



**NTNU – Trondheim**  
Norwegian University of  
Science and Technology

# Development of Membrane Materials for Gas-liquid Membrane Contactors for CO<sub>2</sub> Capture from Natural Gas

**Tina Tomasa**

Chemical Engineering and Biotechnology

Submission date: June 2013

Supervisor: May-Britt Hägg, IKP

Co-supervisor: Karen Nessler Seglem, IKP

Norwegian University of Science and Technology  
Department of Chemical Engineering



# PREFACE

This thesis is written as a final part of my master degree from the Norwegian University of Science and Technology (NTNU) at the Department of Chemical Engineering in 2013.

The master thesis is a part of an already ongoing Ph.D-work at NTNU in collaboration with SINTEF Materials and Chemistry, and it is a continuation of my project work from the fall 2012.

I would like to express my sincere gratitude to my supervisor Karen Nessler Seglem for letting me work on her project and for the teaching, guidance and support she has given me. I am very grateful for the time she has spent on my work and for all the useful comments and input on the report.

I would also like to thank my supervisor Professor May-Britt Hägg for letting me work for the membrane group. I would also like to thank Senior Engineer Suzana Villa Gonzales for letting me use the FT-IR spectroscopy at the Department of Chemistry, Tom-Gøran Skog for showing me how to use the microscopy, Zhongde Dai for showing me TGA and Maria Teresa Guzman Gutierrez for showing me DSC. I would also like to thank Vajiheh Nafisi for showing me some smart tricks in the laboratory.

Lastly, I would like to thank my family for their love, encouragement and support, and my friends who have turned five years of study in to good memories for life.

I declare that this is an independent work according to the exam regulations of the Norwegian University of Science and Technology (NTNU).



# ABSTRACT

In this work, membrane materials are developed with the purpose to be used in a gas-liquid membrane contactor for CO<sub>2</sub> capture from natural gas. The amine, methyl diethanolamine (MDEA), is to be used in the liquid phase as the absorbent. This requires a hydrophobic membrane material with high permeabilities and good compatibility with the absorption liquid.

Poly(1-trimethylsilyl-1-propyne) (PTMSP) is a glassy, high free volume polymer, which achieves the highest gas permeabilities of all known polymers. The permeabilities are however known to be unstable over time due to physical aging of PTMSP. Thermal crosslinking of PTMSP with the bis(azide) 4,4-diazidobenzophenone (BAA) has showed to increase the membrane's chemical and physical stability. Crosslinking increased the resistance towards solvents such as toluene. The gas permeabilities of the membranes were tested for three different gases: N<sub>2</sub>, CH<sub>4</sub> and CO<sub>2</sub> at 2, 4 and 6 bar. The gas permeability decreased upon crosslinking but was stable with time. This decrease in permeability is related to the decrease in fractional free volume (FFV) upon crosslinking. Addition of nanoparticles have shown to increase the permeabilities again. Referring to the project work from the fall 2012, addition of nanoparticles of the size 15 nm decreased the permeabilities. They might have blocked the free volume. Clusters (1-3 μm) of TiO<sub>2</sub> nanoparticles with the primary size 21 nm was used in this work and showed promising results as the permeability increased with increasing nanoparticle content.

Several membranes of pure PTMSP, crosslinked PTMSP, and crosslinked nanofilled PTMSP membranes were exposed to distilled water, 2M MDEA and 4.2M MDEA up to 10 weeks (4 weeks for crosslinked nanofilled membranes). Permeation of pure PTMSP showed the same trend as the aging curve. Crosslinked PTMSP showed a decreasing trend the longer the membranes stayed in the solutions. Based on the selectivities, this trend might have been caused by the reduction in the solubility coefficients. Crosslinked nanofilled membranes on the other hand, showed approximate 90% lower permeability than corresponding membranes which have not been in contact with any solutions.

Fourier Transform Infrared (FT-IR) spectroscopy was used to characterize the membrane materials to see the presence of chemical groups and to see how they change upon crosslinking. FT-IR spectra of PTMSP with BAA showed a peak at 2122 cm<sup>-1</sup> (azide group), which disappeared after thermal crosslinking of the membrane. This leaves BAA with a reactive bis(nitrene) that is ready to bond with PTMSP. Microscopic pictures have shown how the free volume in crosslinked membrane decreases as the content of BAA increases.

Other characteristic methods like contact angle measurements were used. The requirements are a hydrophobic material, which indicate that the liquid should not wet the surface (contact angle

> 90°). The water contact angles were above 90°. Membranes exposed to solutions showed that the highest contact angles were observed for membranes soaked in 4.2M MDEA, followed by 2M MDEA. The viscosity of polymer solutions were found by using a rheometer and the results were correlated to the permeabilities. Thermogravimetric analysis (TGA) showed thermal degradation of PTMSP at 350°C.

# SAMMENDRAG

I dette arbeidet har ulike membranmaterialer blitt utviklet til bruk i gas-væske membrankontakter for CO<sub>2</sub> fangst fra naturgass. Methyl diethanol amine (MDEA) skal brukes i væskefasen som absorpsjonsvæske. Dette krever et hydrofobt membranmaterial med høye permeabiliteter og god kompatibilitet med absorpsjonsvæsken.

Poly(1-trimethylsilyl-1-propyne) (PTMSP) er en glassy polymer med et høyt fritt volum som oppnår de høyeste permeabilitetene av alle kjente polymerer. Permeabilitetene er kjent for å være ustabile med tiden og PTMSP undergår en slags fysisk aldring. Termisk crosslinking av PTMSP med bis(azide) 4,4-diazidobenzophenone (BAA) har vist å øke membranens kjemiske og fysiske stabilitet. Crosslinking øker motstanden for oppløsning av membraner i gode løsningsmidler som toluen. Gasspermeabilitetene ble testet for tre ulike gasser: N<sub>2</sub>, CH<sub>4</sub> og CO<sub>2</sub> ved 2, 4 og 6 bar. Gasspermeabilitetene avtok som følge av crosslinking, men var stabile med tiden. Avtakingen i permeabilitet er relatert til avtaking i fritt volum når membranen crosslinkes. Tilsetning av nanopartikler har vist å øke permeabilitetene igjen. Referert til prosjektarbeidet fra høsten 2012, har tilsetning av nanopartikler med en størrelse på 15nm vist reduksjon i permeabilitetene. De har muligens blokkert det frie volumet. Kluster på 1-3 µm med TiO<sub>2</sub> nanopartikler med en primærstørrelse på 21nm, ble brukt i dette arbeidet og har vist lovende resultater. Permeabiliteten økte med økende nanopartikkelinnhold.

Mange membraner av ren PTMSP, crosslinket PTMSP og crosslinket nanofylt PTMSP ble utsatt for destillert vann, 2M MDEA og 4.2M MDEA opp til 10 uker (4 uker for crosslinket nanofylte membraner). Permeasjon av ren PTMSP viste samme trend som aldringskurven. Crosslinket PTMSP viste en avtaking i permeabilitet dess lengre de var i løsningene. Basert på selektivitetene kan denne trenden ha blitt forårsaket på grunn av reduksjon i solubilitetskoeffisientene. Crosslinkede nanofyllte membraner viste cirka 90 % lavere permeabilitet enn tilsvarende membraner som ikke har vært i kontakt med noen løsninger.

Fourier Transform Infrarød (FT-IR) spektroskopi ble brukt til å karakterisere membranmaterialene for å se tilstedeværelsen av kjemiske grupper samt hvordan de endrer seg ved crosslinking. FT\_IR spektra av PTMSP og BAA viste en topp ved 2122 cm<sup>-1</sup> (azid gruppe), som forsvant etter termisk oppvarming. Dette gjør at BAA har igjen en reaktiv bis(nitrene) som bindes til PTMSP. Mikroskopiske bilder viste hvordan det frie volumet avtok med økende BAA innhold i membranen.

Andre karakteriseringsmetoder, som kontaktvinkelmåling har blitt brukt. Kravet er et hydrofobt material som indikerer at væske ikke kan fukte overflaten (kontaktvinkler > 90°). Vannkontaktvinklene var mål over 90°. Membraner som ble utsatt for ulike løsninger viste at membraner som lå i 4.2M MDEA hadde de høyeste kontaktvinklene, etterfulgt av de som lå i 2M MDEA. Viskositetene av polymerløsningene ble funnet ved bruk av et rheometer, og disse

resultatene ble knyttet opp mot permeabilitetsresultatene. Thermogravimetrisk analyse ble foretatt og viste en termisk degradering av PTMSP ved 350 °C.



# CONTENTS

PREFACE .....	i
ABSTRACT .....	iii
SAMMENDRAG .....	v
LIST OF SYMBOLS .....	xi
LIST OF FIGURES .....	xv
LIST OF TABLES .....	xix
1. INTRODUCTION .....	1
1.1 Membrane classes for gas separations .....	2
1.2 Polymers and their properties .....	3
1.2.1 State of the polymer .....	3
1.2.2 Crosslinking .....	4
1.2.3 Chain flexibility.....	4
1.3 General gas separation theory.....	5
1.3.1 The solution-diffusion mechanism.....	5
1.3.2 The driving force .....	6
1.3.3 Free volume.....	7
1.3.4 Dual sorption model .....	8
1.4 Mixed matrix membranes .....	9
2. LITERATURE REVIEW OF HIGH FREE VOLUME POLYMERS .....	11
2.1 PTMSP.....	12
2.1.1 Crosslinking of PTMSP .....	12
2.1.2 Addition of nanoparticles to PTMSP .....	13
2.2 Other high free volume polymers .....	14
3. GAS-LIQUID MEMBRANE CONTACTORS.....	17
3.1 Combining membrane separation and absorption .....	17
3.2 Wetting characteristics of membrane-solvent .....	18
3.3 Reaction of CO <sub>2</sub> with alkanolamines.....	19
3.4 Mass transfer in membrane contactors .....	20
3.4.1 Mass transfer in flat sheet membranes .....	20

3.4.2	Mass transfer in hollow fiber membranes .....	23
3.5	Advantages and disadvantages of membrane contactors.....	25
3.6	Literature review of gas-liquid membrane contactors .....	26
4.	THE BACKGROUND OF THE MASTER THESIS .....	29
5.	MATERIALS.....	31
5.1	Polymer.....	31
5.2	Crosslinking Agent .....	31
5.3	Nanoparticles .....	32
5.4	Gases.....	32
5.5	Other chemicals .....	32
6.	EXPERIMENTAL METHODS.....	33
6.1	Design Of Experiments (DOE).....	33
6.2	Membrane preparation.....	35
6.2.1	Preparation of polymer solutions .....	35
6.2.2	Membrane casting .....	35
6.2.3	Amine treated membranes.....	35
6.3	Characterization techniques.....	36
6.3.1	Fourier Transform Infrared Spectroscopy (FT-IR) .....	36
6.3.2	Contact Angle Measurements .....	37
6.3.3	Viscosity Measurements .....	38
6.3.4	Gas Permeability Measurements .....	40
6.3.5	Thermogravimetric analysis (TGA).....	43
6.3.6	Differential Scanning Calorimeter DSC .....	43
6.3.7	Microscope .....	44
6.3.8	Uncertainty analysis .....	44
7.	RESULTS AND DISCUSSION .....	45
7.1	Polymer solutions and membranes .....	45
7.1.1	Viscosity of the polymer solutions.....	46
7.1.2	FT-IR spectroscopy of pure PTMSP .....	47
7.1.3	FT-IR spectroscopy of crosslinked PTMSP .....	47
7.2	Thermal stability.....	49
7.3	Permeation results.....	51
7.3.1	The background of the permeability measurements .....	51

7.3.2	Uncertainty analysis .....	52
7.3.3	Effect of gas and pressure on permeability .....	53
7.3.4	Aging of crosslinked and uncrosslinked PTMSP .....	54
7.3.5	Effect of crosslinking on permeability .....	55
7.3.6	Permeation through crosslinked nanofilled membranes .....	57
7.3.7	Amine treated membranes.....	60
7.4	Water contact angles.....	64
8.	CONCLUSION.....	67
9.	FURTHER WORK .....	69
10.	REFERENCES .....	71
APPENDIX .....		I
A.	FT-IR SPECTROSCOPY RESULTS .....	I
B.	GAS PERMEABILITY CALCULATIONS AND RESULTS .....	VII
B.1	Gas permeability calculations .....	VII
B.2	Gas permeability results.....	VIII
C.	CONTACT ANGLE MEASUREMENTS.....	XIII
D.	RISK ASSESSMENT .....	XVII



# LIST OF SYMBOLS

Symbol	Explanation	Unit
<b>Latin Characters</b>		
A	Area	m <sup>2</sup>
b	Langmuir affinity constant	bar <sup>-1</sup>
C or c	Concentration	m <sup>3</sup> (STP)/m <sup>3</sup>
D	Diffusion coefficient	m <sup>2</sup> /s
d	diameter	m
D <sup>k</sup>	Knudsen diffusion coefficient	m <sup>2</sup> /s
E	Enhancement factor	
J	Flow rate	m <sup>3</sup> (STP)/s
J	Flux	mol/m <sup>2</sup> s
k	Mass transfer coefficient	m/s
K	Overall mass transfer coefficient	m/s
k <sub>D</sub>	Henry's Law constant	m <sup>3</sup> (STP)/m <sup>3</sup> bar
L	Length	m
l	Membrane thickness	m
M	Molecular weight	g/mol
p	Pressure	bar
P	Permeability	Barrer or m <sup>3</sup> (STP)m/m <sup>2</sup> h bar
R	Gas constant	8.3144621 J/Kmol
r <sub>p</sub>	Pore size radius	m
S	Solubility coefficient	m <sup>3</sup> (STP)/m <sup>3</sup> bar
T	Temperature	K
V	Volume	m <sup>3</sup>
v	Velocity	m/s
x	Distance in the x direction	m

Symbol	Explanation	Units
--------	-------------	-------

### Greek Characters

$\alpha$	Selectivity	
$\Delta$	Delta, finite difference	
$\delta$	Thickness	m
$\varepsilon$	Porosity	
$\eta$	Viscosity	Pa·s
$\theta$	Contact angle	°
$\tau$	Tortuosity	
$\Upsilon$	Surface tension	mN/m
$\Upsilon$	Shear rate	1/s

### Subscripts

A	Component A
B	Component B
i	Component i
ieg	Component i at the gas-liquid interface
ie	Component i at the liquid-gas interface
ig	Component i at the gas phase
il	Component i at the liquid phase
im	Component i at the membrane
im int	Component i at the microporous-dense interface
img	Component i at membrane-gas interface
j	Component j
g	Gas
l	Liquid
LG	Liquid-gas
m	Membrane
SG	Solid-gas
SL	Solid-liquid
vdw	van der Waals

Symbol	Explanation
--------	-------------

### Abbreviations

BAA	4,4'-diazidobenzophenone azide
BDD	2,2-bis(trifluoromethyl)-4,5-difluoro-1,3dioxole
DEA	Diethanolamine
DOE	Design of experiments
FFV	Fractional free volume
FS	Fumed silica
FT-IR	Fourier Transform Infrared Spectroscopy
MDEA	Methyl diethanolamine
MEA	Monoethanol amine
MGA	Membrane gas absorption
MMM	Mixed matrix material
NaOH	Sodium hydroxide
PP	Polypropylene
PTFE	Polytetrafluoroethylene
PVFE	Polyvinylidene fluoride
PTMSP	Poly(1-trimethylsilyl-1-propyne)
TEA	Triethanolamine
TFE	Tetrafluoroethylene
T <sub>g</sub>	Glass transition temperature
T <sub>m</sub>	Melting temperature
TiO <sub>2</sub>	Titanium oxide
wt%	Weight percentage

### Conversions

Barrer	$10^{-10} \text{ cm}^3(\text{STP})\text{cm}/(\text{cm}^2\text{s cmHg})$ $27.4 \cdot 10^{-10} \text{ m}^3(\text{STP})\text{m}/(\text{m}^2\text{hbar})$ $3.34 \cdot 10^{-16} \text{ kmolm}/(\text{m}^2\text{s kPa})$
Å	$10^{-10} \text{ m}$





# LIST OF FIGURES

Figure 1.1 Illustration of the three different types of membranes for gas separation, (a) Porous membrane (b) Nonporous membrane and (c) Carrier membrane [7].....	2
Figure 1.2 Tensile modulus E as a function of temperature T for an amorphous polymer [7]..	4
Figure 1.3 Illustration of a membrane process separating two types of gas molecules (blue=O <sub>2</sub> , red =N <sub>2</sub> ) .....	5
Figure 1.4 Selectivity for the gas pair O <sub>2</sub> - N <sub>2</sub> as a function of the permeability of O <sub>2</sub> [5] .....	6
Figure 1.5 Dual sorption theory: Henry's Law and Langmuir-type sorption [7].....	8
Figure 1.6 Illustration of the inorganic dispersed phase embedded in the polymer matrix [24]	9
Figure 2.1 Crosslinking reaction mechanism scheme of PTMSP with bis(azide)s [33, 42, 47, 49].....	13
Figure 3.1 A Liqui-Cel® Extra-Flow membrane contactor [56] .....	17
Figure 3.2 Operation modes for a hydrophobic microporous hollow fiber membrane in a gas-liquid membrane contactor where the pores are (a) non-wetting mode, (b) overall-wetting mode, and (c) partial wetting mode [61]. .....	18
Figure 3.3 Concentration profile of the species <i>i</i> when it moves from gas phase towards liquid phase through a) microporous hydrophobic flat sheet membrane, and b) microporous-dense composite membrane [68].....	21
Figure 3.4 Mass transfer/concentration process in a hydrophobic hollow fiber gas-liquid membrane contactor [70] .....	23
Figure 5.1 Chemical structure of poly(1-trimethylsilyl-1-propyne) (PTMSP) .....	31
Figure 5.2 Chemical structure of 4,4-diazidobenzophenone azide (BAA).....	31
Figure 6.1 Instrumental process of FT-IR spectrometry [85] .....	36
Figure 6.2 Optical tensiometer used to measure contact angle [87] .....	37
Figure 6.3 Contact angles for different drop shapes on a solid surface [88].....	37
Figure 6.4 Rheometer at (a) lifted position (b) a picture of the upper and bottom cylinder, respectively, and (c) rheometer ready to do measurements .....	39
Figure 6.5 Viscosity and shear stress measurements from the software US 200.....	39
Figure 6.6 Flowchart of the single gas permeation setup used in the experiment .....	40
Figure 6.7 Flowchart of a single gas permeation setup.....	41
Figure 6.8 Mounting of membrane in the module: (a) the support for the membrane with a metal sinter in the middle, (b) the membrane is masked with aluminum tape on both sides and put on the metal sinter, (c) the masked membrane is glued to the test cell with aluminum tape, and (d) the top and the bottom of the module are put together .....	41
Figure 6.9 Digitrix II Disc Micrometer used to measure the membrane thickness.....	42
Figure 6.10 TGA Q-500 used in the laboratory .....	43
Figure 7.1 Photograph of membranes containing PTMSP. Membrane from left: pure PTMSP, 3wt% BAA, 20wt% TiO <sub>2</sub> nanoparticles, and 3wt% BAA + 20wt% TiO <sub>2</sub> nanoparticles in the last one to right.....	45

Figure 7.2 Viscosity of some polymer solutions.....	46
Figure 7.3 FT-IR spectra of pure PTMSP .....	47
Figure 7.4 FT-IR spectra of PTMSP with 3wt% BAA before and after crosslinking .....	48
Figure 7.5 TGA curves of pure PTMSP and some crosslinked and filled samples .....	49
Figure 7.6 DSC curve of uncrosslinked PTMSP and uncrosslinked PTMSP with 3wt% BAA .....	50
Figure 7.7 The effect of two different TiO <sub>2</sub> nanoparticle sizes on the CO <sub>2</sub> permeability at 2 bar and room temperature [97] .....	51
Figure 7.8 N <sub>2</sub> permeability of three crosslinked membranes containing PTMSP, 1.5 wt% BAA and 10 wt% TiO <sub>2</sub> nanoparticles.....	52
Figure 7.9 CO <sub>2</sub> , CH <sub>4</sub> and N <sub>2</sub> permeabilities as a function of pressure for crosslinked PTMSP with 3wt% BAA .....	53
Figure 7.10 Stability of crosslinked and uncrosslinked PTMSP, measured as a function of CO <sub>2</sub> permeability at 2 bar and room temperature.....	54
Figure 7.11 Stability of crosslinked and uncrosslinked PTMSP, measured as a function of CO <sub>2</sub> /CH <sub>4</sub> selectivity at 2 bar and room temperature .....	55
Figure 7.12 Microscopic pictures of the surface of (a) Pure PTMSP, (b) PTMSP with 1.5wt% BAA, (c) PTMSP with 2wt% BAA and (d) PTMSP with 3wt% BAA .....	56
Figure 7.13 CO <sub>2</sub> permeability of membranes from DOE at room temperature .....	57
Figure 7.14 CO <sub>2</sub> , CH <sub>4</sub> and N <sub>2</sub> permeability of PTMSP+20wt% TiO <sub>2</sub> nanoparticles at room temperature.....	58
Figure 7.15 CO <sub>2</sub> permeability of PTMSP membranes at 2 bar that have been soaked in distilled water, 2M MDEA and 4.2M MDEA for 10 weeks .....	60
Figure 7.16 CO <sub>2</sub> /CH <sub>4</sub> selectivity of PTMSP membranes at 2 bar that have been soaked in distilled water, 2M MDEA and 4.2M MDEA for 10 weeks .....	61
Figure 7.17 CO <sub>2</sub> permeability of crosslinked PTMSP with 3wt% BAA at 2 bar that have been soaked in distilled water, 2M MDEA and 4.2M MDEA for 10 weeks.....	62
Figure 7.18 CO <sub>2</sub> /CH <sub>4</sub> selectivity of crosslinked PTMSP with 3wt% BAA at 2 bar that have been soaked in distilled water, 2M MDEA and 4.2M MDEA for 10 weeks .....	62
Figure 7.19 CO <sub>2</sub> permeability of crosslinked PTMSP with 2wt% BAA and 20wt% TiO <sub>2</sub> at 2 bar that have been soaked in distilled water, 2M MDEA and 4.2M MDEA for 4 weeks.....	63
Figure 7.20 CO <sub>2</sub> /CH <sub>4</sub> selectivity of crosslinked PTMSP with 2wt% BAA and 20wt% TiO <sub>2</sub> at 2 bar that have been soaked in distilled water, 2M MDEA and 4.2M MDEA for 4 weeks.....	63
Figure 7.21 Contact angle measurements of water on a membrane from fall 2012, containing 5wt% PTMSP and 20wt% TiO <sub>2</sub> .....	64
Figure 7.22 Water contact angle measurement of PTMSP membranes that have been soaked in solutions up to 10 weeks .....	65
Figure 7.23 Water contact angle measurement of crosslinked PTMSP with 3wt% BAA that have been soaked in solutions up to 10 weeks .....	66
Figure 7.24 Water contact angle measurement of crosslinked PTMSP with 2wt% BAA and 20wt% TiO <sub>2</sub> that have been soaked in solutions up to 4 weeks .....	66
Figure A.1 FT-IR spectra of a membrane containing crosslinked PTMSP with 1.5wt% BAA..I	
Figure A.2 FT-IR spectra of a membrane containing crosslinked nanofilled PTMSP with 1.5wt% BAA and 10wt% TiO <sub>2</sub> nanoparticles .....	II

Figure A.3 FT-IR spectra of a membrane containing crosslinked PTMSP with 2wt% BAA in a non-gas tested- and gas tested area .....	III
Figure A.4 FT-IR spectra of a membrane containing nanofilled PTMSP with 20wt% TiO <sub>2</sub> nanoparticles in a non-gas tested- and gas tested area .....	IV
Figure A.5 FT-IR spectra of PTMSP membranes treated with (a) no solution (b) distilled water (c) 2 M MDEA and (d) 4.2 M MDEA for 2 weeks .....	V
Figure A.6 FT-IR spectra of crosslinked PTMSP with 3wt% BAA membranes treated with (a) no solution (b) distilled water (c) 2M MDEA and (d) 4.2M MDEA for 2 weeks .....	VI



# LIST OF TABLES

Table 2.1 Structure and properties of some high free volume polymers at 25°C [27-30] .....	11
Table 2.2 Gas permeabilities of PTMSP and PDMS at low pressures and 35°C .....	12
Table 6.1 Factors defined in DOE.....	33
Table 6.2 Response in DOE .....	34
Table 6.3 Membranes to be synthesized.....	34
Table 6.4 Membranes synthesized in the laboratory. The wt% of PTMSP is given according to toluene, and the wt% of BAA and TiO <sub>2</sub> are given according to PTMSP .....	34
Table 7.1 Gas permeabilities of crosslinked membranes and pure uncrosslinked PTMSP at room temperature .....	55
Table 7.2 Selectivities of gases in pure PTMSP and crosslinked nanofilled PTMSP membranes at room temperature .....	59
Table 7.3 Water contact angle measurements of PTMSP membranes from DOE .....	64
Table B.1 Values of the parameters for gas permeability of N <sub>2</sub> at 2 bar for a pure PTMSP membrane .....	VII
Table B.2 Gas permeabilities of membranes from DOE .....	IX
Table B.3 Permeability and selectivity of pure PTMSP membranes which have been treated with distilled water, 2M MDEA and 4.2M MDEA up to 10 weeks .....	X
Table B.4 Permeability and selectivity of crosslinked PTMSP membranes with 3 wt% BAA which have been treated with distilled water, 2M MDEA and 4.2M MDEA up to 10 weeks. XI	
Table B.5 Permeability and selectivity of crosslinked nanofilled PTMSP membranes with 3wt% BAA and 20wt% TiO <sub>2</sub> which have been treated with distilled water, 2M MDEA and 4.2M MDEA up to 4 weeks .....	XII
Table C.1 Water contact angles of the membranes prepared for DOE .....	XIII
Table C.2 Contact angles of pure PTMSP membranes which have been treated with distilled water, 2M MDEA and 4.2M MDEA up to 10 weeks. The measurements are taken 10 minutes after the drop was in contact with the membrane.....	XIV
Table C.3 Contact angles of crosslinked PTMSP with 3wt% BAA which have been treated with distilled water, 2M MDEA and 4.2M MDEA up to 10 weeks. The measurements are taken 10 minutes after the drop was in contact with the membrane. ....	XV
Table C.4 Contact angles of crosslinked nanofilled PTMSP with 2wt% BAA and 20wt% TiO <sub>2</sub> which have been treated with distilled water, 2M MDEA and 4.2M MDEA up to 4 weeks. The measurements are taken 10 minutes after the drop was in contact with the membrane. XVI	



# Chapter 1

## INTRODUCTION

Carbon dioxide (CO<sub>2</sub>) is one of the major greenhouse gases, which has been in focus in the recent years due to global warming [1]. Natural gas on the other hand is an important energy source having a widely variable composition, depending on the reservoir source. In order to meet the pipeline specifications and regulatory standards, it is necessary to process the natural gas. Removal of acidic gases from natural gas, like CO<sub>2</sub>, is the largest industrial gas separation application today giving a growth area for polymeric membranes. The natural gas reservoirs will become more low-quality reservoirs with higher acid gas content in the future, making the separation process even more attractive [2].

Several techniques for CO<sub>2</sub> capture are under research. One conventional technique for CO<sub>2</sub> capture is column absorption which is quite energy-consuming and hard to operate due to several factors. Studies have shown that a membrane gas absorption process, using a membrane contactor, is a good alternative [1]. The use of a novel membrane technology like membrane contactor is very energy efficient compared to the commercial processes used today. In gas-liquid membrane contactors the advantage of both membrane technology and absorption processes are combined. The membrane acts like a barrier between the absorption liquid and the gas, while the absorption liquid increase the selectivity of the system. Liquids such as alkanamines are frequently used in CO<sub>2</sub> contactors because they increase the CO<sub>2</sub>/N<sub>2</sub> selectivity by more than 100-fold [3].

Separations by the use of membranes are becoming very important in the process industries. Membrane technology for liquid separations has been applied in the industry for many years, in processes like reverse osmosis, ultrafiltration and microfiltration [4]. Membrane technology for gas separation is a relatively young technology [5]. The challenge is to develop new tough, high performance materials which gain acceptance in the industry. Materials should be tailored for a particular gas mixture separation.

In this work, development and testing of membrane materials from a highly permeable dense polymer poly[1-trimethylsilyl-1-propyne] (PTMSP) is investigated for gas separation. The synthesized membranes are meant for use in membrane contactors with an amine, methyl diethanolamine (MDEA), as the liquid phase and natural gas as the gas phase. The membranes are optimized for this process, where important demands for the membrane material in contactors are high permeability, hydrophobicity and good chemical and mechanical compatibility with the liquid absorbent. [6]. Due to fast aging of PTMSP, optimal crosslinking with bis(azide) is necessary to enhance the membrane stability. In order to enhance the

permeability of the membranes, which decreases as the amount of crosslinking agent is added, TiO<sub>2</sub> nanoparticles were added to the polymer solutions.

This chapter provides an introduction to membrane gas theory, starting with a classification of different types of membranes (Chapter 1.1) followed by a description of some polymer properties (Chapter 1.2) since a polymer is used as the membrane material in this work. The transport mechanism through nonporous membranes described in terms of solution-diffusion mechanism is given in Chapter 1.3. Mixed matrix materials are widely studied in order to enhance the selectivity and the permeability of the membrane and the concept is described in Chapter 1.4. A literature review on the topic “high free volume polymers” in Chapter 2 provides some reviews of crosslinking of PTMSP and introduction of nanoparticles to the polymer, something which is done in this experimental work. Important gas-liquid membrane contactor requirements are discussed in Chapter 3. Several mass transfer equations for both flat sheet and hollow fiber membranes are presented, but not used in the experimental part of the work. The background of the master thesis is given in Chapter 4, after the theory and literature reviews are presented in Chapter 1-3.

## 1.1 Membrane classes for gas separations

A large number of materials can be used as the basis for membrane preparation. A normal classification of membranes for gas separation is porous membranes, nonporous membranes and carrier membranes. An illustration of these three types of membranes is given in Figure 1.1 [7].

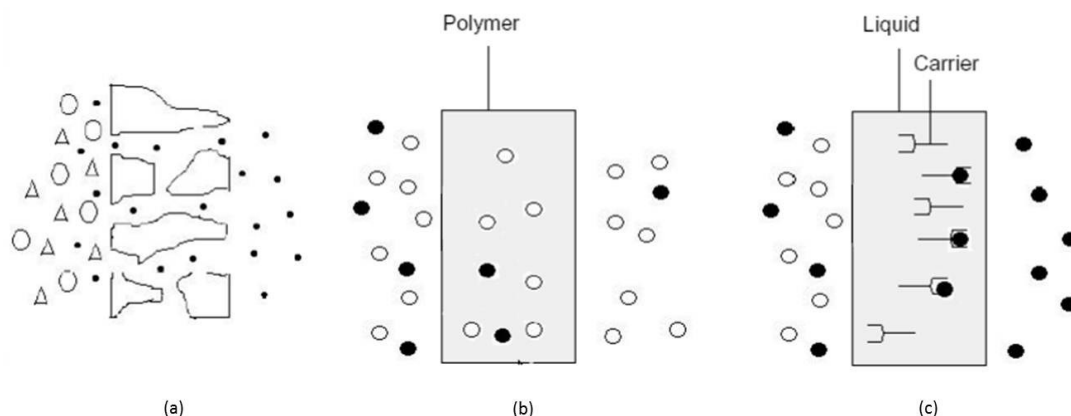


**Figure 1.1** Illustration of the three different types of membranes for gas separation, (a) Porous membrane (b) Nonporous membrane and (c) Carrier membrane [7]

Separation by porous membranes is typically based on size exclusion. They are often made of zeolites, glass, metal or polymer [8]. The small pores in the membrane separate the gases on



the basis of their molecular weight (Knudson diffusion) or size (molecular sieving) [4]. Many membranes of this type are employed, but it is not a commercial membrane for gas separation. Porous membranes are seldom used in gas separation alone, but asymmetric or composite membranes are often used as support for dense membranes [4, 7]. Porous membranes are normally applied in microfiltration and ultrafiltration for liquid separations.

Nonporous membranes are made of dense polymers that are capable of separating molecules of same size or by polarity. This process is based on the solution-diffusion mechanism, where the component with the highest solubility and/or diffusivity will permeate fastest through the membrane. Since the components need to dissolve into the membrane, the properties of the polymeric material will be very important for the separation process [7, 8]. PTMSP, which is used in this experiment, is a dense, nonporous polymer that follows the solution-diffusion mechanism. This mechanism is therefore described in more detail in Chapter 1.3. The rest of the report considers polymer membranes.

The selectivity of carrier membranes is not determined by the membrane material itself, but by a carrier-molecule that allows specific transport. This carrier is either fixed to the membrane matrix or it is mobile when dissolved in a liquid. In the latter case the carrier in liquid is presented in the pores of a porous membrane. The separation depends on the affinity and reactivity of the membrane. With the use of specific tailored carriers, high selectivities can be achieved. This type of membrane is used to remove components that are gaseous or liquid, ionic or non-ionic [7].

## 1.2 Polymers and their properties

Polymers are large molecules (macromolecules) that are built up from many small repeating units called monomers [9]. Since the main membrane material used in the study is the polymer PTMSP, an introduction to some polymer properties is necessary for the further understanding of membrane behavior during gas separation.

### 1.2.1 State of the polymer

The state of the polymer has an important effect on mechanical, thermal and permeation properties of the membrane. Glass transition temperature and the crystallinity of the polymer are important when selecting the membrane material. An amorphous polymer changes from glassy state to rubbery state when heated above the glass transition temperature (Figure 1.2). At this point of transition, the polymer chains change from frozen to flexible. The membrane properties depend upon the polymer state. The rubbery state has generally high permeability and low selectivity, while a glassy polymer generally has low permeability and high selectivity.

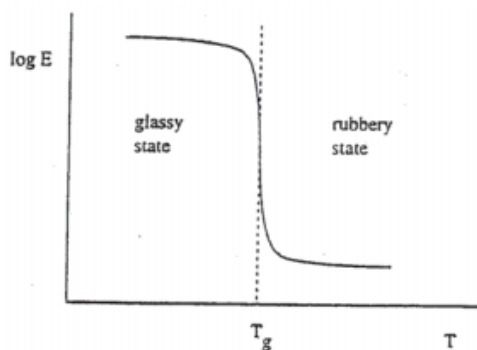


**Figure 1.2** Tensile modulus E as a function of temperature T for an amorphous polymer [7]

Only few polymers can be used as membranes because of the stability. In general,  $T_g$ ,  $T_m$  and degree of crystallinity favors membrane stability.  $T_g$  and  $T_m$  increase with stiff main chains, presence of aromatic groups, large side groups and resonance structure. The degree of crystallinity increases by simple polymer structures and decreases with crosslinking [7, 9, 10].

### 1.2.2 Crosslinking

It is possible to connect two or more macromolecules to each other with covalent bonds, by the means of crosslinking [7]. Crosslinking changes the physical, mechanical and chemical properties of the polymer. Uncrosslinked polymers will normally melt when heated above the melting temperature (thermoplastics) while crosslinked polymers cannot melt because of the reduction of molecular motion during crosslinking of the polymer [11]. Dissolution difference is also an important property change during crosslinking. Uncrosslinked polymers will usually dissolve in an appropriate solvent, while crosslinked polymers become insoluble [7]. The solvent cannot overcome the covalent forces in crosslinkers. The mechanical properties of the polymer depend on the degree of crosslinking. Uncrosslinked or lightly crosslinked polymers tend to be soft and flexible, while heavily crosslinked polymers tend to be very brittle and this brittleness is not affected by the heat [11].

### 1.2.3 Chain flexibility

In order to describe the properties of the polymers, chain flexibility is a factor that has large influence on other parameters, such as the glass transition temperature ( $T_g$ ) and the melting temperature ( $t_m$ ). The chain flexibility is determined by the characteristics of the main chain and the presence of side chains [7]. The chain flexibility is increased when saturated methylene groups ( $-\text{CH}_2-\text{CH}_2-$ ) or oxygen/nitrogen atoms are present. This is because rotation around each  $-\text{C}-\text{C}-$  bond is possible [12].

Introduction of saturated chains make the rotation around the bonds difficult and the chains become very rigid. Introduction of heterocyclic and aromatic groups make the chains rigid as well. The flexible oxygen and nitrogen atoms are often present in a chain together with stiff aromatic or heterocyclic groups which dominate the structure and therefore gives the chain a

rigid character [7]. The flexibility of amorphous polymers is drastically reduced when cooled below the glass transition temperature. Below this temperature, there is no segmental motion [12].

### 1.3 General gas separation theory

The membrane acts like a semipermeable barrier and let only certain types of molecules pass through the membrane. The membrane control the rate of movement of the various molecules [13]. The feed stream is divided into two streams, the retentate and permeate. If air is the feed, the membrane will separate oxygen and nitrogen components by letting the feed gas go through the cross-sectional area of the membrane. The process is illustrated in Figure 1.3.

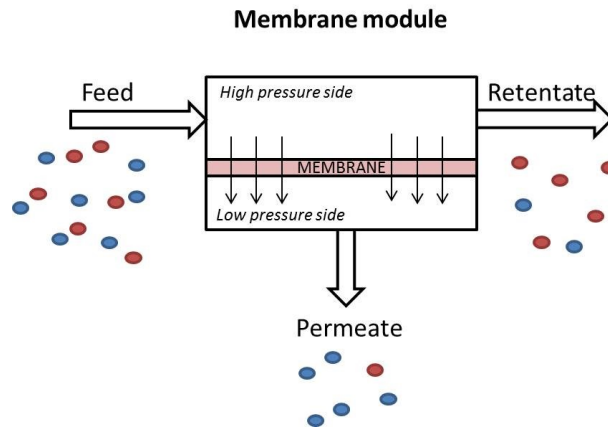


Figure 1.3 Illustration of a membrane process separating two types of gas molecules (blue=O<sub>2</sub>, red =N<sub>2</sub>)

In order to separate two gases, there must be a driving force to make the gas go through the membrane. Membrane separation of gases is a concentration-driven process, which is directly related to the partial pressure of the feed and the gas stream. In this case, the feed is compressed to provide the driving force for the separation of oxygen and nitrogen in air. The membrane is more permeable to oxygen than to nitrogen, and the oxygen will therefore permeate through the membrane to the low pressure permeate side. The remaining stream is enriched in nitrogen and leaves the process as a retentate [4].

#### 1.3.1 The solution-diffusion mechanism

Two important properties of the membrane are the *permeability* and the *selectivity*. The most common type of membranes for gas separation today, is the dense, nonporous, polymeric materials, where the transport takes place as a solution-diffusion process. This means that the gas transport through a polymeric membrane is controlled by the solubility (S) and diffusivity (D) of the gas in the membrane. The permeability is the product of these two factors [4, 5, 7].

$$P = S \cdot D \quad (1.1)$$

The diffusivity is given in  $\text{m}^2 \cdot \text{s}^{-1}$  and the solubility is given in  $\text{m}^3 \text{ (STP)} \cdot \text{m}^{-3} \text{bar}^{-1}$ . The gas permeability is normally given in the common non-SI unit called Barrer ( $1 \text{ Barrer} = 27.4 \cdot 10^{-10} \text{m}^3 \text{ (STP)} \cdot \text{m} \cdot \text{m}^{-2} \cdot \text{h}^{-1} \cdot \text{bar}^{-1}$ ).

The ability of a membrane to separate two molecules is given as the ratio between their permeabilities. This is defined as the ideal selectivity ( $\alpha_{A/B}$ ) and is given as [4]:

$$\alpha_{A/B} = \frac{P_A}{P_B} = \frac{D_A S_A}{D_B S_B} \quad (1.2)$$

Studies of polymer-membrane performances over the last years have revealed a trade-off between the selectivity and the permeability for many different polymers. Highly permeable polymers exhibit low selectivities and vice versa. The limit of the performance was demonstrated by Robeson in 1991, who made a double logarithmic plot of the selectivity of  $\text{O}_2/\text{N}_2$  versus the permeability of  $\text{O}_2$ , as shown in Figure 1.4. The dots in the diagram represent the  $\text{O}_2/\text{N}_2$  performances of several polymers. The cross-hatched area is very attractive where materials like molecular sieves and mixed matrix are most likely to be found [14].

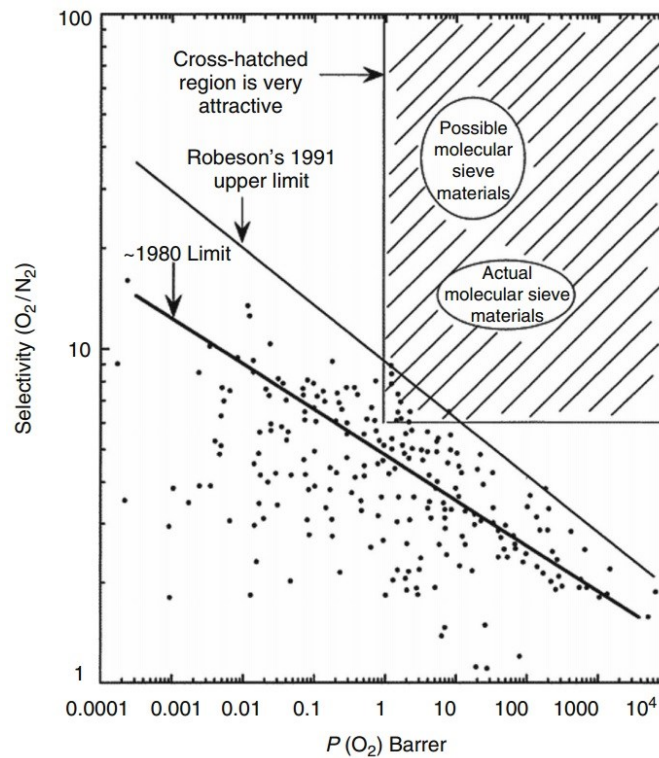


**Figure 1.4** Selectivity for the gas pair  $\text{O}_2$ -  $\text{N}_2$  as a function of the permeability of  $\text{O}_2$  [5]

### 1.3.2 The driving force

The transport of solution-diffusion mechanism takes place with a flux based on Fick's law (Eq. 1.3). Transport through the membrane takes place because of a driving force that acts upon the components on the feed side of the membrane. The permeation rate is in many cases

proportional to the driving force. This means that the flux and the driving force is proportional, and the relationship is given by:

$$J = -D \frac{dc}{dx} \quad (1.3)$$

where  $J$  is the flux of the component ( $\text{m}^3(\text{STP})\cdot\text{s}^{-1}$ ),  $D$  is the diffusion coefficient ( $\text{m}^2\cdot\text{s}^{-1}$ ) and  $dc/dx$  is the concentration gradient for a component over the length  $x$  (m), or in the case of gases a partial pressure gradient between feed and the permeate [5]. Under steady-state conditions, applied for membranes, this equation can be integrated to give:

$$J_i = \frac{D_i(c_{0,i} - c_{l,i})}{l} \quad (1.4)$$

where  $c_{0,i}$  and  $c_{l,i}$  are the concentrations ( $\text{m}^3(\text{STP})\cdot\text{m}^{-3}$ ) in the membrane on the upstream side and downstream side, respectively, and  $l$  is the membrane thickness (m) [7].

The solubility coefficient ( $S$ ), also known as the sorption coefficient, gives the pressure normalized amount of gas sorbed in the membrane.  $S$  is usually low for gases in polymers, but depends on the properties and the state of the polymer (glassy or rubbery) [5]. In ideal systems, the sorption coefficient ( $S$ ) of gases in polymers is relatively constant [15]. For ideal systems the concentrations are related to the partial pressure by Henry's law, where the gas concentration ( $c_i$ ) is proportional to applied pressure ( $p_i$ ) [5]:

$$c_i = S_i p_i \quad (1.5)$$

Henry's law is mostly usable to amorphous polymers where the temperatures are above  $T_g$ , because the solubility behavior is often much less complicated than in the glassy state. Crystallinity in the polymer limits the gas transport [7].

Combining Eq. 1.4 with Eq. 1.5 and Eq. 1.1 gives

$$J_i = \frac{P_i(p_{0,i} - p_{l,i})}{l} = \frac{P_i}{l} \Delta p_i \quad (1.6)$$

Here the flow rate is proportional to the permeability and the difference in partial pressure, and inversely proportional to the membrane thickness [7].

### 1.3.3 Free volume

The free volume is described as static void created by inefficient chain packing [16]. As already mentioned, the permeability of a gas through a dense polymer is described in terms of a solution-diffusion mechanism (Eq. 1.1). The diffusion coefficient ( $D$ ) for a given gas varies from polymer to polymer in a larger degree than the solubility coefficient ( $S$ ). But for dense polymer PTMSP it is the opposite. The diffusion coefficient is affected by many parameters, where the free volume of the polymer is important. The solubility coefficient depends on the free volume as well, but in a much less extent. The permeability coefficient will be strongly correlated to this parameter [17].

The most applied method to estimate the fractional free volume (FFV) of a polymer is given by:

$$FFV = \frac{V - 1.3V_{vdw}}{V} \quad (1.7)$$

where  $V$  is the experimentally observed volume of the polymer and  $1.3V_{vdw}$  is the occupied van der Waals volume, calculated by the group-contribution method of Bondi. The factor 1.3 is estimated from the packing densities of molecular crystals at absolute zero [17-19].

### 1.3.4 Dual sorption model

The most common model used to describe and analyze sorption of gas molecules in glassy polymers, is the dual sorption model. Rubbery polymers are in a hypothetical thermodynamic equilibrium, where the sorption isotherm is linear, hence obeys Henry's law [20]. This means that the gas concentration inside the polymer is proportional to applied pressure. This is observed with gases in elastomers [7]. Glassy polymers on the other hand, are assumed to be in a non-equilibrium state, where the sorption isotherm is rather curved than linear; the permeability decreases with increasing pressure at low feed pressures. Such behavior has been described by the dual-mode sorption, which assumes that two mechanisms happen at the same time: sorption according to Henry's Law and Langmuir type sorption (Figure 1.5). The latter describe sorption in porous solids. The dual sorption is expressed by [7, 20]:

$$C = C_D + C_H = k_D p + \frac{C'_H b p}{1 + b p} \quad (1.8)$$

where  $C$  is the total gas concentration [ $m^3(STP).m^{-3}$ ],  $C_D$  is the gas concentration based on Henry's Law,  $C_H$  is the gas concentration based on Langmuir sorption,  $k_D$  is the Henry's Law constant [ $m^3(STP).m^{-3}bar^{-1}$ ],  $b$  and  $C'_H$  is the hole solubility coefficient [ $bar^{-1}$ ] and the saturation solubility coefficient [ $m^3(STP).m^{-3}$ ] of Langmuir, respectively.

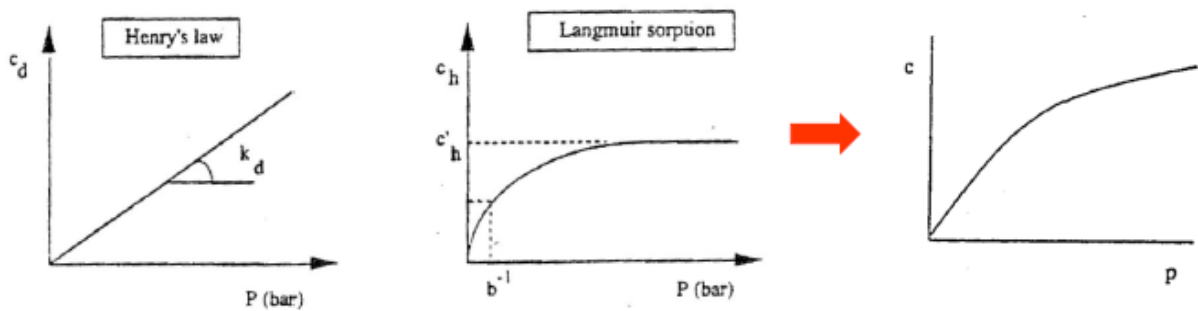
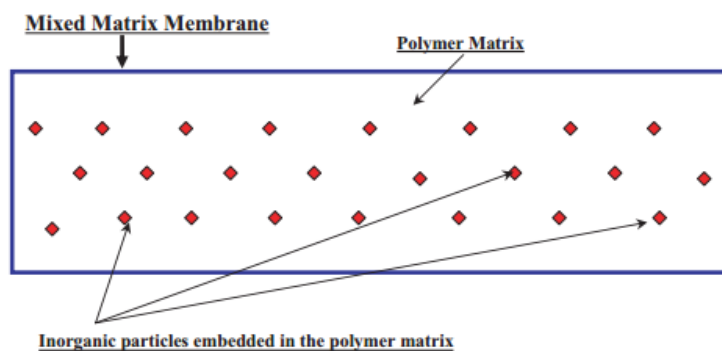


Figure 1.5 Dual sorption theory: Henry's Law and Langmuir-type sorption [7]

The permeability will however begin to increase as the driving pressure is further elevated. This increase occurs when the membrane is exposed to high concentration levels of a gas, like CO<sub>2</sub>, that result in interactions between the gas and the polymer. This may cause changes in the polymer characteristics, and most membrane materials will swell upon the sorption giving a looser matrix, increased free volume and segmental mobility. This unwanted phenomenon is known as plasticization, and results in swollen polymers which losses its selective properties [21].

## 1.4 Mixed matrix membranes

As mentioned earlier, polymeric membranes are restricted by the trade-off between the gas permeability and selectivity, as suggested by the Robeson plot [22]. A new type of membrane material with high permselectivity is needed to expand the market of membranes. The future membrane material which provides a solution of the trade-off problem is mixed matrix material (MMM). This type of material consists of inorganic fillers embedded in a polymer matrix as illustrated in Figure 1.6. The concept of the MMMs is to enhance the separation properties. The fillers might disrupt the molecular packing of the polymer, which affects the local free volume and the molecular transport [5, 23]. Fabrication of MMMs usually involves difficulties with dispersion of inorganic particles in the polymer matrix and the contact of particles with the polymer matrix. Particle size, particle pore size, dispersed pore size and polymer type, and properties are also important when making MMM [24].



**Figure 1.6** Illustration of the inorganic dispersed phase embedded in the polymer matrix [24]

The inorganic materials which are used in MMMs are either of porous or nonporous type. The porous fillers acts like molecular sieves and separate the gases by the shape or size. The nonporous fillers can improve the separation properties of for instance CO<sub>2</sub> by increasing the solubility of the gas in the membrane and thus reducing the diffusion. Nanoparticles may

increase the free volume between the polymer chains and thus increase the diffusion [24]. The nanoparticles used in this work are nonporous TiO<sub>2</sub>.

A review of mixed matrix membranes can be found somewhere else in the literature [24, 25]. The next chapter (Chapter 2) considers some reports of nanoparticles in PTMSP and other high free volume polymers.



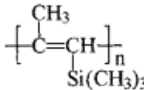
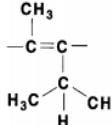
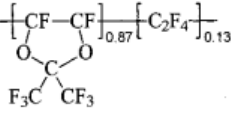
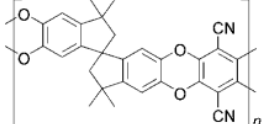
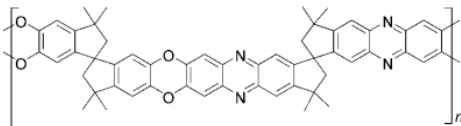
## Chapter 2

# LITERATURE REVIEW OF HIGH FREE VOLUME POLYMERS

Low free volume polymers are often used in membrane applications as molecular sieves for recovery of small molecules like hydrogen or air separations. For separation of large molecule components, like organic vapors or carbon dioxide, from a small component mixture, more efficient membrane materials are required [26].

This section gives a literature review of some high free volume polymers. The structures and properties of some high free volume polymers discussed in this chapter are given in Table 2.1.

**Table 2.1** Structure and properties of some high free volume polymers at 25°C [27-30]

Polymer	FFV [-]	O <sub>2</sub> permeability [barrer]	O <sub>2</sub> /N <sub>2</sub> selectivity [-]	Structure
PTMSP	0.34	6100	1.8	
PMP	0.32	2700	2.0	
AF2400	0.33	1600	2.0	
PIM-1	0.22-0.24	370	4.0	
PIM-7		190	4.5	

## 2.1 PTMSP

Poly[1-trimethylsilyl]-1-propyne] (PTMSP) is the polymer used in this work, and has therefore received its own section. PTMSP is a polymer which has received much attention since it was synthesized for the first time in 1983 by the research group of Higashimura and Masuda [31, 32] at Kyoto University in Japan. PTMSP is a glassy polymer which achieves highest permeabilities for gases and organic vapors. This is mainly due to the loose and flexible packing of the chains which results in an open polymer network, and thus high FFV of 0.34 and unusual free volume distribution [26, 33-35]. The high FFV of PTMSP is almost twice the value of conventional polymers with low free volume. In general, polymers with higher FFV are more permeable.

PTMSP obtains the highest oxygen permeability coefficient of all known polymers ( $P_{O_2} = 6000$  barrer at  $25^\circ\text{C}$ ), but obtain low selectivities ( $P_{O_2}/P_{N_2} = 1.8$ ) [31]. Poly(dimethylsiloxane) (PDMS) was regarded as the most permeable polymer before the synthesis of PTMSP [31]. A comparison between gas permeabilities of PTMSP and PDMS at  $35^\circ\text{C}$  are given in Table 2.2. Note that the permeability measurements in Table 2.1 and Table 2.2 are performed at different temperatures.

**Table 2.2** Gas permeabilities of PTMSP and PDMS at low pressures and  $35^\circ\text{C}$

Gas	Permeability PTMSP [barrer] [36]	Permeability PDMS [barrer] [37]
H <sub>2</sub>	15 000	890
O <sub>2</sub>	9 000	800
N <sub>2</sub>	6 600	400
CO <sub>2</sub>	27 000	3 800
CH <sub>4</sub>	15 000	1 200
C <sub>2</sub> H <sub>6</sub>	31 000	3 300
C <sub>3</sub> H <sub>8</sub>	38 000	4 100

A permeability experiment simulation of PTMSP to a series of gases and vapors shows an increase in permeability in following order: C<sub>3</sub>H<sub>8</sub> > C<sub>2</sub>H<sub>6</sub> > CO<sub>2</sub> > CH<sub>4</sub>/H<sub>2</sub> > O<sub>2</sub> > N<sub>2</sub> > CF<sub>4</sub>. This is because the selectivity is dominated by high solubility and low diffusivity [38]. Ichiraku et al. [39] reported that the high gas permeability of PTMSP results primarily from a substantial gas solubility due to large excess of free volume in this polymer.

### 2.1.1 Crosslinking of PTMSP

PTMSP is however limited by a fast physical ageing caused by relaxation of non-equilibrium excess free volume [27]. Modifications to PTMSP are necessary to improve its chemically and physically stability. PTMSP has been modified by blending it with rubbery polymers [40], brominated it [41], had nanoparticles added to it [16, 33, 42-46], and it has been crosslinked [33, 42, 43, 47-49]. Jia et al. [49] crosslinked PTMSP with bis(azide)s to stabilize the polymer.

Gas permeabilities of PTMSP/bis(azide)s showed a decrease. This decrease is consistent with the fractional free volume (FFV) decrease which occurs during crosslinking. The mechanical stability was improved with permeabilities and separations factors similar or higher than those of PDMS. The permeability of pure PTMSP membranes stored under vacuum for a month declined with 70 %, while crosslinked membranes were approximately unchanged. Crosslinked PTMSP membranes were insoluble in common PTMSP solvents such as toluene [49]. A reaction mechanism scheme for crosslinking of PTMSP with bis(azide)s has been proposed from several experiments [33, 42, 47, 49].

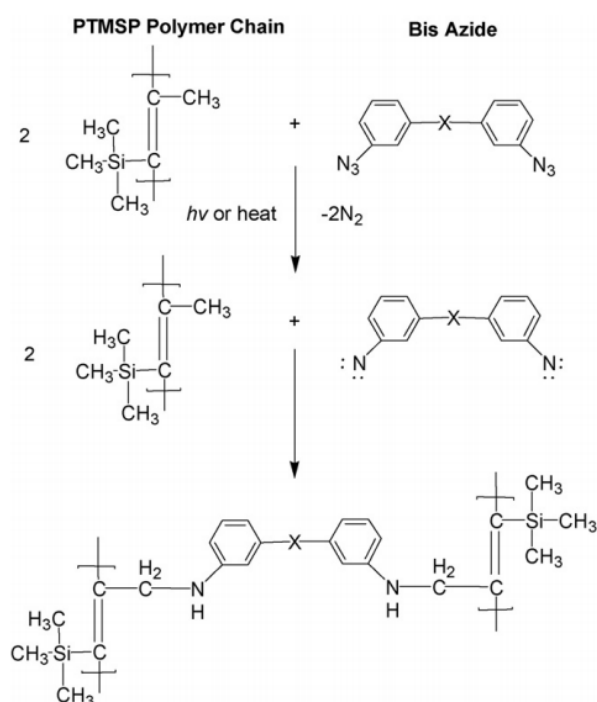


**Figure 2.1** Crosslinking reaction mechanism scheme of PTMSP with bis(azide)s [33, 42, 47, 49]

The reactive bis(nitrene) will react with a C-H bond in PTMSP [33, 42, 47]. The bis(nitrene) can react with the allylic C-H bond or the C-H bonds in  $Si(CH_3)_3$ . Since the allylic C-H bonds are much weaker (85 kcal/mol) than the C-H bonds in  $Si(CH_3)_3$  (100 kcal/mol), it is most likely that the allylic methyl group should be favored [50].

### 2.1.2 Addition of nanoparticles to PTMSP

The permeability reduction caused by crosslinking could be counteracted by adding nanoparticles to the films. Merkel et al. [16] reported that addition of nanoscaled Fumed Silica (FS) to the glassy PTMSP increases the permeability of gas and vapor, but the selectivity of for instance n-butane/methane decreases with increasing FS content. Another experiment [23] with PTMSP showed the same trend as the experiment of Merkel et al., that addition of FS to PTMSP made the hydrocarbon-selective PTMSP less selective for hydrocarbons as the loading of FS

increased. This reduction of the vapor/permanent gas selectivity for filled PTMSP is explained by the polymer's microporous nature, leading to an increased influence of Knudsen diffusion. An experiment of Kelman [43] showed that addition of 30 wt% FS nanoparticles increased the permeability of crosslinked PTMSP by approximately 80%.

The work of Shao [42] with nanoparticles (FS and TiO<sub>2</sub>) in PTMSP resulted in improved permeation (an increase of 38-66% for PTMSP with FS and an increase of 35-63% for PTMSP with TiO<sub>2</sub>) and slightly reduced selectivities of CO<sub>2</sub>/N<sub>2</sub>, CO<sub>2</sub>/CH<sub>4</sub> and CH<sub>4</sub>/N<sub>2</sub>. When crosslinking the PTMSP membrane with 4,4-diazidobenzophenone (BAA), the permeabilities decreased, while the selectivities increased. When adding nanoparticles together with BAA, the permeabilities and selectivities were again increased.

Matteucci et al. [44] investigated the dispersion of TiO<sub>2</sub> nanoparticles in PTMSP, and how different loadings of nanoparticles affect the density and gas permeability of the membrane. This research group was the first to report that some of the particles are dispersed individually or in nanoscale aggregates at low particle loadings. High particle loadings formed micron-sized aggregates. The higher the nanoparticle loading in a sample is, the stronger tendency they have to aggregate, which would act to increase the spacing between particle aggregates. Formation of aggregates may be caused by the polymers inability to disperse particles at high loadings. Addition of nanoparticles with a nominal volume fraction of 0.35 resulted in a density that was 40 % lower than in unfilled PTMSP. Thus, the gas permeability of N<sub>2</sub>, CH<sub>4</sub> and CO<sub>2</sub> increased to more than four times higher than in unfilled PTMSP. Nominal volume fractions below 0.07 showed a decrease in void volume fraction and gas permeability, where the nanoparticles block/fill the free volume of PTMSP. Matteucci et al. [45] looked also at the gas transport properties of MgO filled PTMSP nanocomposites. In films containing 75 nominal volume percent MgO, the gas permeability coefficients of H<sub>2</sub>, N<sub>2</sub>, CH<sub>4</sub> and CO<sub>2</sub> were 17-50 times higher than in unfilled PTMSP.

### 2.2 Other high free volume polymers

Poly(4-methyl-2-pentyne) (PMP) was synthesized by Masuda et al. [51] in 1982, a highly rigid, glassy high free volume polymer. The first gas permeability report of PMP was made by Marisato and Pinnau [30] in 1996, where the gas permeabilities decreased in the following order: n-C<sub>4</sub>H<sub>10</sub> > CO<sub>2</sub> > H<sub>2</sub> > C<sub>3</sub>H<sub>6</sub> > CH<sub>4</sub> > He > O<sub>2</sub> > N<sub>2</sub>. The permeability of O<sub>2</sub> in PMP is reported to 2700 barrer at 25 °C. The CH<sub>4</sub>/N<sub>2</sub>, C<sub>2</sub>H<sub>6</sub>/N<sub>2</sub>, C<sub>3</sub>H<sub>8</sub>/N<sub>2</sub> and n-C<sub>4</sub>H<sub>10</sub>/N<sub>2</sub> selectivity of PMP are 2.2, 2.8, 3.5 and 30, respectively. This is similar behavior to PTMSP. Since the permeability is higher for large molecules, the selectivity must be dominated by high solubility and low diffusivity. Merkel et al. [16, 52, 53] investigated how addition of nanoparticles, Fumed Silica (FS), to PMP improved the permeability and selectivity for large organic molecules. PMP is less permeable than PTMSP, but more stable in time and solvent resistant [30].

Other high free volume polymers are made of random copolymers of tetrafluoroethylene and 2,2-bis(trifluoromethyl)-4,5-difluoro-1,3-dioxole (TFE/BDD). TFE/BDD is an amorphous

random copolymer that exhibits high permeability and excellent chemical resistance. One of the TFE/BDD copolymers that is commercially available is known under the trade name Teflon AF2400 [38]. AF2400 has a FFV of 0.32 which is comparable to the FFV of PTMSP (0.34). Although their FFVs are comparable, PTMSP achieves higher permeabilities. This indicates that the FFV does not describe the permeability properties alone, but the distribution of the free volume is also an important factor. [29, 38]. The cavity size distribution in PTMSP is estimated to 11.2 Å and only 8.2 Å for AF2400 [38].

Polymers of intrinsic microporosity (PIMs) were synthesized by McKeown et al. [28, 54, 55]. These materials are obtained when there are no single bonds in the backbone. Rotation cannot occur and the packing becomes less effective, increasing the free volume [28, 54, 55]. McKeown and Budd believe that PIMs are solutions of the combination of the properties of conventional microporous (pore sizes < 2 nm) materials and polymers. PIM-1 and PIM-7 show O<sub>2</sub>/N<sub>2</sub> selectivities which are much higher than other polymers of similar permeability, and lie above the Robeson plot (from Figure 1.4). For both PIM-1 and PIM-7, the permeability order is CO<sub>2</sub>>H<sub>2</sub>>He>O<sub>2</sub>>Ar>CH<sub>4</sub>>N<sub>2</sub>>Xe. In most glass polymers, He>CO<sub>2</sub>, something which is not the case here [55].



## Chapter 3

# GAS-LIQUID MEMBRANE CONTACTORS

### 3.1 Combining membrane separation and absorption

Membrane contactors have in the recent years received more attention as an effective gas separation tool [5]. It may be considered as a combination of gas absorption technology and membrane technology, giving the process a number of advantages compared to conventional absorption towers. The large contact area per volume and the gas/liquid mass transfer without dispersion of one phase within another makes the membrane contactor process attractive [7]. The membrane acts like a barrier for inter-phase mass transfer, where the absorbent liquid will provide the selectively for the separation without mixing the two phases with each other. The decoupling of the two phases eliminates operation problems like foaming, channeling, entrainment and flooding, which is a common problem with the commercial absorption towers [56]. The separation process of gas/liquid membrane contactors is named membrane gas absorption (MGA), where the concentration difference is the driving force.

The most challenging and attractive applications of membrane contactors are CO<sub>2</sub> capture from combustion of flue gas and natural gas treatment (gas sweetening and dehydration) [57]. A number of different membrane configurations have received attention: flat sheet, spiral wound, rotating annular and hollow fiber. Hollow fiber is the configuration which has received most attention and is available for industrial use. This is due to the compact units and high specific surface area [56]. The high specific area of hollow fiber membrane contactors allows a 65-75% reduction in weight and size compared to conventional towers [58]. Qi and Cussler [59, 60] reported a specific surface area that is 30 times higher than conventional absorption towers. The most known design for concentration driven hollow fiber processes is the Liqui-Cel® Extra-Flow module, which is shown in Figure 3.1 [56].

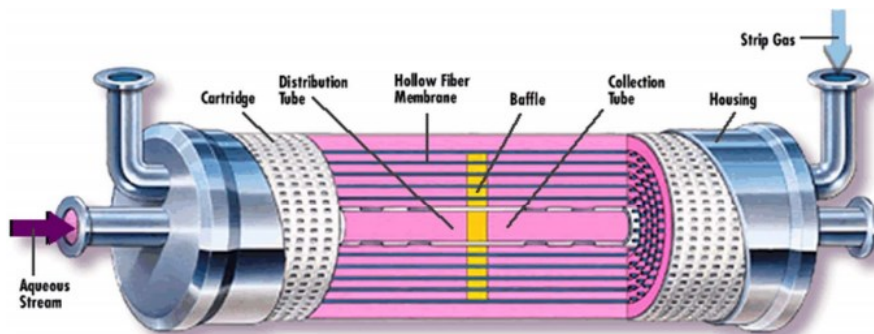


**Figure 3.1** A Liqui-Cel® Extra-Flow membrane contactor [56]

### 3.2 Wetting characteristics of membrane-solvent

Microporous polymer membranes are mostly used in the membrane contactor process. In gas-liquid membrane contactors, the membrane micropores can be filled with either gas or liquid, depending on the hydrophobicity of the membrane. If a hydrophobic membrane is used with an aqueous solution that does not wet the membrane, then the pores of the membrane are filled with gas (Figure 3.2a). On the other hand, a hydrophilic membrane will be wetted by the aqueous solution, and the pores will then be filled with liquid (Figure 3.2b) [7]. Even though a membrane is hydrophobic, liquids such as alkanoamines can partly penetrate into the pores of the membrane as illustrated in Figure 3.2c, where the membrane pores will be gradually wetted over a period of time [61].

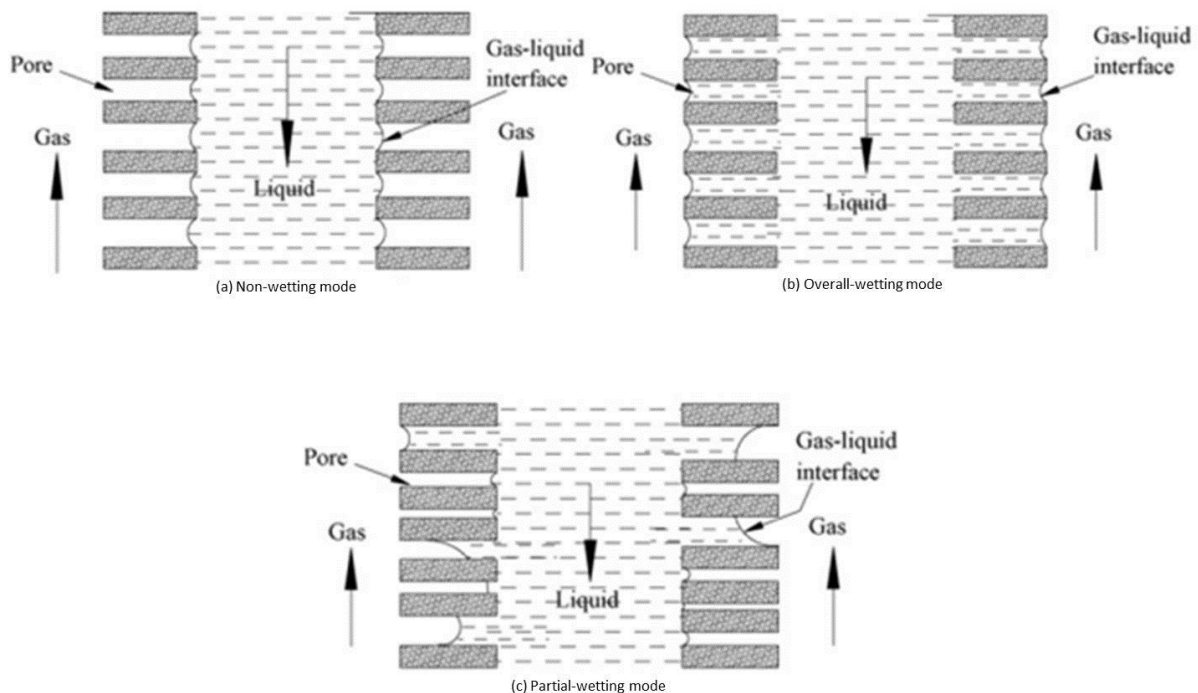


**Figure 3.2** Operation modes for a hydrophobic microporous hollow fiber membrane in a gas-liquid membrane contactor where the pores are (a) non-wetting mode, (b) overall-wetting mode, and (c) partial wetting mode [61].

It is advantageous to operate with a membrane contactor where the pores of the membrane remain completely gas-filled (non-wetted) over longer operational time. This is because the mass transfer coefficient for the process is highest for a gas-filled membrane compared to the liquid filled membrane. In the case of the membrane pores being filled with liquid, the gas to be absorbed also has to diffuse through the stagnant liquid inside the pores, something which increases the mass transfer resistance considerably [62].



The wetting of the membrane is described by the interactions between the membrane and the liquid. The pressure that is required to force water to enter the pore into a hydrophobic membrane can be found by the Young-Laplace equation. This minimum breakthrough pressure ( $\Delta P$ ) for ideal cylindrical pores is given by Eq. 3.1 [6, 63].

$$\Delta P = \frac{2Y_L \cos\theta}{r_p} \quad (3.1)$$

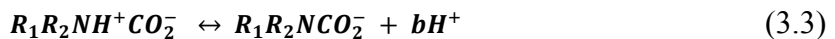
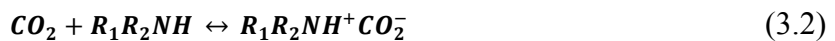
Here  $Y_L$  is the surface tension of the liquid,  $\theta$  is the contact angle between the liquid phase and the membrane, and  $r_p$  is the pore size radius. The key to long term non-wetting applications of gas-liquid membrane contactors is high break through pressure, where the operating pressures are lower than the break through pressure. From Eq. 3.1 it can be observed that high break through pressure can be achieved by using solvents with high surface tension ( $Y_L$ ), increasing the contact angle ( $\theta$ ) and reducing the pore size radius ( $r_p$ ). Liquid absorbents need to have good chemical compatibility with the membrane materials in order to keep the long-term stability of the system [6].

In order to eliminate pore wetting, it is proposed to use a membrane with a dense top layer. The major disadvantage is the introduction of an additional mass transfer resistance compared to the conventional microporous membranes [64].

### 3.3 Reaction of CO<sub>2</sub> with alkanolamines

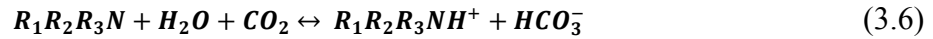
The most used liquids for acid gas treatments today are alkanolamine solvents which constitute of approximately 90% of all processes today [65]. The reaction of CO<sub>2</sub> with commercial alkanolamines such as monoethanolamine (MEA), diethanolamine (DEA) and N-methyldiethanolamine (MDEA) are presented in this section.

The reaction of MEA and DEA with dissolved CO<sub>2</sub> is described by the formation of zwitterions (Eq. 3.2). In the second step the zwitterion is deprotonated by a base to produce carbamate and a base as shown in Eq. 3.3 [65, 66]:



where  $R_1$  is an alkyl group,  $R_2$  is a H for MEA or an alkyl group for DEA,  $b$  denotes a base; H<sub>2</sub>O, OH<sup>-</sup> or amine. The contributions of H<sub>2</sub>O and OH<sup>-</sup> are often neglected in rate of CO<sub>2</sub>

reaction because their concentrations are much smaller compared to amine [66]. MDEA is a tertiary amine and undergoes a base-catalyzed hydration of CO<sub>2</sub>. The complete mechanism includes three reactions [67]:



## 3.4 Mass transfer in membrane contactors

The membrane structure is important to consider when it comes to mass transfer. This is because the structure has a significant influence on the mass transfer. Even though hollow fiber is the most common membrane module for industrial use, flat sheet membranes are often used for testing at laboratory scale because of the easier preparation method. In this section, simple mass transfer theory for both flat sheet and hollow fiber membranes are presented. The membranes that are considered in the next sections are all hydrophobic, leaving the pores gas filled when separating CO<sub>2</sub> gas from natural gas. The liquid absorbent is an amine. The mass transfer equations presented in this section are not further used in the report, but they are of great importance for the understanding of the process and the impact on the membrane properties.

### 3.4.1 Mass transfer in flat sheet membranes

In this section the mass transfer of microporous and microporous-dense composite membranes are considered. Schematic diagram of the two types of flat sheet membrane contactors are shown in Figure 3.3 a and b, respectively. The shape of the two profiles formed are caused by resistances due to the mass transfer when a component  $i$  (e.g.  $i=CO_2$ ) is transferred from the gas phase to the liquid phase [68].

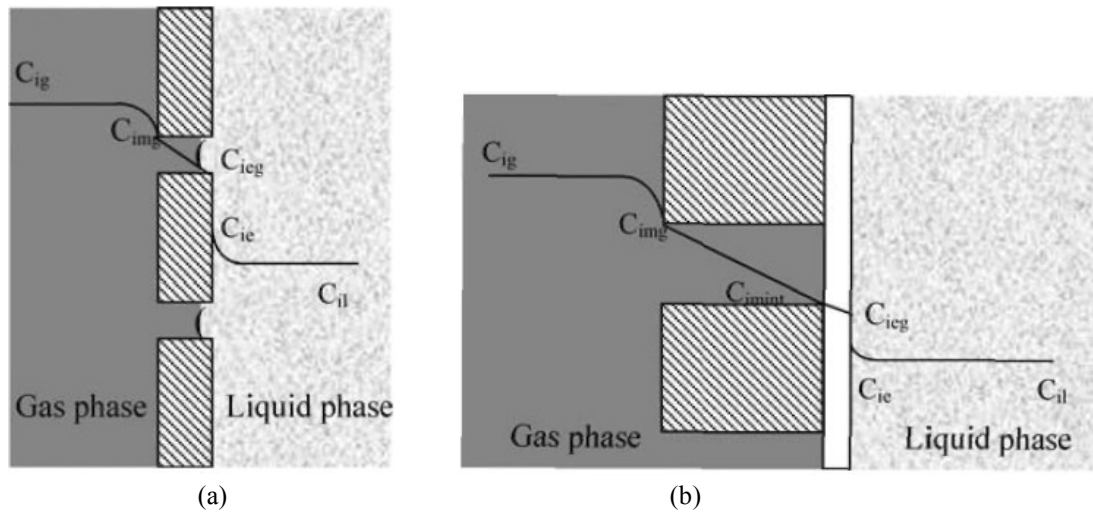


**Figure 3.3** Concentration profile of the species  $i$  when it moves from gas phase towards liquid phase through a) microporous hydrophobic flat sheet membrane, and b) microporous-dense composite membrane [68]

The mass transfer consists of three steps: (1) diffusion of a gaseous  $\text{CO}_2$  from the bulk gas phase to the outer surface of the membrane; (2) diffusion through the membrane pores to the gas-liquid interface; (3) dissolution into the liquid phase and then chemical reaction of  $\text{CO}_2$  and liquid. Thus, the overall mass transfer ( $1/K$ ) consists of three resistances in series which is given by the resistance-in-series-model. This means that the overall mass transfer coefficient can be related to the sum of the partial resistances in series in the gas ( $k_g$ ), membrane ( $k_M$ ) and liquid ( $k_L$ ) [61, 69]:

$$\frac{1}{K} = \frac{1}{k_g} + \frac{1}{k_M} + \frac{1}{mk_L} \quad (3.7)$$

This general equation is valid in a system with a non-wetted membrane. The variable  $m$  represents the distribution coefficient of  $\text{CO}_2$  between the gas and liquid phases. For chemical absorption;  $k_L = E \cdot k_L^\circ$ , where  $E$  is the enhancement factor due to chemical reaction and  $k_L^\circ$  is the physical mass transfer coefficient.

Referring to Figure 3.3a, at steady-state the flux of component  $i$  through the gas film is equal to the flux through the membrane and as well the flux in the liquid film. This can be expressed by following equation [68]:

$$J_i = k_{ig}(C_{ig} - C_{img}) = k_{im}(C_{img} - C_{ieg}) = k_{il}(C_{ie} - C_{il}) \quad (3.8)$$

where  $k_{ig}$ ,  $k_{im}$  and  $k_{il}$  are the mass transfer coefficient for component  $i$  in the gas phase, in the hydrophobic membrane, and in the liquid phase, respectively.  $C_{ig}$ ,  $C_{img}$ ,  $C_{ieg}$ ,  $C_{ie}$  and  $C_{il}$  are the concentration of component  $i$  in the gas phase, at the gas-membrane interface, at the gas-liquid interface, at the liquid-gas interface, and in the liquid phase, respectively.

In hydrophobic membranes used for gas-liquid transfer the species are transferred mainly by Knudsen flow. The expression for the membrane mass transfer coefficient is then:

$$k_{im} = \frac{D_{ig}^k \varepsilon}{\tau \delta} \quad (3.9)$$

with:

$$D_{ig}^k = \frac{2r_p}{3} \left( \frac{8RT}{\pi M_i} \right)^{0.5} \quad (3.10)$$

where  $D_{ig}^k$  is the Knudsen diffusion coefficient for component  $i$ ;  $\varepsilon$  is the membrane porosity;  $\tau$  is the membrane tortuosity;  $\delta$  is the membrane thickness;  $M_i$  is the molecular weight of component  $i$ ;  $r_p$  is the membrane pore radius;  $R$  is the gas constant and  $T$  is the temperature.

The principle of the flux is the same for microporous and microporous-dense composite flat sheet membranes. For the latter there is an additional resistance offered by the dense layer. Referring to Figure 3.3b, the gas has also to diffuse through the dense layer in addition to the gas film, membrane pores and the liquid film. The equality of flux at steady-state can be expressed as [68]:

$$J_i = k_{ig}(C_{ig} - C_{img}) = k_{im}(C_{img} - C_{im\ int}) = k_{im}^d(C_{im\ int} - C_{ieg}) = k_{il}(C_{ie} - C_{il}) \quad (3.11)$$

where  $C_{im\ int}$  is the concentration of component  $i$  at the microporous-dense interface and  $k_{im}^d$  is the mass transfer coefficient in the dense membrane for component  $i$ .

The mass transfer coefficient for the microporous-dense composite membrane is given as a function of the individual microporous and dense skin mass transfer coefficient:

$$\frac{1}{k_{im}^{md}} = \frac{1}{k_{im}} + \frac{1}{k_{im}^d} \quad (3.12)$$

where  $k_{im}^{md}$  is the microporous-dense composite mass transfer coefficient and  $k_{im}^d$  is the dense skin mass transfer coefficient. The dense skin mass transfer coefficient is dependent on the permeability of component  $i$ :

$$k_{im}^d = f(Pe_i) \quad (3.13)$$

To minimize the additional resistance caused by the dense layer, the membranes should have high CO<sub>2</sub> flux. The chemical reaction of CO<sub>2</sub> and amines in the liquid phase happens fast; therefore a highly permeable membrane material is needed [57]. Hydrophobic, high free volume polymers are being considered as good materials for gas-liquid membrane contactors [64]. Some of the polymers having high CO<sub>2</sub> permeability are mentioned in Chapter 2, where PTMSP is the polymer with the highest gas permeabilities.

### 3.4.2 Mass transfer in hollow fiber membranes

Hollow fiber is the configuration of membrane module which is the most used in the industry. Gas absorption into the liquid flowing through a hollow fiber membrane is described by the same model as in the previous section for flat sheet membranes; the resistance-in-series-model. The process consists of the same three steps: (1) transfer of gas from bulk gas phase to the membrane surface, (2) transfer through the membrane pores, and (3) transfer from the membrane-liquid interface to the bulk of the liquid. This process is shown in Figure 3.4.

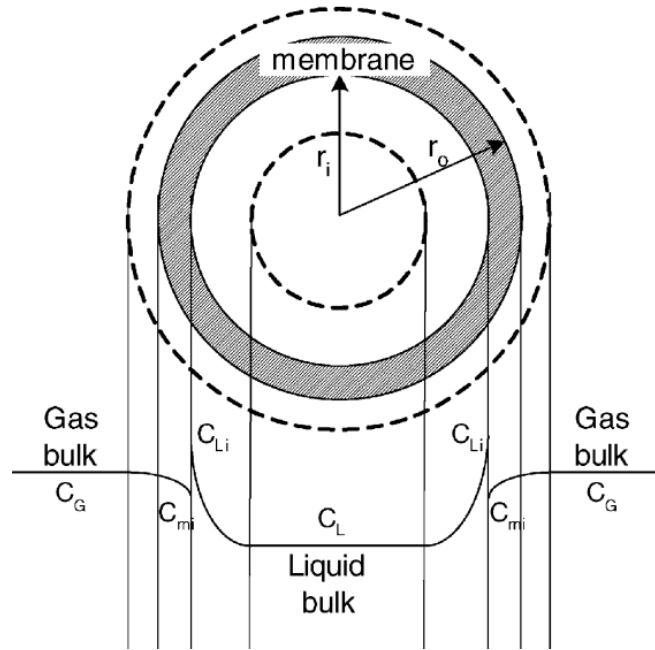


**Figure 3.4** Mass transfer/concentration process in a hydrophobic hollow fiber gas-liquid membrane contactor [70]

The total mass transfer coefficient ( $K_0$ ) can be expressed by a resistance in series model [6]:

$$\frac{1}{K_0} = \frac{m}{k_g d_0 / d_i} + \frac{m}{k_m d_{lm} / d_i} + \frac{1}{Ek_l} \quad (3.14)$$

### 3. GAS-LIQUID MEMBRANE CONTACTORS

---

where  $k_g$ ,  $k_m$  and  $k_l$  are the mass transfer coefficients of the gas phase, membrane and liquid phase, respectively;  $d_o$ ,  $d_i$  and  $d_{lm}$  are the outer, inner and log mean diameters, respectively;  $m$  is the distribution coefficient between gas and liquid phase and  $E$  is the enhancement factor due to chemical reaction.

To describe mass transfer for hollow fiber membranes, the two most commonly used hollow fiber geometries are the shell and tube configuration. The tube side mass transfer coefficient can be described by the L ev eque's equation [68]:

$$Sh = 1.62 \left( \frac{d^2 v}{LD} \right)^{0.33} \quad (3.15)$$

where  $v$  is the fluid velocity,  $d$  is the fiber diameter,  $L$  is the length of the fiber and  $D$  is the diffusion coefficient of the species into the fluid. For the shell side there is no general expression to describe the mass transport due to several factors like: maldistribution of flow, stagnant zones, splitting and demixing of streams, and channeling.

### 3.5 Advantages and disadvantages of membrane contactors

The membrane contactor has several advantages compared to the conventional gas absorption processes with packed towers [1, 5-7, 56]:

- The process is integrated into one piece of equipment, utilizing both the membrane separation and absorption qualities. The size and weight of this compact unit is smaller, making it attractive for offshore use.
- The contact surface area per unit contactor volume is high and constant (500-1500 m<sup>2</sup>/m<sup>3</sup>), resulting in an easier prediction of the membrane contactor performance and reduced footprint.
- The scale up of a membrane contactor process is usually linear by adding new membrane modules.
- The gas and the liquid flow operate on opposite sides of the membrane. It is therefore easy to achieve flexible operations without flooding, entrainment, channeling or foaming. There is also a reduction in solvent loss.
- There is no convective flow through the membrane pores and only diffusive transport can occur, something that makes membrane contactors less exposed to fouling.
- Economic advantages like lower investment and pumping costs.

There are also some disadvantages identified by using membrane contactors instead of conventional gas absorption processes [1, 6, 7, 56]:

- Another mass transfer resistance is added to the process from the membrane itself. This resistance can reduce the total mass transfer and lower the selectivity.
- Wetting of the membrane by the liquid will lead to a reduction in the mass transfer.
- There is a limitation in the break through pressure according to the Laplace equation (Eq. 3.1).
- Membranes are subjected to fouling, but this tends to be bigger problem for pressure driven processes than for concentration driven processes like membrane contactors.
- Shell side bypassing in membrane contactors result in a loss in efficiency. There are several designs developed to reduce this problem.
- The membranes will have to be replaced regularly due to their finite lifetime, resulting in replacement costs.

#### 3.6 Literature review of gas-liquid membrane contactors

In this section a review on membrane contactors for CO<sub>2</sub> capture is given with focus on the membrane materials used. As already mentioned several time, the gas-liquid membrane contactors are widely tested for separation processes, especially gas absorption, in order to replace the conventional absorption towers. The hollow fiber membrane contactor offers much higher contact area per unit volume. This is possible by using highly porous membrane structures. The most common membrane materials for CO<sub>2</sub> removal in such systems are polypropylene (PP), polyvinylidene fluoride (PVDF) and polytetrafluoroethylene (PTFE) [6]. Since the hydrophobicity of the membrane material is of great importance in this project work, a short review on the membrane liquid systems with PP, PVDF and PTFE are given.

Qi and Cussler [59, 60] were the first to develop the idea for the use of hollow fibers in gas-liquid membrane contactors. This was as an alternative for packed towers for removal of CO<sub>2</sub>. They used microporous hollow fibers of PP membranes in contact with sodium hydroxide (NaOH). Qi and Cussler developed a mass transport theory which was confirmed by their results, and compared the membrane contactor with the packed columns. Additional membrane resistance was confirmed. Mainly microporous hollow fiber membranes were used in following researches to avoid the mass transfer resistance [69].

One of the major concerns when selecting the liquid absorbents is the surface tension of the liquid. For gas membrane absorption processes, it is shown that the gas mass transfer is highest for non-wetting modes [69]. A study by Falk-Pedersen and Dannström [71] suggests the GORE-TEX® PTFE is the only material that is not wetted by alkanamines. Dindore et al. [72] selected some materials and put them in different adsorbents to investigate the compatibility. Only PTFE and PP membranes were compatible with some of the selected organic solvents. Rest of the membranes showed incompatibility with the solvents in terms of morphological damage, swelling, shrinkage, color change or dissolution.

An investigation of hollow fiber gas-liquid membrane contactors by Nishikawa et al. [73] has confirmed the stability of PTFE membranes. The membrane showed a stable performance over 660 hours due to high hydrophobicity and chemical stability. The volumetric mass transfer coefficient is found to be more than five times larger than the one of conventional packed tower.

A study of PTFE hollow fibers for high pressure applications in membrane contactors, was investigated by Marzouk et al. [74] for the first time. Experimental data of on CO<sub>2</sub> absorption in water, NaOH and amine were successfully obtained. The CO<sub>2</sub> removal of a gas mixture increased with increasing feed pressure (up to 50 bar) and concentration of the liquid. CO<sub>2</sub> absorption increase was in the order of NaOH > amine > water.

Rangwala [75] studied the CO<sub>2</sub> absorption in water, aqueous NaOH and aqueous diethanolamine (DEA) in gas absorption membranes, and received promising results. The mass transfer results for hollow fiber PP membranes were 3 to 9 times higher than for packed



columns. Wang et al. [76] used two types of PP microporous hollow fiber membranes, Celgard X-40-200 and Celgard X-50-215, to expose them to DEA and study the surface properties of the membranes. It was found that both of them suffered from changes in terms of morphology and surface roughness after being exposed to DEA. Another study by Yan et al. [77] showed that the absorption liquid of aqueous potassium glycinate, with high surface tension and thus lower wetting problem, showed better results than monoethanolamine (MEA) and methyl diethanolamine (MDEA). This was with regard to both wetting and reactivity towards CO<sub>2</sub>. Other studies of PP in MEA have shown that the PP fibers are very sensitive to only small variations in feed pressure, which result in performance loss. In addition, high liquid losses are observed for PP fibers at elevated temperatures [78].

Yeon et al. [79] used porous PVDF in a membrane contactor for removal of CO<sub>2</sub> from flue gas in absorbers like MEA and triethanolamine (TEA). The process showed a higher CO<sub>2</sub> removal efficiency than the conventional absorption tower. The CO<sub>2</sub> absorption rate per unit volume of the membrane contactor was 2.7 times higher than that of the packed column. Another study within the same research group [80], was the study of the absorption rate per surface area of CO<sub>2</sub> in PVDF and PTFE membranes in contact with MEA. PVDF showed the highest absorption rate.

One of the experiments which has been carried out in order to compare the three commercial membrane materials ( PTFE, PP and PVDF) for liquid-gas contactors is the experiment of Khaisri et al. [81]. CO<sub>2</sub> absorption in both physical and chemical solvents were investigated, and the performance was ranked as PTFE > PVDF > PP. PVDF is an alternative to PTFE. The stability of those two materials was tested continuously for 60 hours. PTFE maintained the absorption performance, while PVDF did loose performance. Franco et al. [82] studied the performance of PTFE, PP and PVDF microporous hollow fiber membranes in aqueous solutions of MEA. With respect to the CO<sub>2</sub> performance, the membranes were ranked in the order PTFE > PP > PVDF. Both wettability and performance test have shown that PVDF is not a proper material to be used with MEA. The capacity of PP drops over time.

PP, PVDF and PTFE have all some limitations in the performance in gas membrane absorption processes. Therefore, wide researches for development of new membrane materials for gas absorption processes are under exploration. Nguyen et al. [57] explored the possibility to design tailor made dense skin composite hollow fiber membranes for CO<sub>2</sub> absorption in amine solvents, in order to test the wetting phenomena. PTMSP and AF2400 were used as dense skin layers which were coated on PP hollow fibers. The performance of the permeability was tested before and after exposure to amines. The PTMSP performance was much lower than that of AF2400. The authors suspect an accelerated ageing during the drying phase of the coating process. AF2400 showed similar performance to the porous PP membrane. This demonstrates the proof of the study that added mass transfer resistance of thin dense layers is small enough.



## Chapter 4

# THE BACKGROUND OF THE MASTER THESIS

The membranes that are developed in this work are to be used in a membrane contactor with MDEA for the removal of CO<sub>2</sub> from natural gas. Even though gas-liquid membrane contactors offers several advantages as discussed in Chapter 3, there are some great challenges when it comes to the selection of the membrane material for the application. Because the membrane is exposed to a liquid up to several operational days, some undesirable effects due to the liquid contact may result in gradual changes in the membrane structure or partly wet the membrane. This might affect the mass transfer coefficient. To minimize this, a hydrophobic, dense, chemical stable polymer is needed. High permeability is also required in order to keep up the fast chemical reaction between CO<sub>2</sub> and the liquid [57].

PTMSP is the polymer used in this work. This is because the polymer achieve the highest permeabilities of all known synthetic membranes [31]. The desired membrane is the one minimizing the wetting problem and which have a minimal impact on the mass transfer coefficient. The solution is to make a thin dense skin of the hydrophobic PTMSP, coated on a microporous support [57]. The dense skin layer should prevent penetration of water into the membrane pores. Chemical and physical stability of PTMSP is improved by crosslinking the polymer with the bis azide BAA, and addition of inorganic TiO<sub>2</sub> nanofillers increase the permeability again after crosslinking.

This work is a continuation of my project from fall 2012, where SINTEF Materials and Chemistry developed a nanoparticle solution containing 15 nm TiO<sub>2</sub> nanoparticles which was used as membrane material together with PTMSP and BAA. The permeability results were not promising as the permeability decreased when the weight percent of nanoparticles increased, filling/blocking the free volume of PTMSP [83]. Merkel et al. [53] investigated how the nanoparticle size affect the gas permeability. His research team tested the permeability of PMP with different particle diameters of fumed silica (FS). The permeability was presented as a function of the primary particle diameter (nm), where the permeability decreased as the particle diameter increased. In this work, commercial TiO<sub>2</sub> nanoparticles which were used by Lei Shao [42] are tested since they showed the wanted permeability trend as the nanoparticle content increased.

As stated in Chapter 2.1.2, Matteuci et al. [44] revealed that individually dispersed 3 nm sized TiO<sub>2</sub> nanoparticles in PTMSP showed a decrease in permeability at low particle loadings. At

approximately 7 vol. % of nanoparticles the permeability was at the lowest and began to increase as the particle loading further increased. New attempts from SINTEF Materials and Chemistry have been made to develop more nanoparticle solutions containing larger nanoparticle sizes: 15-400 nm and  $>1 \mu\text{m}$ . The Ph.D. student Karen Nessler Seglem is working with those solutions. In this work, commercial nanoparticles have been used with a diameter of 21 nm, appearing in clusters with sizes of 1-3  $\mu\text{m}$ . The nanoclusters are introduced by the producer on purpose by covalently binding the nanoparticles. As the particles used by Shao showed the wanted results, these were further explored through this work to be used as comparison for the particles developed by SINTEF Materials and Chemistry.

# Chapter 5

## MATERIALS

### 5.1 Polymer

The polymer used in this study is the high free volume poly(1-trimethylsilyl-1-propyne) (PTMSP), which is purchased from Gelest (Lot.: 4A-22048). The structure of PTMSP is shown in Figure 5.1.

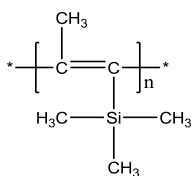


**Figure 5.1** Chemical structure of poly(1-trimethylsilyl-1-propyne) (PTMSP)

### 5.2 Crosslinking Agent

The gas permeability of PTMSP decreases dramatically with time [34]. Since PTMSP undergoes physical aging over time, a crosslinking agent needs to be added to the polymer to increase the chemical stability as indicated in Chapter 2.1.1. As crosslinking agent for PTMSP, the bis(aryl azide): 4,4-diazidobenzophenone (BAA) is used (Figure 5.2). This crosslinking agent is synthesized in the laboratory by others.

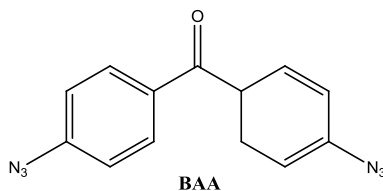


**Figure 5.2** Chemical structure of 4,4-diazidobenzophenone azide (BAA)

### 5.3 Nanoparticles

Titanium dioxide (Aeroxide® TiO<sub>2</sub> T 805, Evonik-Degussa, Germany) nanoparticles used in this study are kindly provided by Grolman Nordic AS. The nanoparticle size is 21 nm, but they are delivered as covalently bounded aggregates in the range of 100-250nm. The BET specific surface area is 45±10 m<sup>2</sup>/g. SINTEF Material and Chemistry have measured the particle size to 1-3 μm.

### 5.4 Gases

The gases used in the gas permeability tests were N<sub>2</sub>, CH<sub>4</sub> and CO<sub>2</sub>, all provided by Yara.

### 5.5 Other chemicals

Toluene (Lot.: STBB3628) with a purity of 99.8 %, is purchased from Sigma-Aldrich and used as the solvent in the experimental work. The amine used in membrane contactor tests is N-methyldiethanolamine (Lot.: MKBF6506V) with a purity of ≥99 %, purchased from Sigma-Aldrich.

# Chapter 6

## EXPERIMENTAL METHODS

### 6.1 Design Of Experiments (DOE)

In this work it is interesting to find an optimal membrane composition which examines different membrane properties such as permeability, contact angle and viscosity. The polymer (PTMSP) concentration is 2wt% according to the solvent throughout the experimental work. The composition of nanoparticles (TiO<sub>2</sub>) varies from 0 to 20wt% and the composition of the crosslinker (BAA) varies from 0 to 3wt% according to PTMSP. This setup gives many different combinations because of all the possible parameter variations. In order to test all these membranes for gas permeability, viscosity measurements and contact angle measurements, it was constructed a selected set of experiments, in which all relevant factors were varied simultaneously. This is called statistical experimental design, or, Design Of Experiments (DOE).

DOE is a useful tool in any design project when variations are present. In this case, the selected factors are the variations in weight percentages of BAA crosslinker and TiO<sub>2</sub> nanoparticles, and the feed pressure during the gas permeability measurements. The program that was used for DOE is MODDE 9.1, where screening is selected as the objective and a 2<sup>4</sup> full factorial design is used. Table 6.1 shows the factors that were defined in the software, Table 6.2 shows the response in DOE which is not any further analyzed, and

Table 6.3 shows the membranes to be synthesized. The focus of DOE in this project is to do the experimental design, not to fit the values in the software.

**Table 6.1** Factors defined in DOE

Name	Abbr	Units	Type	Use	Settings
wt%nanoparticle	nano	%	Quantitative	Controll	0 to 20
wt%crosslinker	cross	%	Quantitative	Controll	0 to 3
Pressure	P	Bar	Quantitative	Controll	2 to 6

**Table 6.2** Response in DOE

Name	Abbr	Units
Permeability N2	PN2	Barrer
Permeability	PCH4	Barrer
Permeability	PCO2	Barrer
Contact angle	CA	Degrees
Viscosity	Visc	Ns/m <sup>2</sup>

**Table 6.3** Membranes to be synthesized

Experimental Number	Experimental Name	Run Order	Incl/Excl	Nanoparticles [wt%]	Crosslinker [wt%]	Pressure [bar]
1	N1	3	Incl	0	0	2
2	N2	6	Incl	20	0	2
3	N3	4	Incl	0	3	2
4	N4	8	Incl	20	3	2
5	N5	5	Incl	0	0	6
6	N6	2	Incl	20	0	6
7	N7	11	Incl	0	3	6
8	N8	7	Incl	20	3	6
9	N9	1	Incl	10	1.5	4
10	N10	10	Incl	10	1.5	4
11	N11	9	Incl	10	1.5	4

In order to achieve an overall understanding of the membrane properties, some additional membranes outside DOE were synthesized. A list of all membrane compositions used in the work are given in Table 6.4. All membranes are casted from toluene solutions containing 2wt% PTMSP. Further in the report, the membrane will be referred to as PTMSP and not 2wt% PTMSP.

**Table 6.4** Membranes synthesized in the laboratory. The wt% of PTMSP is given according to toluene, and the wt% of BAA and TiO<sub>2</sub> are given according to PTMSP

Membrane composition		
wt% PTMSP	wt% BAA	wt% TiO <sub>2</sub>
2	None	None
2	1.5	None
2	2.0	None
2	3.0	None
2	None	20.0
2	1.5	10.0
2	2.0	20.0
2	3.0	20.0



## 6.2 Membrane preparation

### 6.2.1 Preparation of polymer solutions

PTMSP, BAA and TiO<sub>2</sub> nanoparticles were dissolved in toluene to make homogenous solutions at different weight percentages. The polymer concentrations was 2wt%, the crosslinker concentrations varied from 0 to 3wt % and the nanoparticle concentrations varied from 0 to 20wt%. All solutions were put on an automatic rotator for 24 hours to get a homogenous solution. Before the solution was casted on Teflon plate, ultrasonic cavitation was used in solutions containing nanoparticles at intensity of 6-7 ampere for 3 minutes to disperse the nano-sized particles in the solution.

### 6.2.2 Membrane casting

Polymer solution was poured on a Teflon plate and covered with a funnel to allow slow and constant solvent evaporation. The casted membranes were dried in a fume cupboard at room temperature for 7 days. The membranes were then placed in a vacuum oven for 24 hours to evaporate the residual solvent. All membranes containing BAA were crosslinked by heating the membranes in vacuum for 90 minutes at 180 °C.

### 6.2.3 Amine treated membranes

Membranes consisting of pure PTMSP and crosslinked PTMSP with 3wt% BAA were put in MDEA solutions for 1 day, 1-, 2-, 3-, 4-, 6-, 8- and 10 weeks. The membranes were placed in 100ml beaker with 10 ml of distilled water (which is used as reference), 2M MDEA and 4.2M MDEA, and covered with a plastic film. The chosen MDEA concentrations were elected on the basis of the modeling work of Karl Anders Hoff [84], who has used 2M and 4.2M MDEA in his study of CO<sub>2</sub> absorption in a membrane contactor. His work is not further considered in this report.

After the desired stay in the solutions, the membranes were washed with distilled water for 1 day, air dried for 2 days and vacuum dried for 1 day. Crosslinked nanofilled PTMSP membranes with 2wt% BAA and 20wt% TiO<sub>2</sub> nanoparticles were also placed in distilled water, 2M MDEA and 4.2M MDEA, but for 2 and 4 weeks.

## 6.3 Characterization techniques

### 6.3.1 Fourier Transform Infrared Spectroscopy (FT-IR)

Fourier Transform Infrared Spectroscopy (FT-IR) is a chemical analytical technique, which detects vibration characteristics of functional groups in order to characterize or identify the molecules. When the IR radiation pass through a sample, some of the radiation will absorb by the sample and some will pass through (be transmitted). FT-IR measures the intensity versus the wavelength or the wavenumber of light [48, 85].

The IR radiation is normally split into two beams, one with a fixed length and the other with a variable length. The different distances between the two pathlengths result in variations in intensities: an interferogram. Fourier transformation converts this interferogram into one spectral point of the more familiar form of the frequency domain [86]. A normal instrumental process is shown in Figure 6.1 [85]. Membranes in this work were tested on a Thermo Nicolet.

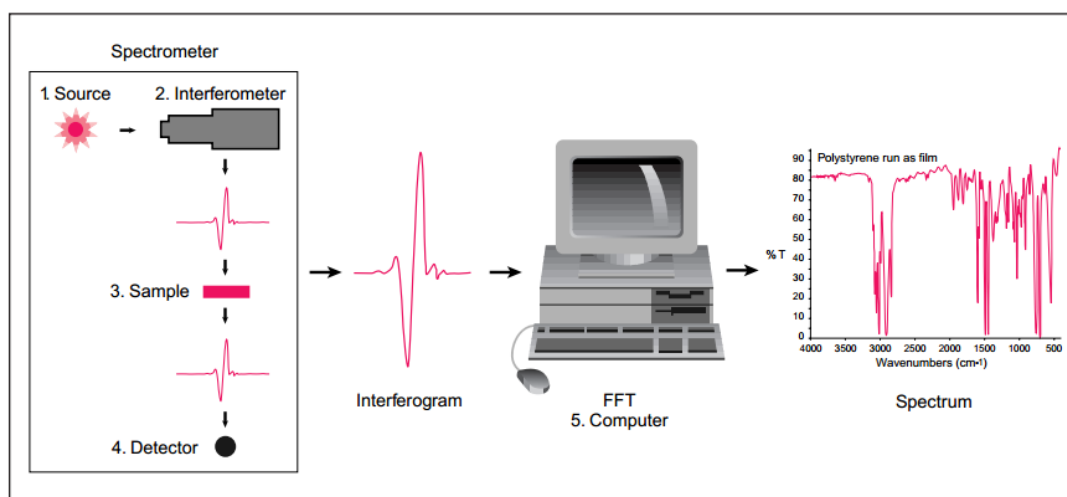


**Figure 6.1** Instrumental process of FT-IR spectrometry [85]

### 6.3.2 Contact Angle Measurements

The contact angles between membrane and water were measured by Theta Lite Optical Tensiometer, delivered by Biolin Scientific (Figure 6.2). The software, OneAttention, was used for the Young-Laplace equation to fit the water-drop profile.



Figure 6.2 Optical tensiometer used to measure contact angle [87]

The contact angle,  $\theta$ , is a measure of the wetting on the membrane by water. The contact angle is predicted in terms of the interfacial free energies between three phases: solid, liquid and gas. The contact angle is the angle between the solid and the tangent to the drop at the three phase intersection as indicated in Figure 6.3.

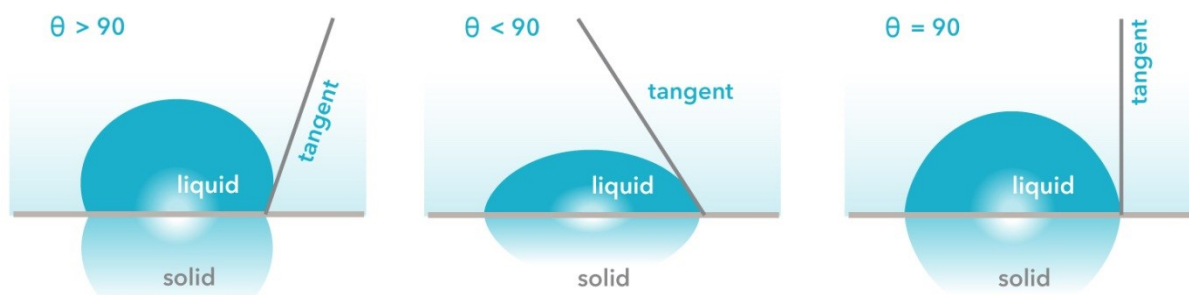


Figure 6.3 Contact angles for different drop shapes on a solid surface [88]

The balance can be described by the Young equation:

$$\cos(\theta) = \frac{Y_{SG} - Y_{SL}}{Y_{LG}} \quad (6.1)$$

where  $\gamma_{SG}$ ,  $\gamma_{SL}$  and  $\gamma_{LG}$  is the surface tension between solid-gas, solid-liquid and liquid-gas respectively. Values below  $90^\circ$  indicate that the liquid wets the surface, while values above  $90^\circ$  indicate poor wetting [88, 89].

The local operation manual for the apparatus was used when doing the contact angle measurements. The software OneAttention was opened and the sessile drop method was selected. A calibration ball was placed on a magnetic holder on the sample stage. The ball was brought into the image on the screen and zoomed appropriately by adjusting the zoom lens. When the calibration ball was in the center and focused, “calibration” was pressed.

Experimental parameters were set, and the calibration ball was replaced by a membrane. A manual dispenser was used to place a water drop on the membrane surface. When the drop touched the surface, the recording was started and measured for 10 minutes. Several pictures were taken. Only the last one, after 10 minutes, was used as the result.

Curve fitting and the data analysis were done after the images have been taken. An appropriate baseline, which denotes the level of the solid surfaces, was selected manually for the contact angle measurements.

### 6.3.3 Viscosity Measurements

The viscosity of the polymer solutions was measured by a rheometer (Rheometer Physica MCR 100) at room temperature ( $21^\circ\text{C}$ ). The rheometer is a high precision apparatus, controlled directly from the US 200 software. The measuring system DG 26.7 and the measuring cell TEK 150PC were used. The local operation manual for the apparatus from the lab was followed when doing the measurements.

The upper part of the rheometer was moved to the lifting position (Figure 6.4a), and a white protection cylinder from the measuring system was removed by rotation. The measuring system was taken out from the box, consisting of two cylinders (Figure 6.4b). The bottom cylinder was placed in a hole at the bottom of the apparatus and filled with 4 ml of the polymer solution. The upper cylinder was coupled to the motor (Figure 6.4c). When the apparatus was set, the “meas position” button was pressed so that the upper part of the rheometer moved to the measuring position. The “NF Reset” -button reset the normal force to zero and the Pelitier water was turned on.

## 6. EXPERIMENTAL METHODS

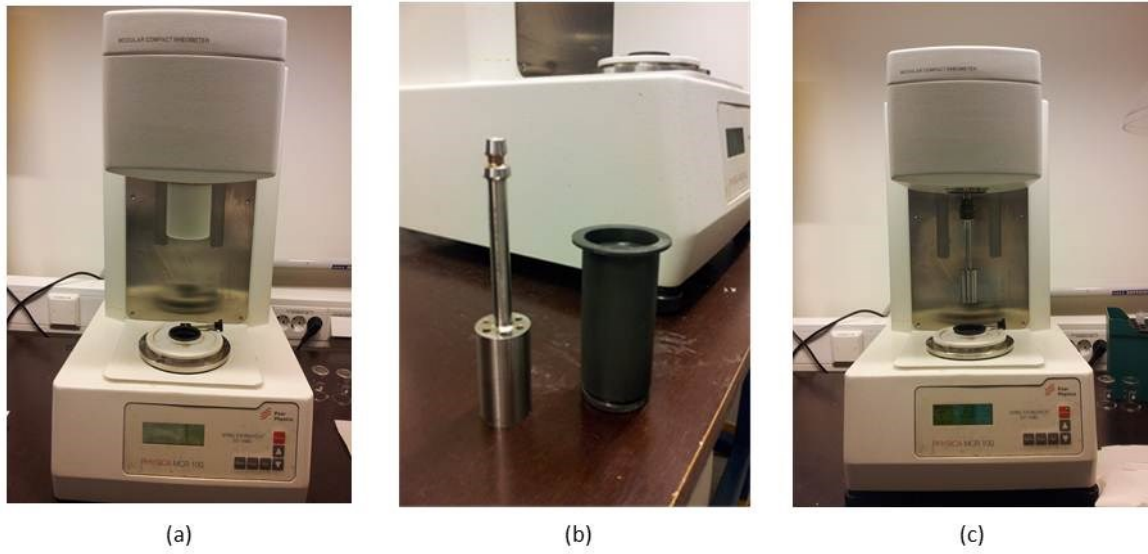


**Figure 6.4** Rheometer at (a) lifted position (b) a picture of the upper and bottom cylinder, respectively, and (c) rheometer ready to do measurements

The viscosity is measured by positioning the cylinders concentrically and filling the gap between them with a fluid. By rotating the inner cylinder in different velocities, shear stress in the liquid is generated at different shear rates. For Newtonian fluids, the graph of shear rate against the shear stress is a line. The slope gives the viscosity. The measurements were taken at shear rates from 100 to 1000 1/s. For Newtonian fluids, the viscosity has a constant value and the two curves in Figure 6.5 overlap.

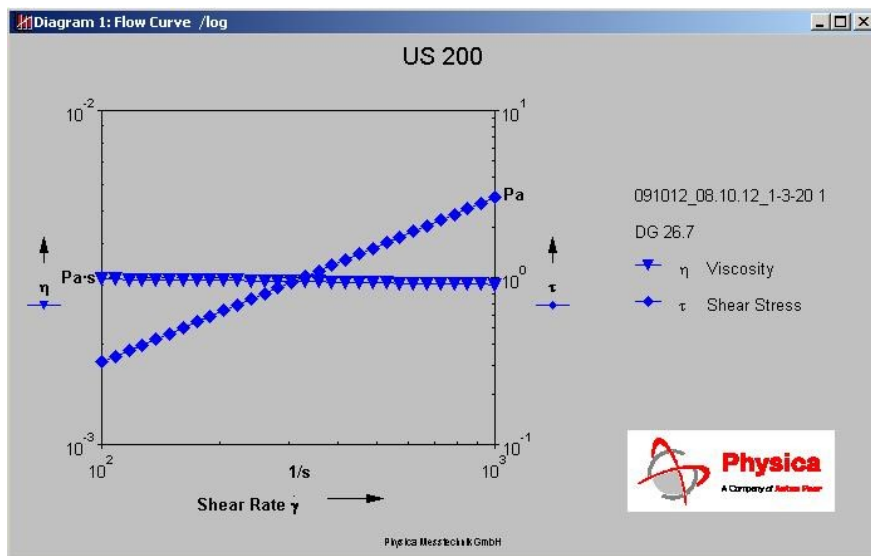


**Figure 6.5** Viscosity and shear stress measurements from the software US 200

## 6. EXPERIMENTAL METHODS

The data series were analyzed by setting the data to be evaluated as Newtonian fluid. The viscosity was calculated for 30 points data series by fitting a line with zero intercept to the data ( $y=ax$ ). The fitted parameter is the viscosity of the tested fluid for the current temperature.

When finishing the measurements for one solution, the apparatus had to be cleaned. The upper part of the rheometer was moved to the lifting position. The upper cylinder was removed first and then the bottom cylinder. The tested polymer solution was disposed. The cylinders were carefully washed first in toluene, then with water and distilled water. The parts were dried by using soft cloth to avoid scratches. The cylinders were put back to its box, and the white protection cylinder was attached to the rheometer.

### 6.3.4 Gas Permeability Measurements

The gas permeability measurements were performed in two different single chamber apparatuses as shown in Figure 6.6 and Figure 6.7. The procedure is described only for Figure 6.6, but the principles are the same for both. The local operation manual for the apparatus was followed when doing the gas permeability measurements. Permeability for three gases was tested in the following order:  $N_2$ ,  $CH_4$  and  $CO_2$ , to avoid possible effects on the membrane.  $N_2$  and  $CH_4$  are considered to be non-interacting gases, while  $CO_2$  may show some interaction [7]. Each gas was tested at 2, 4 and 6 bar.

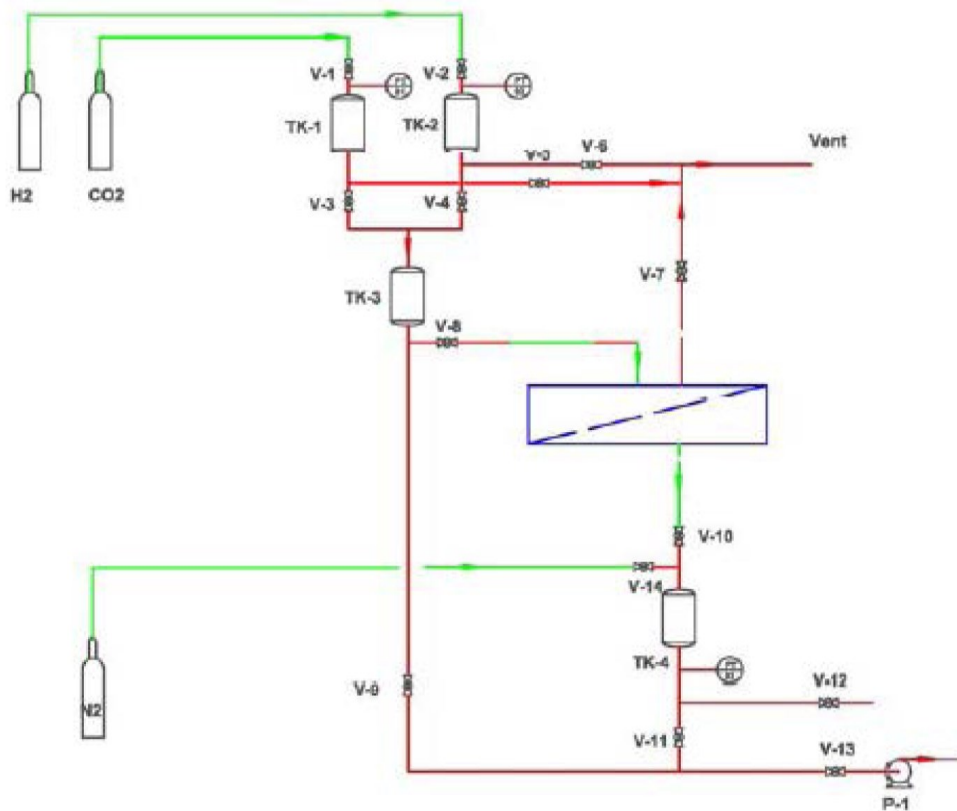


**Figure 6.6** Flowchart of the single gas permeation setup used in the experiment

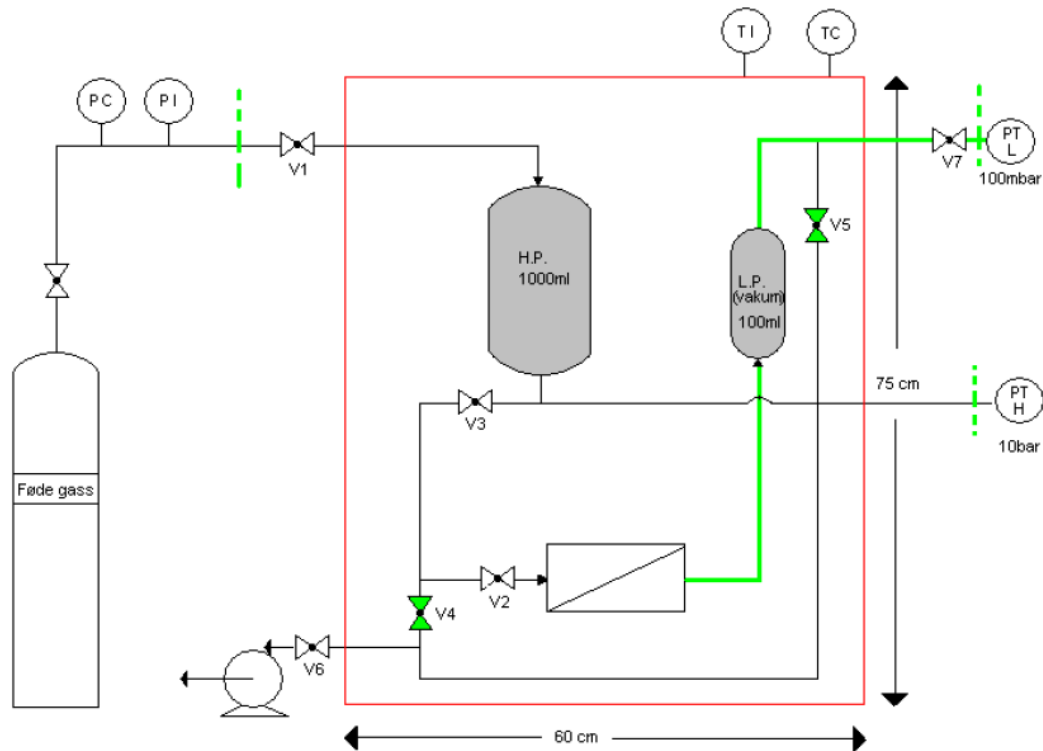


**Figure 6.7** Flowchart of a single gas permeation setup

The first step was to mount the membrane inside the module. This was done stepwise as shown in Figure 6.8. The membrane was masked with aluminum tape on both sides leaving a membrane cross sectional area of  $1.54 \text{ cm}^2$ . The masked membrane was then placed on a metal sinter on the bottom part of the module. The metal sinter is a protection for the membrane. A wider tape was put on top of the masked membrane to prevent gas leakage from feed side to permeate side. Two O-rings (one at the upper and one at the bottom part of the module) sealed the membrane module when the upper part and the bottom part were put together. The module was then connected to the gas permeation system.



**Figure 6.8** Mounting of membrane in the module: (a) the support for the membrane with a metal sinter in the middle, (b) the membrane is masked with aluminum tape on both sides and put on the metal sinter, (c) the masked membrane is glued to the test cell with aluminum tape, and (d) the top and the bottom of the module are put together

## 6. EXPERIMENTAL METHODS

The next step was to evacuate the system by closing all valves except V4, V9, and V13, and opening the vacuum pump. The LabView program file was opened. After two minutes valve V11 and V10 were slowly opened and the Low pressure sensor showed decrease in pressure. Valve V8 was also slowly opened and the High pressure sensor showed decrease in pressure. The system was left like this overnight to achieve vacuum.

A leak test was performed by closing valve V8 and V11, and the vacuum pump for some minutes to see if there was an increase in pressure (leakage). After the leak test, valve V9 and V13 were closed as well, and the vacuum pump was turned off. The gas was brought into the high pressure storage by opening V2, while the permeate side was kept at vacuum. When the pressure at the feed side was adjusted to the desired value, valve V2 was closed. The file was saved, which means that the logging in LabView ® started. Valve V8 was slowly opened to let the gas go through the membrane. The pressure rise was measured by a MKS Baraton® 0-100mbar pressure transducer. The system was left for 2-5 minutes. The permeate pressure transducer was logged in LabView ®. The plot of  $dp/dt$  was calculated by linear regression in Microsoft Excel. The gas permeability is based on the constant variable/volume pressure method and is given by [48]

$$P = \frac{l}{A T p_0} \frac{V T_0}{(p_1 - p_2)} \frac{dp}{dt} \quad (6.2)$$

where  $P$  is the gas permeability ( $1 \text{ Barrer} = 27.4 \cdot 10^{-10} \text{ m}^3(\text{STP})\text{m}\cdot\text{m}^{-2}\text{h}^{-1}\text{bar}^{-1}$ ),  $l$  is the film thickness ( $\mu\text{m}$ ),  $A$  is the membrane area ( $\text{cm}^2$ ),  $V$  is the volume in the chamber ( $\text{cm}^3$ ),  $T_0 = 273.15 \text{ K}$  is the standard temperature,  $T$  is the gas temperature (K),  $p_0 = 1.0133 \text{ bar}$  is the standard pressure,  $p_1$  and  $p_2$  are the feed and permeate pressure (mbar), respectively, and  $dp/dt$  is the steady state pressure change (bar/s). The membrane thickness was measured by a Digitrix II Disc Micrometer as shown in Figure 6.9. The thickness of the membrane was measured at five places on the surface and the mean value was used.



**Figure 6.9** Digitrix II Disc Micrometer used to measure the membrane thickness



### 6.3.5 Thermogravimetric analysis (TGA)

Thermogravimetric analysis (TGA), TGA Q-500<sup>®</sup> (Figure 6.10), was used to measure changes in the physic-chemical properties of the membranes at elevated temperatures as a function of increasing temperature [90]. The change in mass weight percent was measured as a function of increasing temperature. Local operation manual was used for the TGA instrument.



**Figure 6.10** TGA Q-500 used in the laboratory

Purge N<sub>2</sub> gas flow was switched on at 1.1-1.4 bar. An alumina pan was used in a platinum basket for all the sample runs. The sample holder was tare from the software. The sample was loaded with 5-10mg of the membrane. In the software, the balance purge flow and the sample purge flow was set to 10 and 90 mL/min, respectively. The running segment description was set to ramp 5 °C/min to 600 °C. The start button was pressed. When the test was completed, the sample was unloaded and the basket was cleaned. The results were analyzed in the software Universal Analysis.

### 6.3.6 Differential Scanning Calorimeter DSC

Differential Scanning Calorimeter (DSC) is a thermal analyzer which measures the energy change when sample is heated, cooled or held isothermally, as a function of the temperature. From the detected energy changes it is possible to find different temperature transitions of the material which occur during the heating. The transitions are melting temperatures, glass transitions and more complex events [91]. Local operational manual was used for DSC Q-100<sup>®</sup> instrument.

The RCS system and purge N<sub>2</sub> gas was turned on at 1.1-1.4 bar. Alumina pans were loaded with 5-10 mg of sample and covered with a lid. The sample pan and a reference pan was loaded in

to the cell. The software wizard was used to set the parameters. The flow rate was set to 50 mL/min and the sample was ramped 10 °C/min to 350 °C. The start button was pressed. The sample was unloaded and thrown away when the measurements were completed. The results were analyzed in the software Universal Analysis.

### 6.3.7 Microscope

A binocular microscope ZEISS Axio Lab.A1® was used to look at the membrane surfaces. An Infinity 60 N-C camera was connected to the microscope, making it possible to take pictures in the software Deltapix Camera. Transmitted light was sent through an objective “A-plan” 40x0.25 Ph. Transmitted light polarization was used at low angles to get clear pictures.

### 6.3.8 Uncertainty analysis

Standard deviation (s) was used to find how much variation exists from the average (mean) value ( $\bar{X}$ ). Eq. 6.3 shows how to determine the mean value.  $x_i$  represents the data sets and n the number of experiments. The standard deviation is found by taking the square root of the average of the squared differences of the values from their average value Eq. 6.4 [92].

$$\bar{X} = \sum_{i=1}^n \frac{x_i}{n} \quad (6.3)$$

$$s = \sqrt{\frac{1}{n} \sum_{i=1}^n (x_i - \bar{x})^2} \quad (6.4)$$

## Chapter 7

# RESULTS AND DISCUSSION

### 7.1 Polymer solutions and membranes

There were eight different polymer solutions, and thus membrane compositions, prepared for the experimental work. All solutions contained 2 wt% PTMSP in toluene, where different weight percentages of BAA and TiO<sub>2</sub> nanoparticles were put into the solutions. The solutions were casted on a porous Teflon support, with an approximate membrane thickness of 30-40 μm. This thickness is the half of the size from the experiments carried out the fall 2012. Thinner membranes were prepared due to reduced membrane resistance and because basically, the membranes are to be used as a thin coating on a support. Pictures of some of the membranes containing maximum weight percentages of BAA (3 wt%) and TiO<sub>2</sub> (20 wt%) in this experimental work, are given in the figure below.



**Figure 7.1** Photograph of membranes containing PTMSP. Membrane from left: pure PTMSP, 3wt% BAA, 20wt% TiO<sub>2</sub> nanoparticles, and 3wt% BAA + 20wt% TiO<sub>2</sub> nanoparticles in the last one to right.

It can be observed that the membranes made of pure PTMSP are transparent as well as membranes containing an addition of 3wt% BAA. Addition of 20wt% TiO<sub>2</sub> nanoparticles (the two membranes to the right in Figure 7.1), gives less transparent membranes.

### 7.1.1 Viscosity of the polymer solutions

The viscosity of the polymer solutions made for DOE were measured as a function of the share rate (Figure 7.2). The three solutions that have achieved the highest viscosities are the solutions containing nanoparticles.

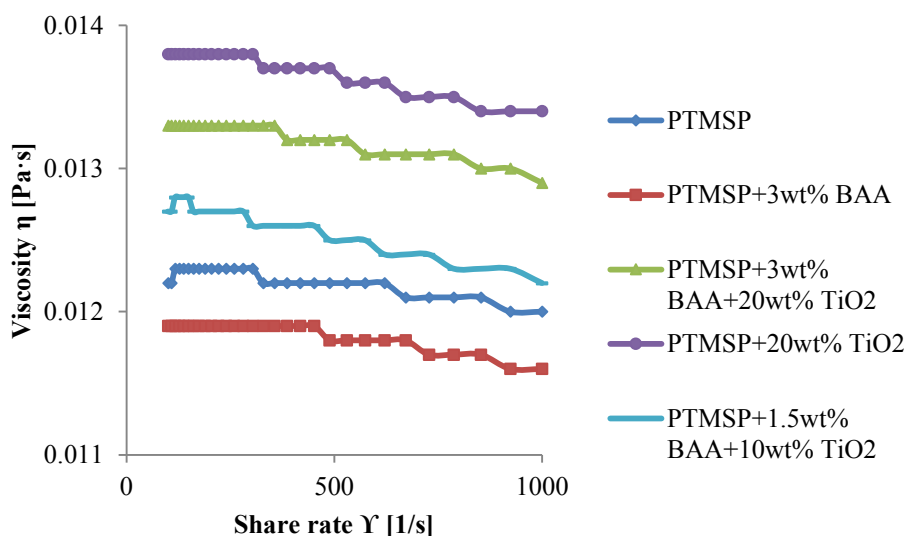


Figure 7.2 Viscosity of some polymer solutions

The most viscous polymer solution contains PTMSP with 20wt% TiO<sub>2</sub>, and achieves the highest permeabilities (presented in Chapter 7.3.6) of all membranes prepared for this work. The viscous solution require less drying time when casted into a membranes, making the chain packing very loose and inefficient. These membranes result in higher free volume and thus high gas permeability. Referring to the project work from fall 2012 [83], membranes casted from toluene with 1 and 5wt% PTMSP showed large difference in viscosity and thus permeability. Permeabilities of membranes containing 5wt% PTMSP were much higher than for those with 1wt% PTMSP, even though the polymer mass was the same when casted. The drying time is an important factor due to longer and thus denser packing for 1wt% PTMSP, resulting in less free volume and lower gas permeability.

All polymer solutions containing BAA, have been crosslinked after membrane casting. This means that they do not follow the same trend as the most viscous polymer solution which was not crosslinked. The chemistry and the chain packing become more complex.

### 7.1.2 FT-IR spectroscopy of pure PTMSP

In order to confirm the PTMSP structure, FT-IR spectroscopy was used. Figure 7.3 shows the FT-IR spectra of PTMSP casted from a toluene solution containing 2wt% PTMSP. The polymer exhibits an absorption band at  $1557\text{ cm}^{-1}$ , which is in the region of C=C stretching. Other absorption bands are exhibited at  $1243\text{ cm}^{-1}$  and  $829\text{ cm}^{-1}$  which are assignable to SiC-H and C-Si stretching, respectively. The two peaks in the area of  $2900\text{--}3000\text{ cm}^{-1}$  indicate methyl groups and C-H stretching [31, 86].

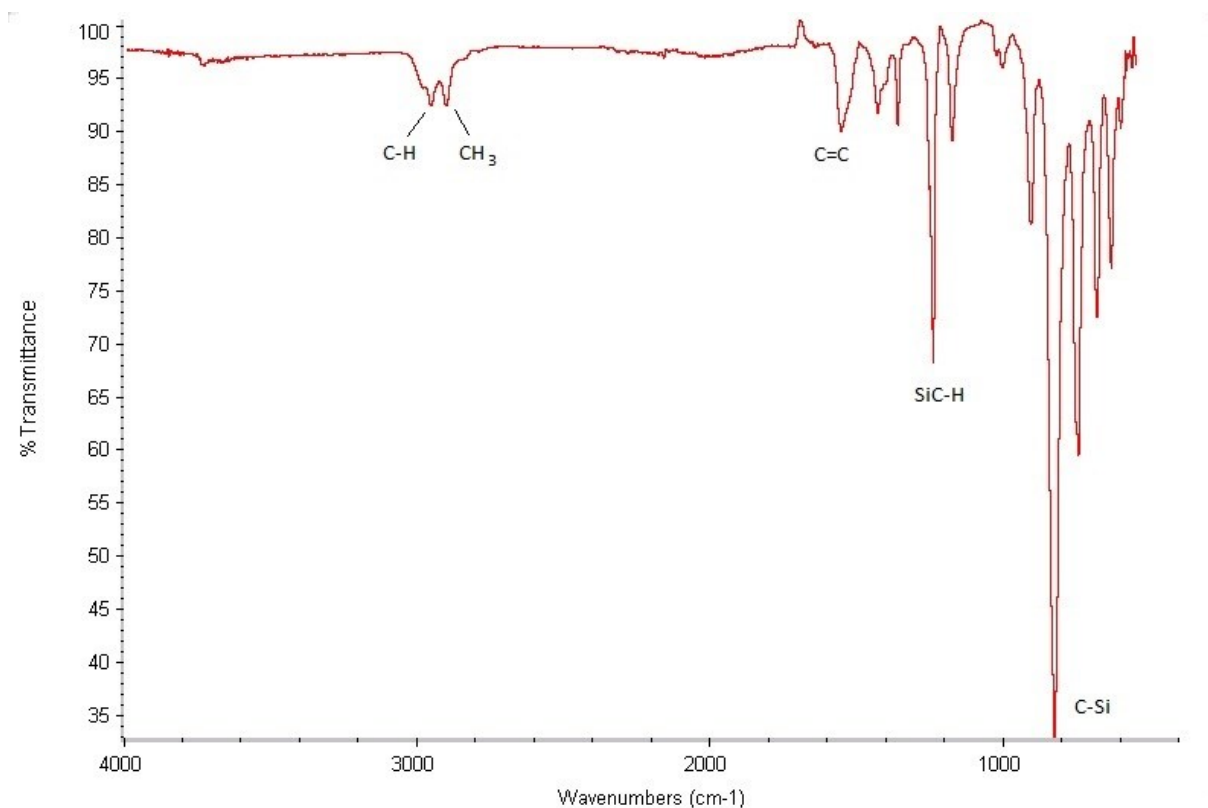


Figure 7.3 FT-IR spectra of pure PTMSP

### 7.1.3 FT-IR spectroscopy of crosslinked PTMSP

Crosslinking makes PTMSP insoluble in solvents that normally dissolve the uncrosslinked polymer. In this experiment, 1.5wt%, 2wt% and 3wt% bis azide BAA was dissolved in a PTMSP solution before casting. The casted and vacuum dried membrane were easily dissolved in toluene before crosslinking, and after thermal crosslinking the membranes containing 1.5- and 2wt% BAA were still soluble in toluene while membranes containing 3wt% BAA were insoluble in toluene. From the literature, crosslinked PTMSP with BAA have shown that the membrane is insoluble in toluene when the bis(azide) crosslinker 3,3'-diazidodiphenylsulfone concentration is above 2.4wt% [47].

In order to see if crosslinking has happened, FT-IR spectroscopy was used to identify the components in the sample. A FT-IR spectra is given in Figure 7.4 for a membrane before

## 7. RESULTS AND DISCUSSION

crosslinking and after crosslinking. This membrane was casted from a toluene solution containing 2wt% PTMSP with 3wt% BAA. FT-IR spectrums of other membranes prepared in this experiment are attached in Appendix A.

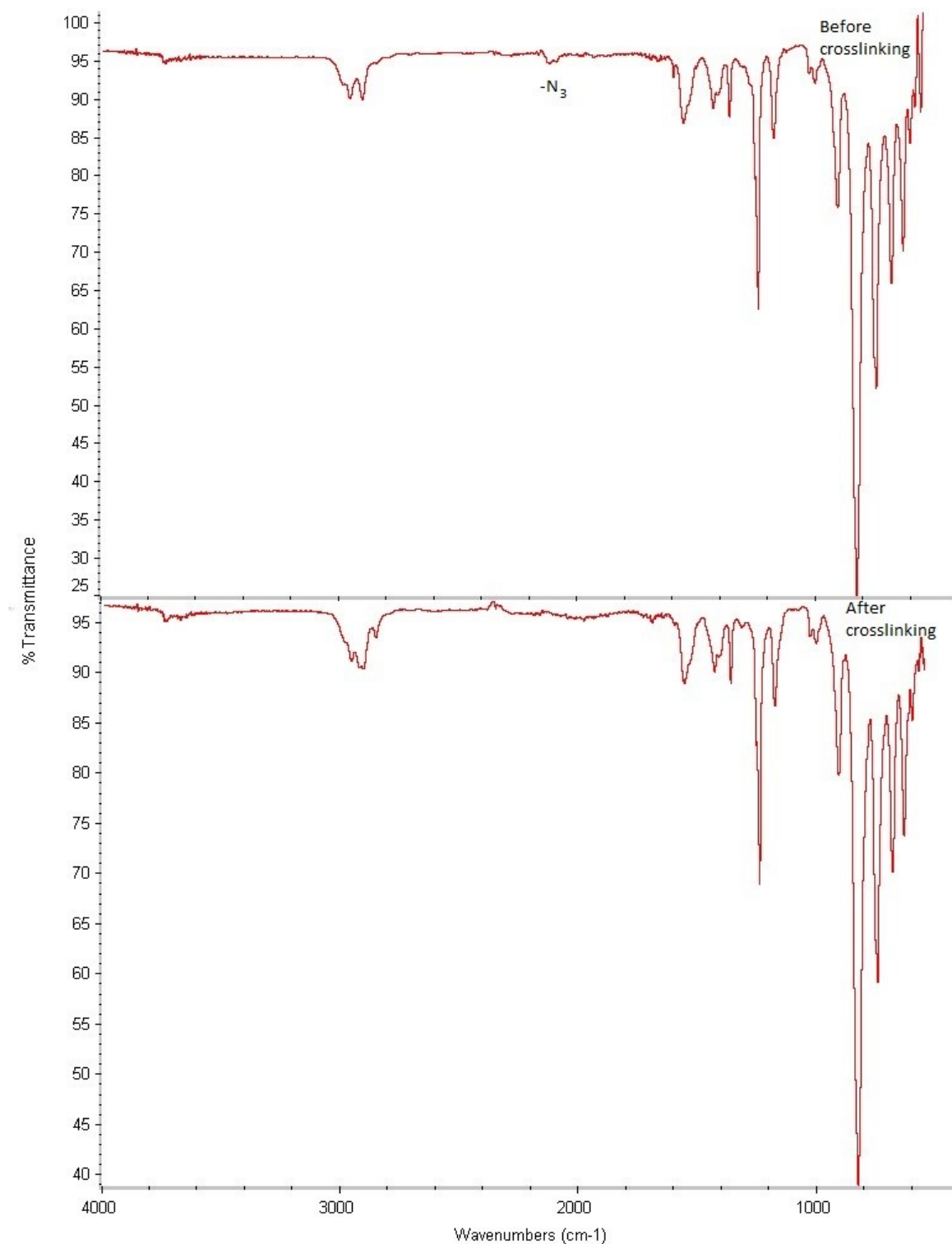


**Figure 7.4** FT-IR spectra of PTMSP with 3wt% BAA before and after crosslinking

The main difference which can be observed from the two FT-IR spectra is that the intensity of the peak at a wavelength of  $2122\text{ cm}^{-1}$ , the azide group ( $\text{N}_3^-$ ) of BAA, decrease during crosslinking. This indicate conversion of the bis(azide) crosslinker to a reactive bis(nitrene) when heating the membrane up to  $180\text{ }^\circ\text{C}$  in vacuum oven. These results show good agreement with the crosslinking mechanism which was presented earlier in Figure 2.1.

It was confirmed that exposure of pure PTMSP membranes and membranes containing PTMSP with 3wt% BAA in different concentrations of MDEA does not affect the chemical structure of the polymer. No peaks are observed in the region of  $\text{C}=\text{O}$  and  $\text{C}-\text{O}$ , which can be seen from Figure A.5 and Figure A.6 in Appendix A.

For membranes with nanoparticles (Figure A.2 and Figure A.4 in Appendix A) the intensity at wavelengths between  $500$  and  $700\text{ cm}^{-1}$  are higher than the membranes without nanoparticles. This might have something to do with the coordination of the molecules (octahedral, tetrahedral) [93].

## 7.2 Thermal stability

Thermogravimetric analysis (TGA) was used to analyze the thermal stability of the PTMSP membranes. Figure 7.5 shows the thermogravimetric degradation profile of pure PTMSP and some crosslinked and nanofilled samples.

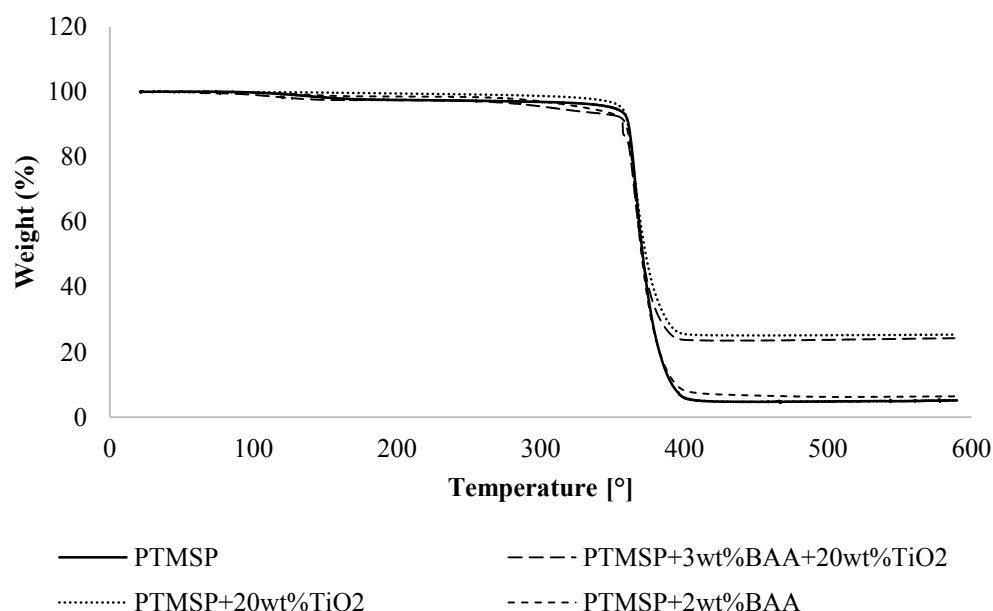


**Figure 7.5** TGA curves of pure PTMSP and some crosslinked and filled samples

The thermal degradation happens around  $350\text{ }^\circ\text{C}$  for all membranes. From the literature [31] it is described that when PTMSP undergoes thermal degradation in air, the degradation begins at

the carbon-carbon double bonds in the main chain. The difference in mass % left after the degradation for the four membrane compositions is caused by the nanoparticles which have not degraded at 600 °C. This conclusion is drawn since approximate 25wt% of the total sample weight was left for the membrane containing 20wt% nanoparticles and approximate 5wt% was left for the membrane containing pure PTMSP. Sitter et al. [94] have reported that all of the polymer became degraded at 750 °C, but the silica nanofillers remained.

DSC of pure PTMSP and uncrosslinked PTMSP with 3wt% BAA was performed up to temperatures before the thermal degradation occurred. As expected from the literature [95], the thermal analysis of pure PTMSP showed no glass transition or melting point below the degradation temperature of the thermal decomposition. The degradation process was observed to be exothermic up to 320°C. At this temperature decomposition of the sample took place. These results indicate that the polymer is very rigid: it is easier to break primary bonds than to achieve rotation mobility by using thermal energy [96].

DSC was also used to detect the crosslinking temperature of PTMSP membranes containing 3wt% BAA as shown in Figure 7.6. It is observed an increase in heat flow which begins at approximately 180°C and have a peak top at 200°C. This peak corresponds to the decomposition of BAA. Thus, the crosslinking temperature is 180°C as expected from the literature [49].

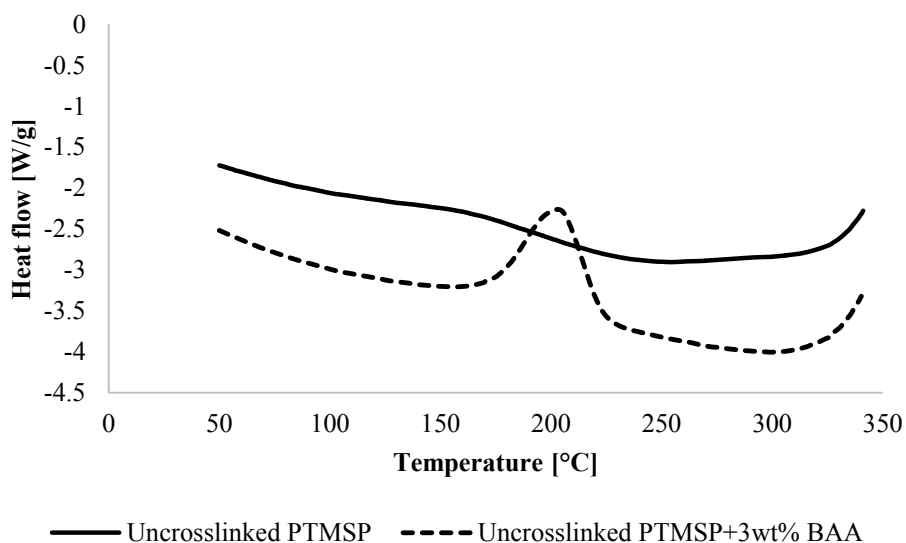


**Figure 7.6** DSC curve of uncrosslinked PTMSP and uncrosslinked PTMSP with 3wt% BAA



### 7.3 Permeation results

In this section, several permeation experiments have been performed. First, an background of the permeability results are given according to selection of nanoparticles, followed by an uncertainty analysis, effect of gas and pressure on the permeability, aging of crosslinked and uncrosslinked PTMSP with BAA, effect on permeability by crosslinking membranes and crosslinking nanofilled membranes, and at last, permeation of membranes treated with amine solutions. The permeation results are also given in tables in Appendix B.

#### 7.3.1 The background of the permeability measurements

Referring to the project work from fall 2012 [83], nanoparticles of the size of 15 nm were used in PTMSP membranes. Commercial nanoparticles which Lei Shao used in his experiments [42], were used in this work. The nanoparticles have a primary size of 21nm. The producer of the nanoparticles informed that the particles are covalently bonded as aggregates in the range of 100-250nm. SINTEF Material and Chemistry have measured the particle sizes up to 1-3  $\mu\text{m}$ . The result from the works are presented in Figure 7.7. The  $\text{CO}_2$  permeability measurements were performed by Seglem [97].

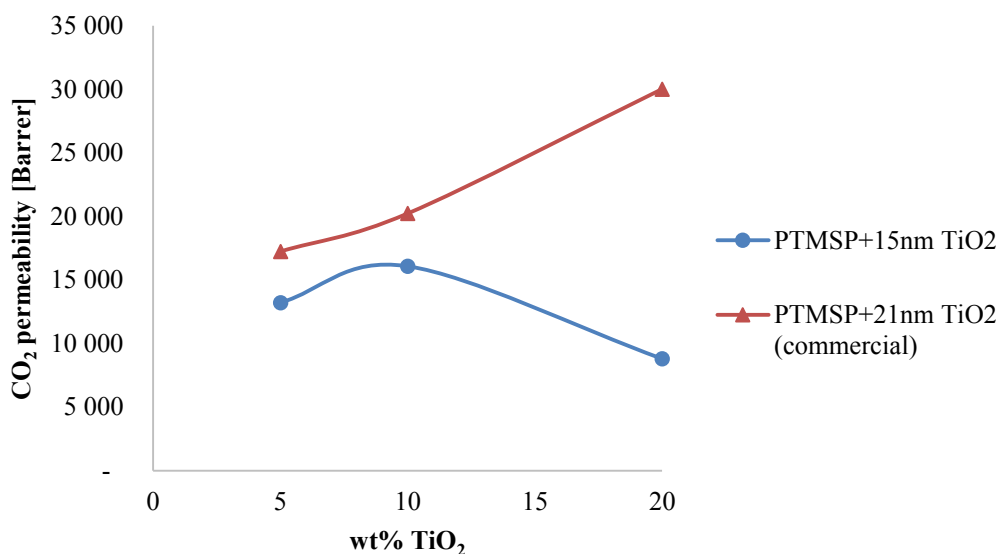


**Figure 7.7** The effect of two different TiO<sub>2</sub> nanoparticle sizes on the CO<sub>2</sub> permeability at 2 bar and room temperature [97]

The smallest nanoparticles of 15nm, which were used during the fall 2012, showed first an increase in permeability at 10wt% TiO<sub>2</sub>. As the nanoparticle loading was further increased, the permeability decreased dramatically. The nanoparticles might have begun to occupy the free volume as the particle content further increased. The commercial nanoparticles on the other

hand, showed an increasing effect on the CO<sub>2</sub> permeability as the nanoparticle loading increased. Those nanoparticles might have increased the free volume by disrupting the chain packing. This increasing permeability trend is the reason that commercial nanoparticles of the primary size 21nm are used in this work.

### 7.3.2 Uncertainty analysis

From the DOE, three crosslinked nanofilled PTMSP membranes with 1.5wt% BAA and 10wt% TiO<sub>2</sub> were tested for gas permeability to see how stochastic the results are (Figure 7.8). The three same type of membranes showed differences in permeability. They were all casted from the same polymer solution at the same day and crosslinked at the same time to minimize the random error. Some of the random error is introduced by the difference in membrane surface from one parallel to the other (macrovoids or crooked distribution of the density on the membrane surface), the gas permeation equipment and/or by the membrane thickness measurement. Membranes that have not been crosslinked are also affected by the aging of the membranes, something which is presented later.

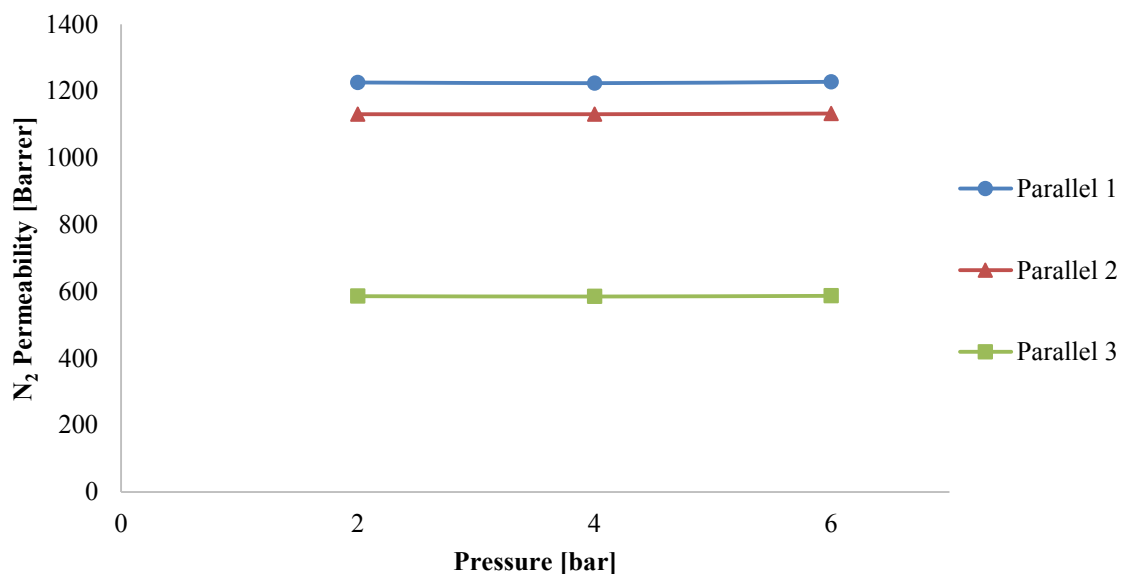


**Figure 7.8** N<sub>2</sub> permeability of three crosslinked membranes containing PTMSP, 1.5 wt% BAA and 10 wt% TiO<sub>2</sub> nanoparticles.

As can be seen from Figure 7.8, the CO<sub>2</sub> permeabilities of the two first parallels are close in value, while the last parallel has a much lower permeability. From these results, a standard deviation is calculated to be around  $\pm 2300$  barrer.

DOE was used to achieve high degree of spreading and variation in the results. The permeability of two parallels of every membrane was measured due to the high uncertainty in the measurements. Some membranes with high permeability distribution was measured three times,

and the two membranes closest in value was used for DOE. It would have been better to measure even more parallels, but it was both limitations in time and laboratory equipment to make all the membranes at the same time to reduce preparation errors and to test all of them. The laboratory limitations are: not enough membrane preparation equipment (funnels and porous supports), not enough space in the oven and the oven is not always available since it is shared with others.

### 7.3.3 Effect of gas and pressure on permeability

The  $N_2$ ,  $CH_4$  and  $CO_2$  permeabilities at 2, 4 and 6 bar is shown for crosslinked PTMSP with 3wt% BAA in Figure 7.9.

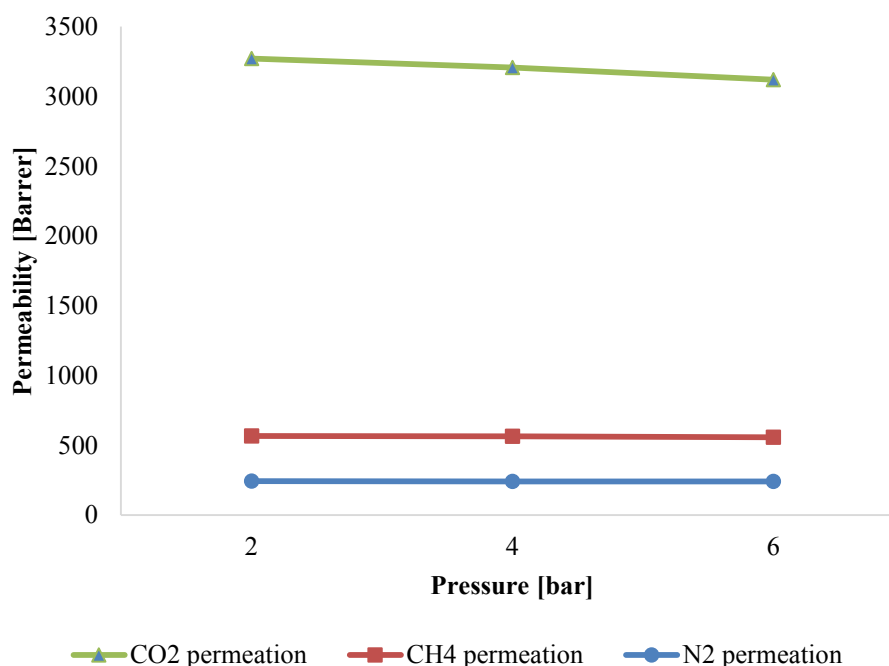


**Figure 7.9**  $CO_2$ ,  $CH_4$  and  $N_2$  permeabilities as a function of pressure for crosslinked PTMSP with 3wt% BAA

It is observed that the  $CO_2$  achieve the highest permeabilities among the gases, followed by  $CH_4$  and at last  $N_2$ . The diffusivity of the smallest  $N_2$  is highest, but the high solubility of  $CO_2$  in PTMSP overcomes the diffusivity [98]. It is also observed a slight decrease in the  $CO_2$  permeabilities as the pressure increase. The permeabilities of  $CH_4$  and  $N_2$  remains almost constant. This is in agreement with the dual sorption model described in Chapter 1.3.4. Sanders [99] has introduced a theory on how microvoids are introduced in the membrane as low concentrated penetrant passes through the membrane. His microvoids became saturated at higher levels of penetrant and thus result in a decrease in gas permeability.

### 7.3.4 Aging of crosslinked and uncrosslinked PTMSP

The stability of uncrosslinked PTMSP and crosslinked PTMSP containing 3wt% BAA was studied over a period of 3 months. The membranes were stored in air and the CO<sub>2</sub> permeability was measured at 2 bar (Figure 7.10). The age (days) of the membranes are counted from the day the polymer solutions were casted to form membranes.

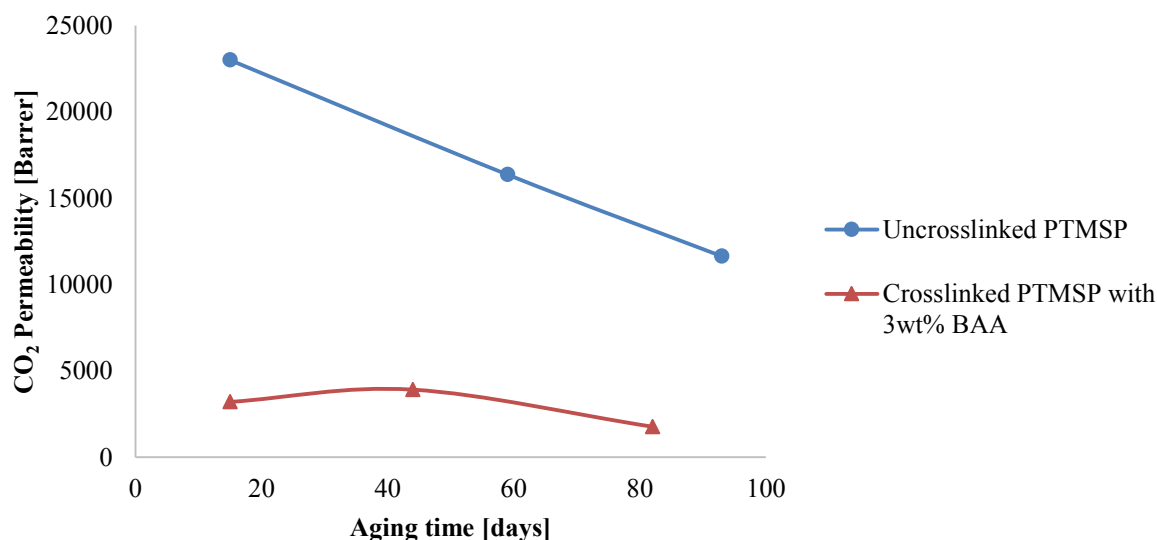


**Figure 7.10** Stability of crosslinked and uncrosslinked PTMSP, measured as a function of CO<sub>2</sub> permeability at 2 bar and room temperature

The results show that the uncrosslinked membranes are unstable over time. The permeability was halved after an aging time of 93 days in proportion to the permeability after 15 days. These results are comparable to the literature as described in Chapter 2.1 where this fast physical aging occurs due to relaxation of nonequilibrium excess free volume [49]. The membranes that were crosslinked with 3wt% BAA for 1 and a half hour showed a more stable trend with only a slight decrease in permeability. Crosslinking of PTMSP resulted in an improved permeability stability. Even though the CO<sub>2</sub> permeability has decreased dramatically with time, the permeability is still much higher than the polymer PDMS, which was regarded as the most permeable polymer before the synthesis of PTMSP [31].

The change in CO<sub>2</sub>/CH<sub>4</sub> selectivity with the aging of the membrane is given in Figure 7.11. It is observed that the CO<sub>2</sub>/CH<sub>4</sub> selectivity as well as the permeability of crosslinked membranes are stable over time. Uncrosslinked PTMSP shows both unstable and lower CO<sub>2</sub>/CH<sub>4</sub> selectivity than crosslinked membranes. The selectivity after 60 days, might be a random error. Aging impact the hole sizes differently. The narrow hole sizes will no longer be able to serve as diffusion pathways for the permeates. Consequently, the small gas molecules are most affected by the ageing of the membranes [35].

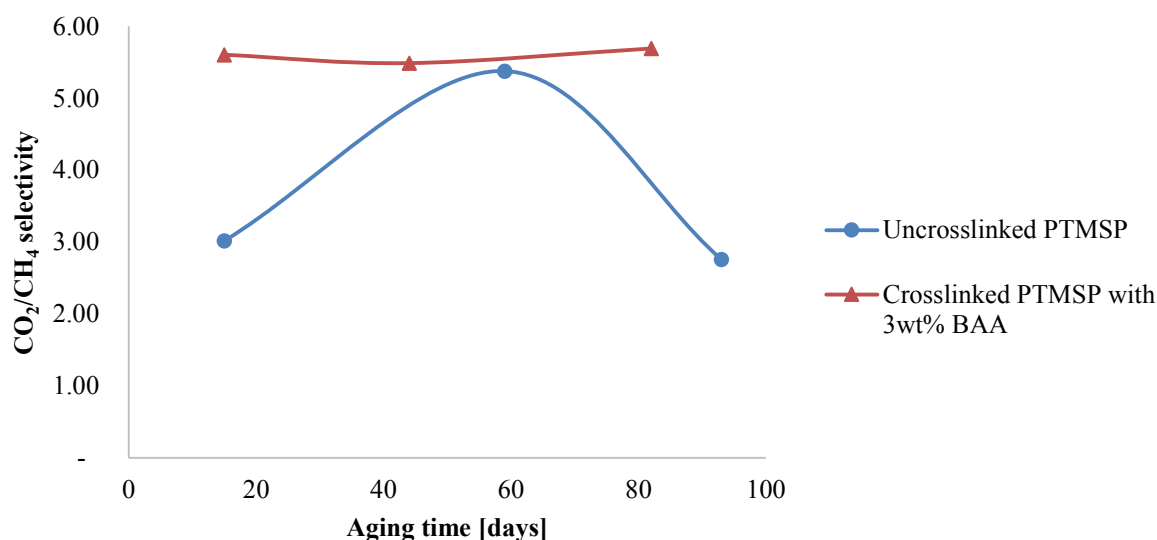


**Figure 7.11** Stability of crosslinked and uncrosslinked PTMSP, measured as a function of CO<sub>2</sub>/CH<sub>4</sub> selectivity at 2 bar and room temperature

### 7.3.5 Effect of crosslinking on permeability

PTMSP membranes with the crosslinker BAA were tested for gas permeability. Membranes with different weight percentages of BAA were tested: 0, 1.5, 2 and 3wt%. The results are presented in Table 7.1.

**Table 7.1** Gas permeabilities of crosslinked membranes and pure uncrosslinked PTMSP at room temperature

Wt% BAA	Permeability [Barrer]								
	N <sub>2</sub>			CH <sub>4</sub>			CO <sub>2</sub>		
	2 bar	4 bar	6 bar	2 bar	4 bar	6 bar	2 bar	4 bar	6 bar
0	3 505	3 533	3579	5 327	7 602	7 729	20 446	20 891	20 869
1.5	-	-	-	2 213	2 229	2 213	8 950	8 840	8 361
2	-	-	-	753	775	767	3 971	3 924	3 751
3	242	240	241	566	564	556	3 271	3 208	3 121

It is observed that membranes made of pure PTMSP achieves the highest CO<sub>2</sub> permeabilities. Addition of 1.5wt% BAA reduces the permeability with more than 50% when it is crosslinked. As the amount of BAA was further increased, the permeability decreases. This is in agreement to what is observed in the literature [33, 42, 43, 47-49, 75]. The crosslinker was expected to occupy a lot of the free volume.

A binocular microscope ZEISS Axio Lab.A1® with an Infinity 60 N-C camera was used to take pictures of the membrane surfaces with a 10x zoom. Figure 7.12 shows how the increase of amount BAA affect the membrane surface structure. BAA occupy a lot of the free volume and connect adjacent chains which results in an increased local density as the BAA content



increases. It is observed a decrease in free volume as the BAA content increase from a) pure PTMSP to d) 3wt% BAA. This is in agreement with the results obtained from Jia et. Al [49] where the density is reported to be higher for crosslinked PTMSP with bis (aryl azides) than for pure PTMSP.

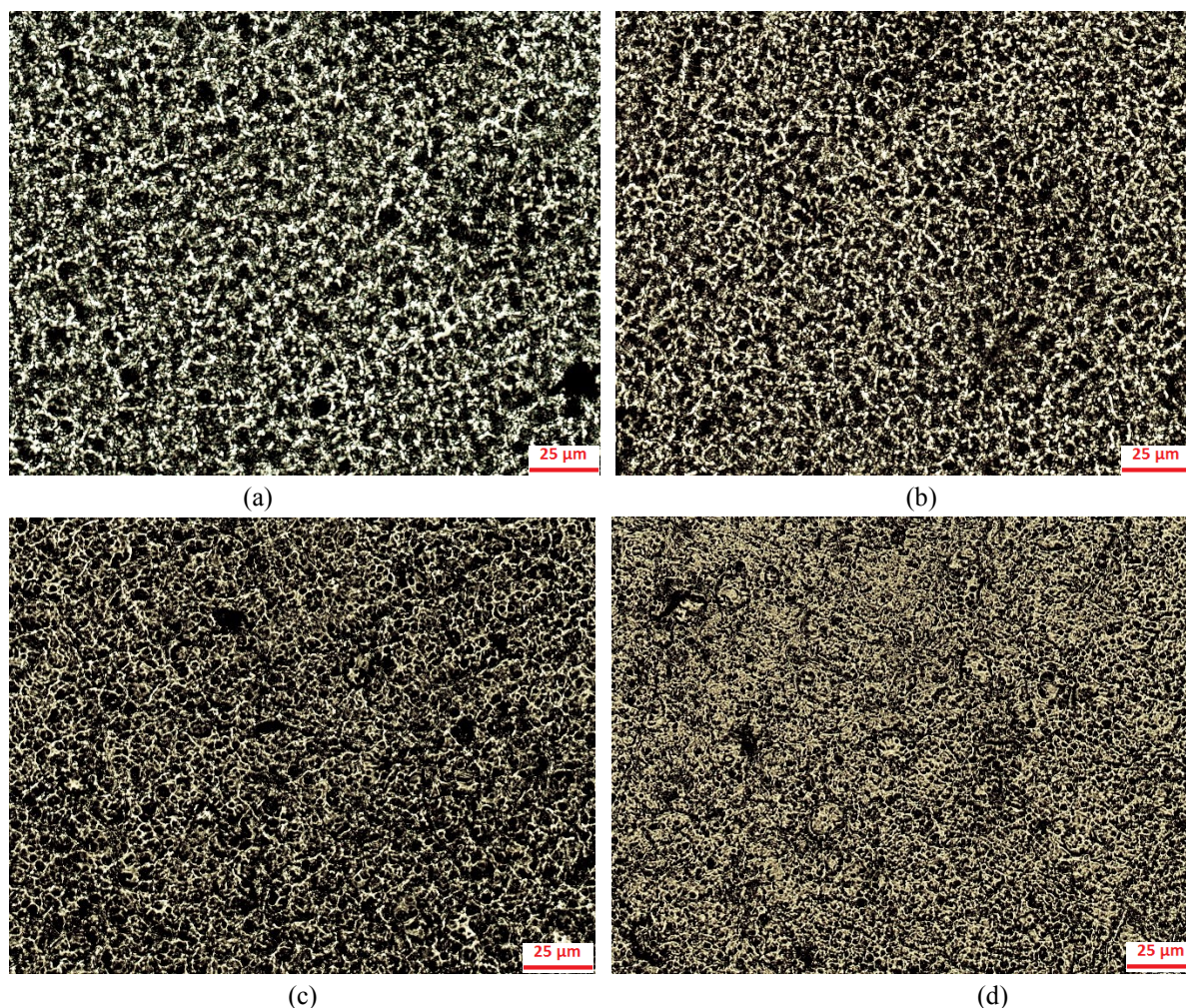


**Figure 7.12** Microscopic pictures of the surface of (a) Pure PTMSP, (b) PTMSP with 1.5wt% BAA, (c) PTMSP with 2wt% BAA and (d) PTMSP with 3wt% BAA

According to literature [42, 43], sorption measurements remain constant as the wt% BAA increases. This means that the decrease in permeability is caused decrease in diffusivity as the free volume decrease. The selectivities of crosslinked membranes are discussed in Chapter 7.3.6.

A large uncertainty of membranes is caused by the effect of annealing on the membrane structure and thus the permeability and selectivity of the different membranes. A study by Tasaka et al. [100] showed that the density of PTMSP increased as the polymer was heated at even low ( $<100^{\circ}\text{C}$ ) temperatures. PTMSP casted from benzene solution had low density ( $0.82\text{g}/\text{cm}^3$ ) and high permeability, whereas the annealed sample had higher density

( $0.88\text{g}/\text{cm}^3$ ) and a permeability that was two order of magnitude lower. In this work, membranes containing BAA was thermally crosslinked for 90 minutes. All membranes were not crosslinked at the same time, something which increased the uncertainty in the results. Referring to the project work from the fall 2012 [83], a membrane was thermally treated at  $180^\circ\text{C}$  for 16h to illustrate the principle of the effect of the annealing time. The  $\text{CO}_2$  permeability at 2 bar and room temperature resulted in a decrease from approximate 11 000 barrer (heated for 90 minutes) to approximate 1 000 barrer (heated for 16 hours).

### 7.3.6 Permeation through crosslinked nanofilled membranes

One of the membrane parallels that were prepared for DOE and some additional membranes are shown in Figure 7.13, which presents the  $\text{CO}_2$  permeability as a function of pressure. It was observed that addition of 21nm nanoparticles to pure uncrosslinked PTMSP have increased the membrane permeability and thus produced an even more permeable material. This is because the nanofillers increase the free volume by disrupting the chain packing [16].

The data observed in Figure 7.13 showed also an increase for crosslinked membranes when the nanoparticles were added. An exception is for the membrane containing 3wt% BAA where the gas permeability decreased when 20wt% of nanoparticles were added. The microscopic pictures from Figure 7.12 showed how the free volume decrease as the weight percent of BAA increases. A possible theory for the decrease in permeability for the crosslinked membrane containing 3wt% BAA is that the free volume is too small for the nanoparticles to penetrate in between the chains and create more pathways for molecular transport. Instead the nanoparticles block the free volume which results in a reduced diffusion coefficient, thus reduced permeability.

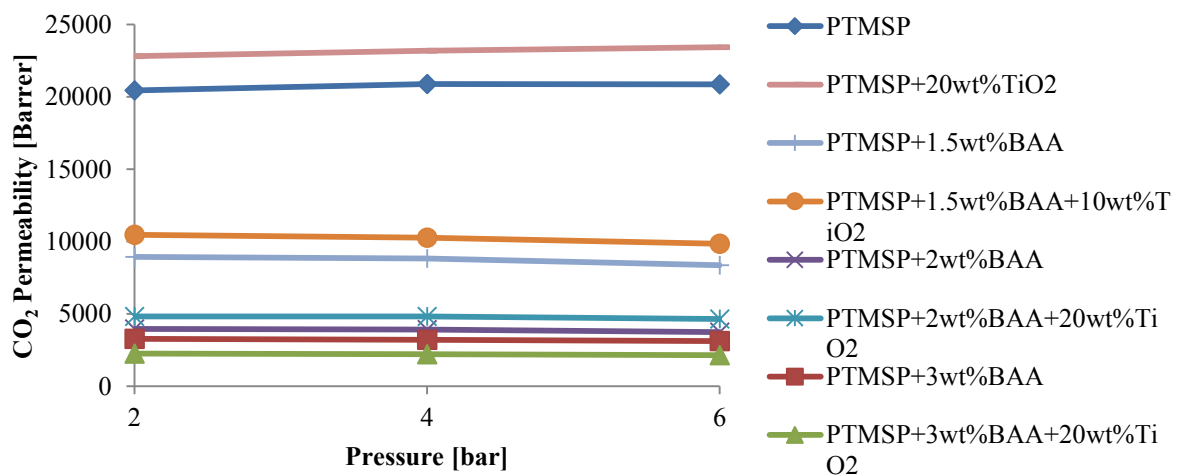
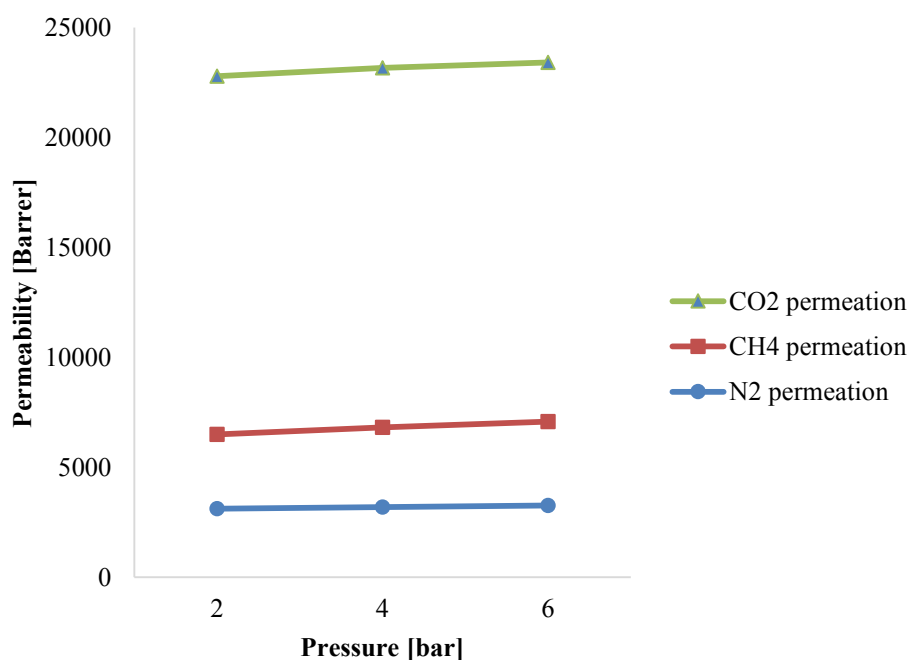


Figure 7.13  $\text{CO}_2$  permeability of membranes from DOE at room temperature

The permeabilities from Figure 7.13 follows a general trend when the pressure is changed. The permeability decreases slightly with increasing pressure. This is due to the dual sorption, which



is described in Chapter 1.3.4. One exception from this trend is the membrane containing PTMSP with 20wt% TiO<sub>2</sub> where the permeability increased slightly as the pressure increased.



**Figure 7.14** CO<sub>2</sub>, CH<sub>4</sub> and N<sub>2</sub> permeability of PTMSP+20wt% TiO<sub>2</sub> nanoparticles at room temperature

The data in Figure 7.14 shows that CO<sub>2</sub> permeation gave the largest permeability increase as the pressure was increased from 2 to 6 bar. This might have been caused by swelling of the membrane as the CO<sub>2</sub> concentration builds up inside the polymer. This can cause changes in the membrane structure. The polymer is said to be plasticized [21]. From the FT-IR spectroscopy results in Figure A.4 in Appendix A, it is observed that something has happened during the gas permeability since the peaks in the region 400-800 cm<sup>-1</sup> vary from the figure before and after gas testing. A possible explanation is that CO<sub>2</sub> have plasticized the nanofilled polymer, and thus changed the chemical structure. If the membrane is plasticized, the segmental mobility of the chain should be enhanced, reducing the glass transition temperature ( $t_g$ ) [21]. As already mentioned from literature [95] and demonstrated with DSC,  $t_g$  for PTMSP is unknown. TGA showed a thermal degradation of PTMSP around 350 °C. Since the polymer degrades before  $t_g$ , it is not possible to determine if plasticization occurs by observing if a depression of the glass transition temperature happens.

From the selectivity results in Table 7.2 it was observed an increase in the CH<sub>4</sub>/N<sub>2</sub>, CO<sub>2</sub>/N<sub>2</sub> and CO<sub>2</sub>/CH<sub>4</sub> selectivities as the wt% of BAA increased. Higher degree of crosslinking resulted in a lower gas permeability and higher selectivity. The reduction in permeability was largest for N<sub>2</sub> and CH<sub>4</sub>, giving higher selectivity increase for CH<sub>4</sub>/N<sub>2</sub>, CO<sub>2</sub>/N<sub>2</sub> and CO<sub>2</sub>/CH<sub>4</sub> as the BAA concentration goes from 0 to 3wt%. Addition of nanoparticles to membranes with crosslinker decreased the selectivities slightly, but improve the permeabilities. These selectivities increases



with increasing wt% of BAA and nanoparticles, because the narrow holes can no longer serve as diffusion pathways. This affect mostly the permeability of the smallest molecule, N<sub>2</sub>, and then the larger: CH<sub>4</sub> and then CO<sub>2</sub> [35].

Table 7.2 Selectivities of gases in pure PTMSP and crosslinked nanofilled PTMSP membranes at room temperature

Membrane composition		Selectivity [-]								
wt% BAA	wt% TiO <sub>2</sub>	CH <sub>4</sub> /N <sub>2</sub>			CO <sub>2</sub> /N <sub>2</sub>			CO <sub>2</sub> /CH <sub>4</sub>		
		2 bar	4 bar	6 bar	2 bar	4 bar	6 bar	2 bar	4 bar	6 bar
None	None	1.52	2.15	2.16	5.83	5.91	5.83	3.84	2.75	2.70
1.5	None	-	-	-	-	-	-	4.04	3.97	3.78
2.0	None	-	-	-	-	-	-	5.27	5.06	4.89
3.0	None	2.34	2.35	2.31	13.52	13.37	12.95	5.78	5.69	5.61
None	20	2.09	2.14	2.17	7.31	7.27	7.18	3.51	3.40	3.31
1.5	10	2.20	2.20	2.17	9.26	9.07	8.69	4.21	4.12	4.00
2.0	20	-	-	-	-	-	-	5.10	5.00	4.80
3.0	20	2.34	2.36	2.32	13.28	13.25	12.82	5.67	5.61	5.52

The selectivities are less important when the membranes are to be used in a membrane contactor with MDEA. The amine will selectively absorb CO<sub>2</sub>. The selectivity is a property of the membrane and it is interesting to see if MDEA is compatible with the membrane material. The CO<sub>2</sub>/CH<sub>4</sub> selectivities of membranes that have been soaked in liquid solutions for weeks are presented in the next section as well as the permeabilities, too see if the liquids have affected the membrane properties.

### 7.3.7 Amine treated membranes

In total 54 membranes were put in different solutions: distilled water, 2M MDEA and 4.2M MDEA for a period up to 10 weeks, and the CH<sub>4</sub> and CO<sub>2</sub> permeability at 2, 4 and 6 bar was measured when the membranes had dried. Permeability, selectivity and aging days of all the 54 membranes put in solutions are given in Table B.3, Table B.4 and Table B.5 in Appendix B. From those membranes, 24 membranes were pure uncrosslinked PTMSP membranes. The CO<sub>2</sub> permeability results of pure PTMSP membranes at 2 bar are presented in Figure 7.15.

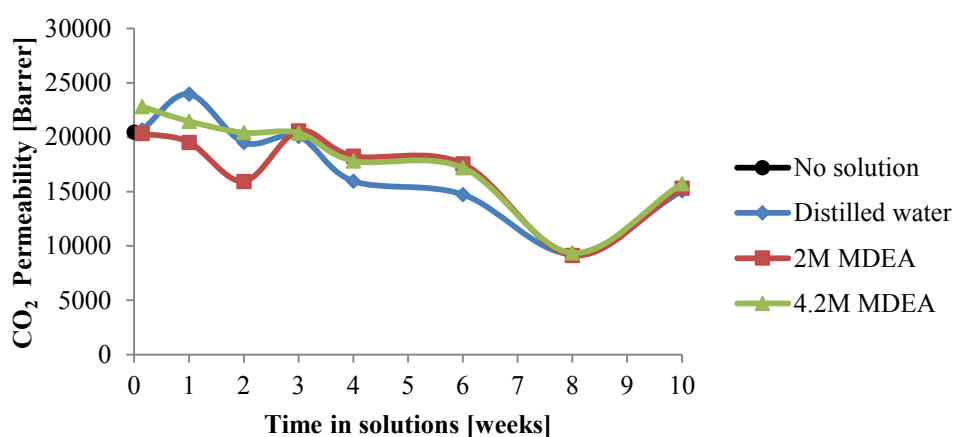


**Figure 7.15** CO<sub>2</sub> permeability of PTMSP membranes at 2 bar that have been soaked in distilled water, 2M MDEA and 4.2M MDEA for 10 weeks

The permeabilities decreased slightly the longer the membranes have stayed in the solutions. The permeabilities followed the same trend as the aging curve in Figure 7.10. This indicates that the contact with solutions did not affect the permeabilities because the hydrophobicity of the membranes. The CO<sub>2</sub>/CH<sub>4</sub> selectivities of pure PTMSP are shown in Figure 7.16. It was observed an increasing selectivity trend for the membranes that have stayed in the solutions up to 4 weeks. After this, the selectivities decreased before they increased again after 10 weeks. Referring to Figure 7.11, the selectivities have changed with the aging of the membranes. The selectivities first increased, and then decreased. This trend is also observed for the membranes that have been in distilled water and amine solutions.

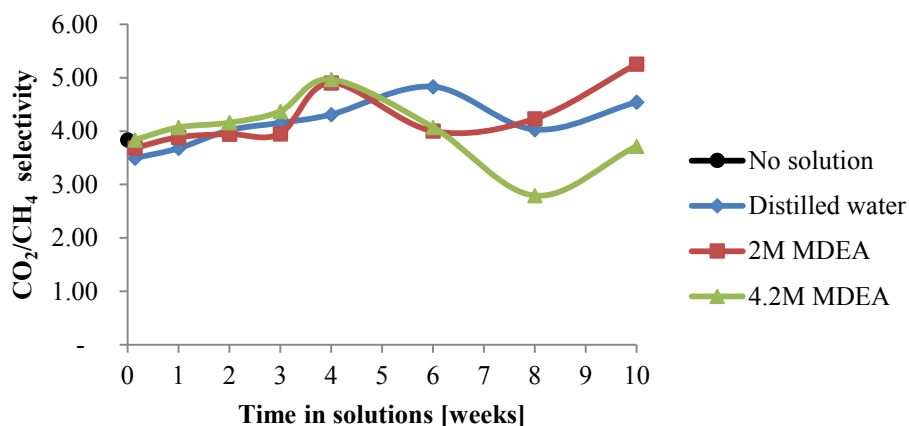


**Figure 7.16** CO<sub>2</sub>/CH<sub>4</sub> selectivity of PTMSP membranes at 2 bar that have been soaked in distilled water, 2M MDEA and 4.2M MDEA for 10 weeks

Crosslinked PTMSP membranes with 3wt% BAA were also put in solutions like the pure PTMSP membranes. Figure 7.17 and Figure 7.18 shows the CO<sub>2</sub> permeabilities and the CO<sub>2</sub>/CH<sub>4</sub> selectivities, respectively. The permeabilities are very high compared to the membrane that has not been in the solution. The permeabilities of the membranes that have been in distilled water have the highest values followed by 2M MDEA and at last 4.2M MDEA. For all membranes the CO<sub>2</sub> permeabilities decreased the longer they stayed in solution. From Figure 7.10 and Figure 7.11 it is observed that the permeability and selectivity is very stable with time for crosslinked membranes. It is concluded that the aging of the membranes have not affected the permeabilities and selectivities. Since the permeability decrease with time, sorption measurements could have been interesting to perform too see if the solubility of CO<sub>2</sub> decreases with the time in solutions.

The selectivities of the crosslinked membranes remained very stable up to 4 weeks, and then decreased slightly and increased again for membranes soaked in 2M MDEA and 4.2M MDEA. The results seems to be a little random, and this might have something do with the uncertainty. From Table B.4 in Appendix B it is observed that not all membranes are prepared the same day, and thus not crosslinked at the same time.

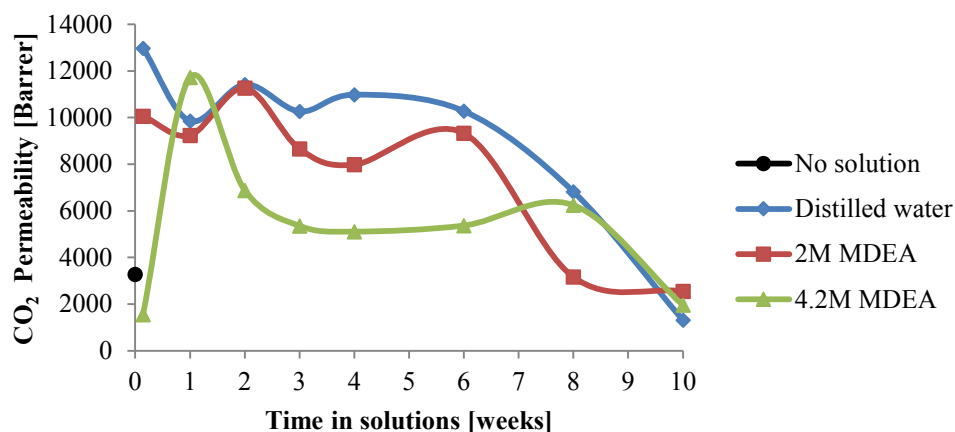


**Figure 7.17** CO<sub>2</sub> permeability of crosslinked PTMSP with 3wt% BAA at 2 bar that have been soaked in distilled water, 2M MDEA and 4.2M MDEA for 10 weeks

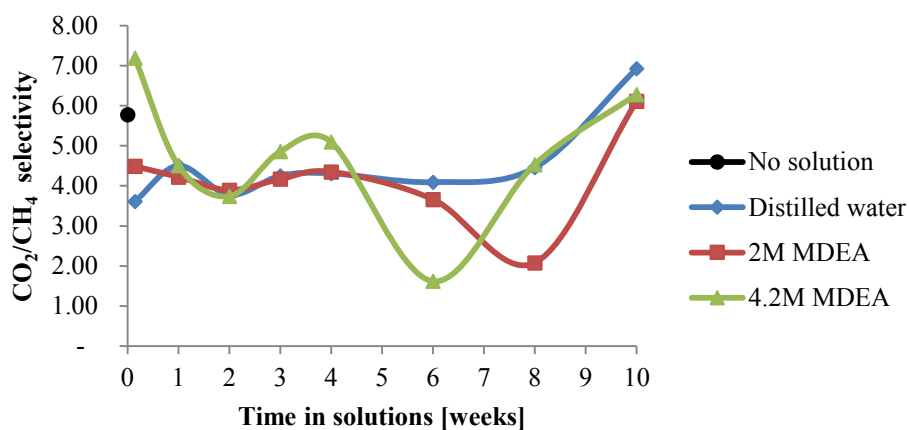


**Figure 7.18** CO<sub>2</sub>/CH<sub>4</sub> selectivity of crosslinked PTMSP with 3wt% BAA at 2 bar that have been soaked in distilled water, 2M MDEA and 4.2M MDEA for 10 weeks

Due to time and equipment limitations as mentioned in Chapter 7.3.2, only 6 membranes containing crosslinked nanofilled PTMSP with 2wt% BAA and 20wt% TiO<sub>2</sub> were put in solutions for 2 and 4 weeks. The CO<sub>2</sub> permeability and CO<sub>2</sub>/CH<sub>4</sub> selectivity results for these membranes are presented in Figure 7.19 and Figure 7.20. The permeabilities of the membranes that have been in solutions have decreased dramatically compared to the membrane that has not been in contact with any solution. This is not good for the work, since the crosslinked nanofilled PTMSP membranes are to be used in a membrane contactor with MDEA. From FT-IR spectroscopy, no traces of any solvents were detected. The nanoparticles are also hydrophobic, something which should have improved the membrane's resistance towards the solutions. This needs to be further explored. Since these results were from the last experiments in the laboratory, there was no time to do further investigations. Some suggestions of further work are given in Chapter 9.

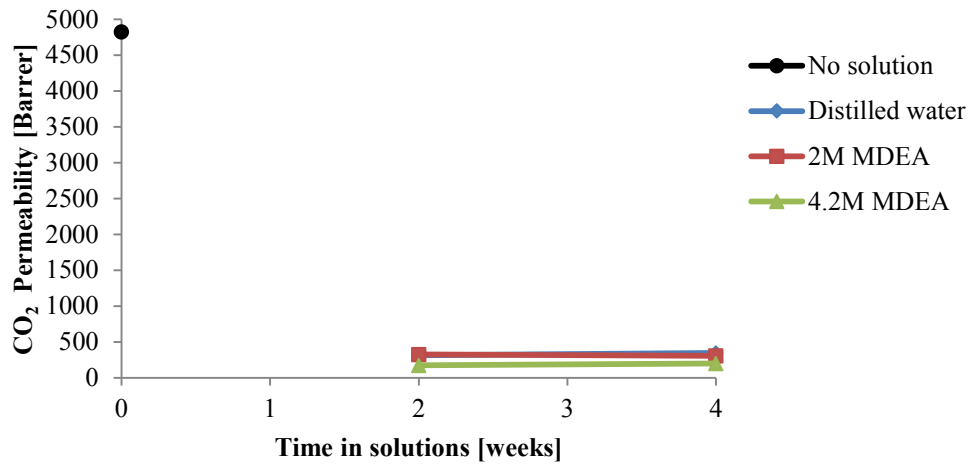


**Figure 7.19** CO<sub>2</sub> permeability of crosslinked PTMSP with 2wt% BAA and 20wt% TiO<sub>2</sub> at 2 bar that have been soaked in distilled water, 2M MDEA and 4.2M MDEA for 4 weeks

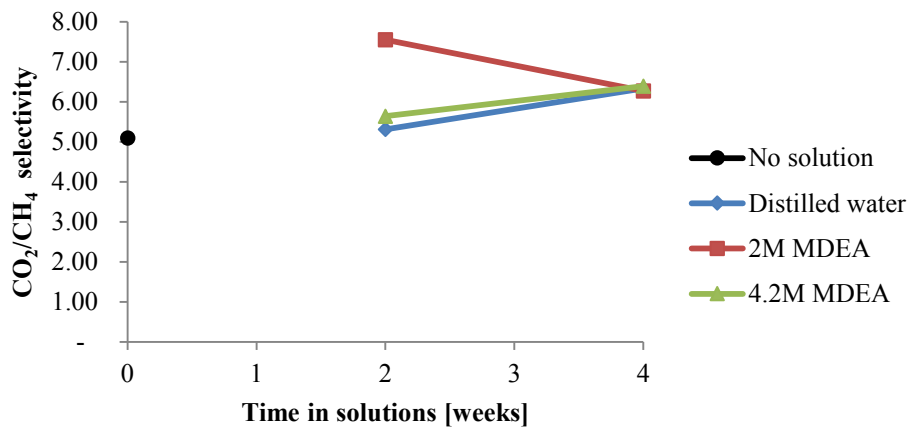


**Figure 7.20** CO<sub>2</sub>/CH<sub>4</sub> selectivity of crosslinked PTMSP with 2wt% BAA and 20wt% TiO<sub>2</sub> at 2 bar that have been soaked in distilled water, 2M MDEA and 4.2M MDEA for 4 weeks

## 7.4 Water contact angles

The water contact angles ( $\theta$ ) were measured for all the membranes produced in the laboratory. The contact angle between the water and the membrane was measured both on left and right side, as illustrated in Figure 7.21.

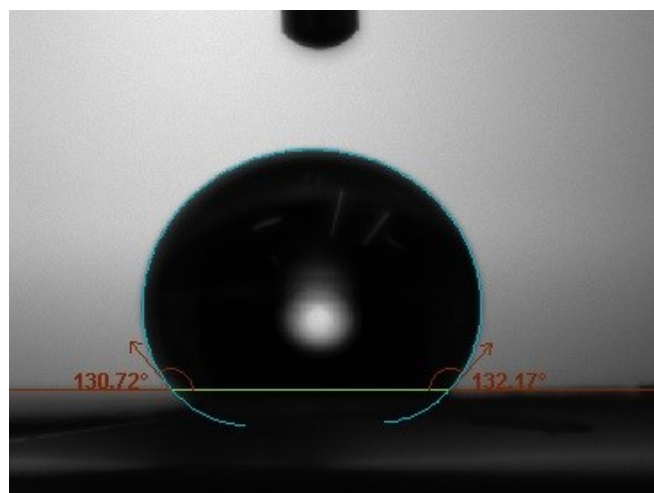


**Figure 7.21** Contact angle measurements of water on a membrane from fall 2012, containing 5wt% PTMSP and 20wt% TiO<sub>2</sub>

All reported contact angle values are given as the mean values of the left and right contact angles. Each membrane was measured three times and the mean value and a standard deviation was calculated. These values were recorded 10 minutes after water deposition since the drop volume began to decrease as the results were recorded any longer due to evaporation. The contact angles of membranes produced for Design Of Experiments (DOE) are presented in Table 7.3 The values of all parallels are given in Table C.1 in Appendix C.

**Table 7.3** Water contact angle measurements of PTMSP membranes from DOE

Membrane Composition		Contact angle, $\theta$ [°]
wt% BAA	wt% TiO <sub>2</sub>	
None	None	124 ± 3.78
1.5	None	96 ± 2.04
2.0	None	95 ± 2.99
3.0	None	102 ± 1.90
None	20.0	136 ± 4.89
1.5	10.0	93 ± 1.27
2.0	20.0	95 ± 2.99
3.0	20.0	79 ± 6.92

All contact angle values, except for one membrane, was above  $90^\circ$ . This indicate poor wetting of the membranes. Since the membranes in this experiment are meant to be used in a gas-liquid membrane contactor with an aqueous amine as liquid phase, poor wetting is desirable. These hydrophobic membranes will not allow the amine to penetrate in the membrane and affect the membrane properties.

The contact angle of pure PTMSP was high compared to the other membranes, but addition of 20wt% nanoparticles increased the contact angles even more, enhancing the hydrophobicity of the membrane. This might be because the roughness of the membrane surface increases when the particles are added as well as the fact that the  $\text{TiO}_2$  nanoparticles are hydrophobic. It was not observed any special contact angle trend from the measurements.

There was a large uncertainty when defining the base line (the green line) in Figure 7.21 for the contact angle measurements, which has probably affected the results most. It was observed that accidental contact of the membrane with the finger reduced the contact angle dramatically. The same membrane was used for many applications, something which made it difficult to do more than three parallels per membrane, due to limitations in the equipment as mentioned earlier.

Contact angles of the other membranes made for amine solutions are presented in Figure 7.22, Figure 7.23 and Figure 7.24. The values of all parallels are given in Appendix C. The contact angles do not show any specific trend other than membranes being soaked in 4.2M MDEA have achieved the highest values. They have become most hydrophobic, followed by the membranes soaked in 2M MDEA. The crosslinked nanofilled membranes do not show the same trend. Here the values appears to be more random, due to uncertainty in the measurements.

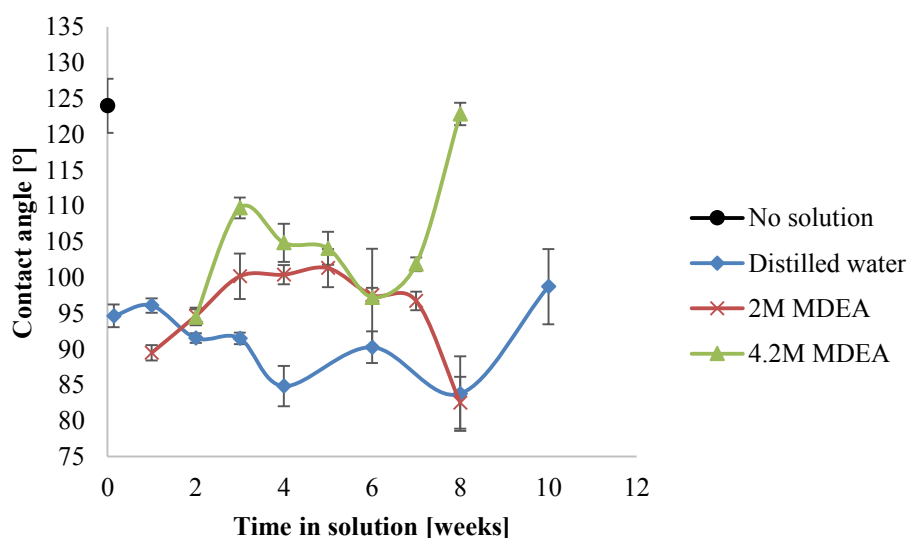


**Figure 7.22** Water contact angle measurement of PTMSP membranes that have been soaked in solutions up to 10 weeks

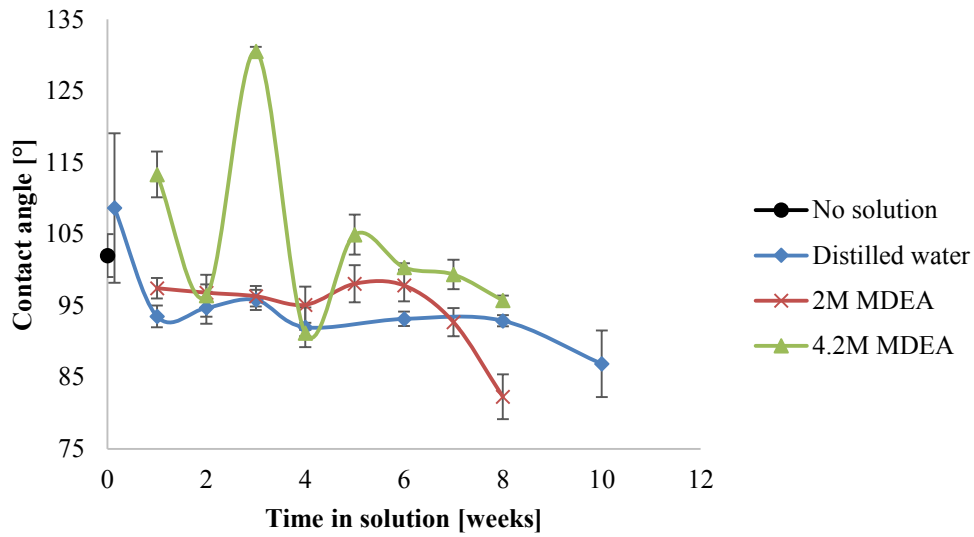


**Figure 7.23** Water contact angle measurement of crosslinked PTMSP with 3wt% BAA that have been soaked in solutions up to 10 weeks

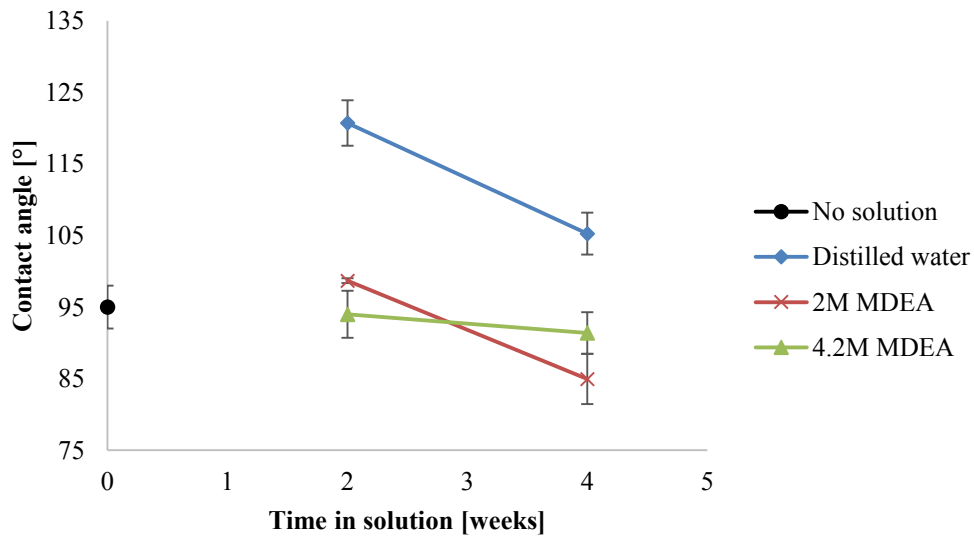


**Figure 7.24** Water contact angle measurement of crosslinked PTMSP with 2wt% BAA and 20wt% TiO<sub>2</sub> that have been soaked in solutions up to 4 weeks



## Chapter 8

### CONCLUSION

Flat sheet membranes of different BAA and TiO<sub>2</sub> compositions have been prepared by precipitation by solvent evaporation. FT-IR spectroscopy before and after crosslinking confirmed that the crosslinking took place as the peak at 2122 cm<sup>-1</sup> (azide group) disappeared after thermal heating of the membrane.

The chemical and physical stability of PTMSP membranes were improved by crosslinking with BAA. Crosslinking had a decreasing effect on the gas permeability, due to decrease in free volume. Based on the increase in CH<sub>4</sub>/N<sub>2</sub>, CO<sub>2</sub>/CH<sub>4</sub> and CO<sub>2</sub>/N<sub>2</sub> selectivities, the permeability is mostly reduced due to the decrease in the diffusion coefficient. The diffusion coefficient of the smallest N<sub>2</sub> molecule decreases most.

Addition of 15nm sized TiO<sub>2</sub> nanoparticles, from the experiments of the fall of 2012, showed a decreasing effect on the permeability as the weight percent of nanoparticles increased. This indicates that the particles blocked the free volume. Clusters of nanoparticles with the primary size of 21nm, have been measured to 1-3µm. Permeation results with these nanoparticles have on the other hand showed an increasing permeability as the particle content increase. In crosslinked nanofilled membranes, the nanoparticles have increased the free volume and thus enhanced the mechanical properties of the membrane.

Membranes which have been exposed to distilled water and 2M MDEA and 4.2M MDEA have shown to not affect the gas permeabilities of membranes containing pure PTMSP. The decrease in permeabilities correspond to the aging trend of the membranes. For crosslinked membranes, which have shown to be stable towards aging, the permeabilities decreased with the time in solution. Based on the selectivities, it is suspected that the decrease in permeability is caused by reduction in the solubility coefficient for the membranes. Crosslinked nanofilled membranes exposed to the different solutions showed large decrease in permeability compared to the non-treated membranes with almost 90%.

Addition of hydrophobic TiO<sub>2</sub> nanoparticles to PTMSP and membranes that have been soaked in MDEA for several weeks have shown to improve the water contact angles. The membranes in 4.2M MDEA gave highest contact angles followed by 2M MDEA and at last distilled water. The values were above 90°, indicating poor wetting of the membranes.

As mentioned, the last experiment with crosslinked nanofilled membranes exposed to MDEA did not show good results. Hence the nanoparticles from SINTEF Materials and Chemistry

## *8. CONCLUSION*

---

should be explored as further work. A compromise between nanoparticles provided by SINTEF and commercial nanoparticles can be the solution in order to enhance the liquid compatibility. The results obtained from this work can be used as a comparison for further work with SINTEF's nanoparticles.

## Chapter 9

### FURTHER WORK

It would have been interesting to see how the different membrane compositions affect the gas permeability by the mean of sorption and diffusion. This makes it easier to describe what actually happens with the membrane. There was a sorption apparatus in the laboratory. If the apparatus was up and running, sorption measurements of the membranes would have been interesting to explore. Sorption measurements of the membranes exposed to distilled water and MDEA could have given a better description of the contact process between the membrane and solution, like if swelling occurs.

The crosslinked nanofilled membranes showed a dramatic reduction in permeability for all membranes that have been in contact with the solutions. Here it is obvious that something has happened which is not good for the work since crosslinked nanofilled membranes are to be used with MDEA in a membrane contactor. The nanoparticles are hydrophobic, so one would have expected that the solutions would not affect the permeabilities. For further work it should be explored if this is caused by the nanoparticles alone, by doing the same experiment with membranes containing only nanoparticles. Preferably experiments with different amounts of  $\text{TiO}_2$  should be performed, to check correlations with nanoparticle loadings.

Scanning Electron Microscopy (SEM) which provides pictures of the membrane surface could have given some information about the nanoparticle distribution, like what has happens before and after exposure to MDEA. Other methods to characterize the membrane surface is by Atomic Force microscopy (AFM) which provides information like pore size and porosity [7]. Contact angles can be predicted by AFM.



# Chapter 10

## REFERENCES

1. Li, J.L. and B.H. Chen, *Review of CO<sub>2</sub> absorption using chemical solvents in hollow fiber membrane contactors*. Separation and Purification Technology, 2005. **41**: p. 109-122.
2. Scholes, C.A., G.W. Stevens, and S.E. Kentish, *Membrane gas separation applications in natural gas processing*. Fuel, 2012. **96**: p. 15-28.
3. Rahaman, M.S.A., et al., *Capturing carbon dioxide from air using fixed carrier facilitated transport membrane*. RSC Advances, 2012. **2**: p. 9165–9172.
4. Noble, R.D. and S.A. Stern, *Membrane separations technology - principles and applications*. Membrane Science and Technology Series 1995, Amsterdam, Netherlands: Elsevier Science B.V.
5. Pabby, A.K., S.S.H. Rizvi, and A.M. Sastre, *Handbook of membrane separations: chemical, pharmaceutical, food, and biotechnological applications*. 2009, Boca Raton: CRC Press, Taylor & Francis Group.
6. Mansourizadeh, A. and A.F. Ismail, *Hollow fiber gas-liquid membrane contactors for acid gas capture: A review*. Journal of Hazardous Materials, 2009. **171**: p. 38-53.
7. Mulder, M., *Basic Principles of Membrane Technology*. 2 ed. 1996, Dordrecht: Kluwer Academic Publishers.
8. R.Konietzny. *Polymers - Membrane based separations*. 2010 [cited 2012 10/17]; Available from: [http://www.chemie.uni-duesseldorf.de/Faecher/Organische\\_Chemie/OC2/staudt/ENGLISCH/forschung/Membrane-based%20Separations](http://www.chemie.uni-duesseldorf.de/Faecher/Organische_Chemie/OC2/staudt/ENGLISCH/forschung/Membrane-based%20Separations).
9. Painter, P.C. and M.M. Coleman, *Fundamentals of polymer science*. 2 ed. 1997, Boca Raton: CLC Press.
10. Ravve, A., *Principles of Polymer Chemistry*, 2012, Springer: New York.
11. Nicholson, J.W., *Chemistry of polymers*. 3 ed. 2006, Dorset: RSC Publisher.
12. Carrahrer Jr, C.E., *Polymer chemistry - an introduction*. 4 ed. 1996, New York: Marcel Dekker.
13. Geankoplis, C.J., *Transport processes and separation process principles*. 4 ed. 2003, New Jersey: Pearson Education, Prentice Hall PTR.
14. Robeson, L.M., *Correlation of separation factor versus permeability for polymeric membranes*. Journal of Membrane Science, 1991. **62**: p. 165-185.
15. Baker, R.W., *Membrane technology and applications*. 2 ed. 2004: Chichester : Wiley.
16. Merkel, T.C., et al., *Effect of nanoparticles on gas sorption and transport in poly(1-trimethylsilyl-1-propyne)*. Macromolecules, 2003. **36**: p. 6844-6855.
17. Park, J.Y. and D.R. Paul, *Correlation and prediction of gas permeability in glassy polymer membrane materials via a modified free volume based group contribution method*. Journal of Membrane Science, 1997. **125**: p. 23-39.
18. Maeda, Y. and D.R. Paul, *Effect of antiplastification on gas sorption and transport. III. Free volume interpretation*. Journal of Polymer Science part B: Polymer Physics, 1987. **25**: p. 1005-1016.
19. Freeman, B., Y. Yampolskii, and I. Pinnau, *Materials science of membranes for gas and vapor separation*. 2006: Wiley.

20. Kanehashi, S. and K. Nagai, *Analysis of dual-mode model parameters for gas sorption in glassy polymers*. Journal of Membrane Science, 2005. **253**: p. 117-138.
21. Ismail, A.F. and W. Lorna, *Penetrant-induced plasticization phenomenon in glassy polymers for gas separation membrane*. Separation and Purification Technology, 2002. **27**(3): p. 173-194.
22. Cong, H., et al., *Polymer-inorganic nanocomposite membranes for gas separation*. Separation and Purification Technology, 2007. **55**: p. 281-291.
23. Chung, T.-S., et al., *Mixed matrix membranes (MMMs) comprising organic polymers with dispersed inorganic fillers for gas separation*. Polymer Science, 2007. **32**: p. 483-507.
24. Aroon, M.A., et al., *Performance studies of mixed membranes for gas separation: A review*. Separation and Purification Technology, 2010. **75**: p. 229-242.
25. Zimmerman, C.M., A. Singh, and W.J. Koros, *Tailoring mixed matrix composite membranes for gas separations*. Journal of Membrane Science, 1997. **137**: p. 145-154.
26. Rutherford, S.W., *Mechanism of sorption and diffusion in a high free-volume polymer*. Industrial & Engineering Chemistry Research, 2001. **40**: p. 1370-1376.
27. Bernardo, P., E. Drioli, and G. Golemme, *Membrane gas separation: A review/state of the art*. Industrial & Engineering Chemistry Research, 2009. **48**: p. 4639-4663.
28. McKeown, N.B., et al., *Polymers of intrinsic microporosity (PIMs): Bridging the void between microporous and polymeric materials*. Chemistry - A European Journal, 2005. **11**(9): p. 2610-2620.
29. Shantarovich, V.P., et al., *Positron annihilation lifetime study of high free volume glassy polymers: Effects on free volume sizes on the permeability and permselectivity*. Macromolecules, 2000. **33**: p. 7453-7466.
30. Morisato, A. and I. Pinnau, *Synthesis and gas permeation properties of poly(4-methyl-2-pentyne)*. Journal of Membrane Science, 1996. **121**: p. 243-250.
31. Nagai, K., et al., *Poly[1-(trimethylsilyl)-1-propyne] and related polymers: synthesis, properties and functions*. Progress in Polymer Science, 2001. **26**: p. 721-798.
32. Masuda, T., E. Isobe, and T. Higashimura, *Poly[1-(trimethylsilyl)-1-propyne]: A new high polymer synthesized with transition-metal catalysts and characterized by extremely high gas permeability*. American Chemical Society, 1983. **105**: p. 7473-7474.
33. Kelman, S.D., et al., *Crosslinking poly[1-(trimethylsilyl)-1-propyne] and its effect on physical stability*. Journal of Membrane Science, 2008. **320**: p. 123-134.
34. Morisato, A., et al., *Polymer characterization and gas permeability of poly(1-(trimethylsilyl)-1-propyne) [PTMSP], poly(1-phenyl-1-propyne) [PPP] and PTMSP/PPP blends*. Journal of Polymer Science B: Polymer Physics, 1996. **34**: p. 2209-2222.
35. Morliere, N., et al., *Impact of thermal ageing on sorption and diffusion properties of PTMSP*. Journal of Membrane Science, 2006. **270**: p. 123-131.
36. Merkel, T.C., et al., *Sorption and transport of hydrocarbon and perfluorocarbon gases in poly[1-(trimethylsilyl)-1-propyne]*. Journal of Polymer Science, Part B, 2000. **38**(2): p. 273-296.
37. Merkel, T.C., et al., *Gas Sorption, Diffusion, and Permeation in Poly(dimethylsiloxane)*. Journal of Polymer Science, Part B, 2000. **38**(3): p. 415-434.
38. Wang, X.-Y., et al., *Cavity size distributions in high free volume glassy polymers by molecular simulation*. Polymer, 2004. **45**: p. 3907-3912.
39. Ichiraku, Y. and S.A. Stern, *An investigation of the high gas permeability of poly(1-(trimethylsilyl)-1-propyne)*. Journal of Membrane Science, 1987. **34**(1): p. 5-18.
40. Nakagawa, T., et al., *Physical modification of poly[1-(trimethylsilyl)-1-propyne] membranes for gas separation*. Journal of Membrane Science, 1994. **94**(1): p. 183-193.
41. Nagai, K., A. Higuchi, and T. Nakagawa, *Gas permeation and sorption in brominated poly[1-(trimethylsilyl)-1-propyne] membrane*. Journal of Applied Polymer Science, 1994. **54**(9): p. 1353-1361.
42. Shao, L., J. Samseth, and M.-B. Hägg, *Crosslinking and stabilization of nanoparticle filled poly(1-(trimethylsilyl)-1-propyne) nanocomposite membranes for gas separations*. Journal of Applied Polymer Science, 2009. **113**: p. 3078-3088.

43. Kelman, S.D., et al., *Crosslinking poly(1-trimethylsilyl-1-propyne) and its effect on solvent resistance and transport properties*. *Polymer*, 2007. **48**(23): p. 6881-6892.
44. Matteucci, S., et al., *Gas transport in TiO<sub>2</sub> nanoparticle-filled poly(1-trimethylsilyl-1-propyne)*. *Journal of Membrane Science*, 2008. **307**(2): p. 196-217.
45. Matteucci, S., et al., *Gas transport properties of MgO filled poly(1-trimethylsilyl-1-propyne) nanocomposites*. *Polymer*, 2008. **49**(6): p. 1659-1675.
46. Kelman, S.D., et al., *The influence of crosslinking and fumed silica nanoparticles on mixed gas transport properties of poly[1-(trimethylsilyl)-1-propyne]*. *Polymer*, 2008. **49**(13-14): p. 3029-3041.
47. Kelman, S.D., *Crosslinking and stabilization of high fractional free volume polymers for the separation of organic vapors from permanent gases*, 2008, Ph.D. Dissertation. The University of Texas at Austin
48. Shao, L., *Crosslinking and stabilization of high free volume polymers for gas separations*, in *Department of Chemical Engineering* 2008, Ph.D Dissertation, Norwegian University of Science and Technology, Norway: Tapir Uttrykk.
49. Jia, J. and G.L. Baker, *Cross-linking of poly[1-(trimethylsilyl)-1-propyne] membranes using bis (aryl azides)*. *Journal of Applied Polymer Science*, 1998. **36**: p. 959-968.
50. Dean, J.A., *Lange's handbook of chemistry*. 15 ed. 1999, McGraw-Hill, New York.
51. Masuda, T., et al., *Polymerization of methylpentynes by transition metal catalysts: monomer structure, reactivity, and polymer properties*. *Polymer Journal*, 1982. **14**: p. 371-377.
52. Merkel, T.C., et al., *Sorption, transport, and structural evidence for enhanced free volume in poly(4-methyl-2-pentyne)/fumed silica nanocomposite membranes*. *Chemistry of Materials*, 2003. **15**: p. 109-123.
53. Merkel, T.C., et al., *Ultrapervious, reverse-selective nanocomposite membranes*. *Science*, 2002. **206**: p. 519-522.
54. Budd, P.M., et al., *Gas separation membranes from polymers of intrinsic microporosity*. *Journal of Membrane Science*, 2005. **251**(2005): p. 263-269.
55. McKeown, N.B. and P.M. Budd, *Polymers of Intrinsic Microporosity (PIMs): organic materials for membrane separations, heterogeneous catalysis and hydrogen storage*. *Chemical Society Reviews*, 2006. **35**(8): p. 675-683.
56. Gabelman, A. and S.-T. Hwang, *Hollow fiber membrane contactors*. *Journal of Membrane Science*, 1999. **159**: p. 61-106.
57. Nguyen, P.T., et al., *A dense membrane contactor for intensified CO<sub>2</sub> gas/liquid absorption in post-combustion capture*. *Journal of Membrane Science*, 2011. **377**: p. 261-272.
58. Falk-Pedersen, O., et al., *CO<sub>2</sub> capture with membrane contactors*. *International Journal of Green Energy*, 2005. **2**: p. 157-165.
59. Qi, Z. and E.L. Cussler, *Microporous hollow fibers for gas absorption Part I. mass transfer in the liquid*. *Journal of Membrane Science*, 1985. **23**: p. 321-332.
60. Qi, Z. and E.L. Cussler, *Microporous hollow fibers for gas absorption Part II. mass transfer across the membrane*. *Journal of Membrane Science*, 1985. **23**: p. 333-345.
61. Lu, J.-G., Y.-F. Zheng, and M.-D. Cheng, *Wetting mechanism in mass transfer process of hydrophobic membrane gas absorption*. *Journal of Membrane Science*, 2008. **308**(1-2): p. 180-190.
62. Kumar, P.S., et al., *New absorption liquids for the removal of CO<sub>2</sub> from dilute gas streams using membrane contactors*. *Chemical Engineering Science*, 2002. **57**(9): p. 1639-1651.
63. B.-S., K. and P. Harriott, *Critical entry pressure for liquids in hydrophobic membranes*. *Journal of Colloid and Interface Science*, 1986. **115**(1): p. 1-8.
64. Trusov, A., et al., *Gas/liquid membrane contactors based on disubstituted polyacetylene for CO<sub>2</sub> absorption liquid regeneration at high pressure and temperature*. *Journal of Membrane Science*, 2011. **383**(1-2): p. 241-249.
65. Paul, S., A.K. Ghoshal, and B. Mandal, *Removal of CO<sub>2</sub> by single and blended aqueous alkanolamine solvents in hollow-fiber membrane contactor: modeling and simulation*. *Industrial & Engineering Chemical Research*, 2007. **46**(8): p. 2576-2588.
66. Alavinasab, A., et al., *Modeling of carbon dioxide absorption in a gas/liquid membrane contactor*. *Desalination and Water Treatment*, 2011. **29**: p. 336-342.

67. Barth, D., C. Tondre, and J.-J. Delpuech, *Kinetics and mechanisms of the reactions of carbon dioxide with alkanolamines: A discussion concerning the cases of MDEA and DEA*. Chemical Engineering Science, 1984. **39**(12): p. 1753-1757.
68. Drioli, E., A. Criscuoli, and E. Curcio, *Membrane contactors: Fundamentals, application and potentialities*. 2006, Amsterdam: Elsevier. xiii, 502.
69. Kreulen, H., et al., *Determination of mass transfer rates in wetted and non-wetted microporous membranes*. Chemical Engineering Science, 1993. **48**(11): p. 2093-2102.
70. Dindore, V.Y., et al., *CO<sub>2</sub> absorption at elevated pressures using a hollow fiber membrane contactor* Journal of Membrane Science, 2004. **235**: p. 99-109.
71. Falk-Pedersen, O. and H. Dannström, *Separation of carbon dioxide from offshore gas turbine exhaust*. Energy Conversion and Management, 1997. **38**: p. 81-86.
72. Dindore, V.Y., et al., *Membrane-solvent selection for CO<sub>2</sub> removal using membrane gas-liquid contactors*. Separation and Purification Technology, 2004. **40**: p. 133-145.
73. Nishikawa, N., et al., *CO<sub>2</sub> removal by hollow-fiber gas-liquid contactor*. Energy Conversion and Management, 1995. **36**: p. 415-418.
74. Marzouk, S.A.M., et al., *Removal of carbon dioxide from pressurized CO<sub>2</sub>-CH<sub>4</sub> gas mixture using hollow fiber membrane contactors*. Journal of Membrane Science, 2010. **351**: p. 21-27.
75. Rangwala, H.A., *Absorption of carbon dioxide into aqueous solutions using hollow fiber membrane contactors*. Journal of Membrane Science, 1996. **112**: p. 229-240.
76. R., W., et al., *Impact of DEA solutions with and without CO<sub>2</sub> loading on porous polypropylene membranes intended for use as contactors*. Journal of Membrane Science, 2004. **229**: p. 147-157.
77. Yan, S., et al., *Experimental study on the separation of CO<sub>2</sub> from flue gas using hollow fiber membrane contactors without wetting*. Fuel Processing Technology, 2007. **88**: p. 501-511.
78. Simons, K., K. Nijmeijer, and M. Wessling, *Gas-liquid membrane contactors for CO<sub>2</sub> removal*. Journal of Membrane Science, 2009. **340**: p. 214-220.
79. Yeon, S.-H., et al., *Application of pilot-scale membrane contactor hybrid system for removal of carbon dioxide from flue gas* Journal of Membrane Science, 2005. **257**: p. 156-160.
80. Yeon, S.-H., et al., *Determination of mass transfer rates in PVDF and PTFE hollow fiber membranes for CO<sub>2</sub> absorption*. Separation Science and Technology, 2003. **38**(2): p. 271-293.
81. Khaisri, S., et al., *Comparing membrane resistance and absorption performance of three different membranes in a gas absorption membrane contactor*. Separation and Purification Technology, 2009. **65**: p. 290-297.
82. Franco, J., et al., *A study of the mass transfer of CO<sub>2</sub> through different membrane materials in the membrane gas absorption process*. Separation and Purification Technology, 2008. **43**(2): p. 225-244.
83. Tomasa, T., *Development of membrane materials for gas-liquid membrane contactors for CO<sub>2</sub> capture from natural gas*, 2012: Specialization project 2012, Department of Chemical Engineering.
84. Hoff, K.A., *Modeling and experimental study of carbon dioxide absorption in a membrane contactor*, in *Department of Chemical Engineering 2003*, Ph.D Dissertation, Norwegian University of Science and Technology, Norway.
85. Nicolet, T. *Introduction to fourier transform infrared spectrometry*. [cited 2012 11/08]; Available from: [www.thermonicolet.com](http://www.thermonicolet.com).
86. Silverstein, R.M., F.X. Webster, and D.J. Kiemle, *Spectrometric identification of organic compounds*. 7 ed. 2005: John Wiley & Sons.
87. scientific, B. *Theta Lite Optical Tensiometer*. [cited 2012 10/15]; Available from: <http://www.attension.com/theta-lite>.
88. *Contact angle*. [cited 2012 10/15]; Available from: [http://www.attension.com/contact-angle?\\_kk=contact%20angle%20measurement&\\_kt=8aec43de-d800-4d3c-8402-7cbba5e92fdc&\\_gclid=CLTC3Kui0bMCFax7cAod\\_wkAvA](http://www.attension.com/contact-angle?_kk=contact%20angle%20measurement&_kt=8aec43de-d800-4d3c-8402-7cbba5e92fdc&_gclid=CLTC3Kui0bMCFax7cAod_wkAvA).
89. Decker, E.L., et al., *Physics of contact angle measurement*. Colloids and Surfaces A: Physicochemical and Engineering Aspects, 1999. **156**: p. 177-189.
90. Coats, A.W. and J.P. Redfern, *Thermogravimetric analysis. A review*. Analyst, 1963. **88**(1053): p. 906-924.



## 10. REFERENCES

---

91. Gabbott, P., *Principles and applications of thermal analysis*. 2008: Blackwell Publishing.
92. Walpole, R.E., et al., *Probability & statistics for engineers and scientists*. 2007: Pearson Prentice Hall.
93. Aruldas, G., *Molecular structure and spectroscopy*. 2001, New Delhi, India: Prentice-Hall.
94. Ditter, K.D., et al., *Silica filled poly(1-trimethylsilyl-1-propyne) nanocomposite membranes: Relation between the transport of the gases and structural characteristics*. Journal of Membrane Science, 2006. **278**: p. 83-91.
95. Schultz, J. and K.-V. Peinemann, *Membranes for separation of higher hydrocarbons from methane*. Journal of Membrane Science, 1995. **110**(1): p. 37-45.
96. Nisoli, E., et al., *Chlorination of poly[1-trimethylsilyl-1-propyne] membrane*. Macromolecules, 1999. **32**: p. 7263-7268.
97. Seglem, K.N., *Development of membrane material for a membrane contactor for natural gas sweetening*, 2013: Norwegian University of Science and Technology, [pers.comm.].
98. Srinivasan, R., S.R. Auvil, and P.M. Burban, *Elucidating the mechanism (s) of gas transport in poly[1-trimethylsilyl-1-propyne] (PTMSP) membranes*. Journal of Membrane Science, 1994. **86**(1-2): p. 67-86.
99. Sanders, E.S., *Penetrant-induced plasticization and gas permeation in glassy polymers*. Journal of Membrane Science, 1988. **37**(1): p. 63-80.
100. Tasaka, S., N. Inagaki, and M. Igawa, *Effect of annealing on structure and permeability of poly(1-trimethylsilyl-1-propyne)*. Journal of Polymer Science: Part B: Polymer Physics, 1991. **29**(6): p. 691-694.



## APPENDIX

## A. FT-IR SPECTROSCOPY RESULTS

Fourier Transform Infrared spectroscopy (FT-IR), Thermo Nicolet, is used to determine the chemical components in the various membranes made in the laboratory. All membranes were tested, but only some results are presented here. Some interesting results have been discovered by testing membranes in “tested areas” which have been in contact with the various gases ( $N_2$ ,  $CH_4$  and  $CO_2$ ) and can be seen in Figure A.3 and Figure A.4. Other results show that long-term exposure of PTMSP in distilled water, 2M MDEA and 4.2 M MDEA indicate chemical stability of the polymer (Figure A.5 and Figure A.6).

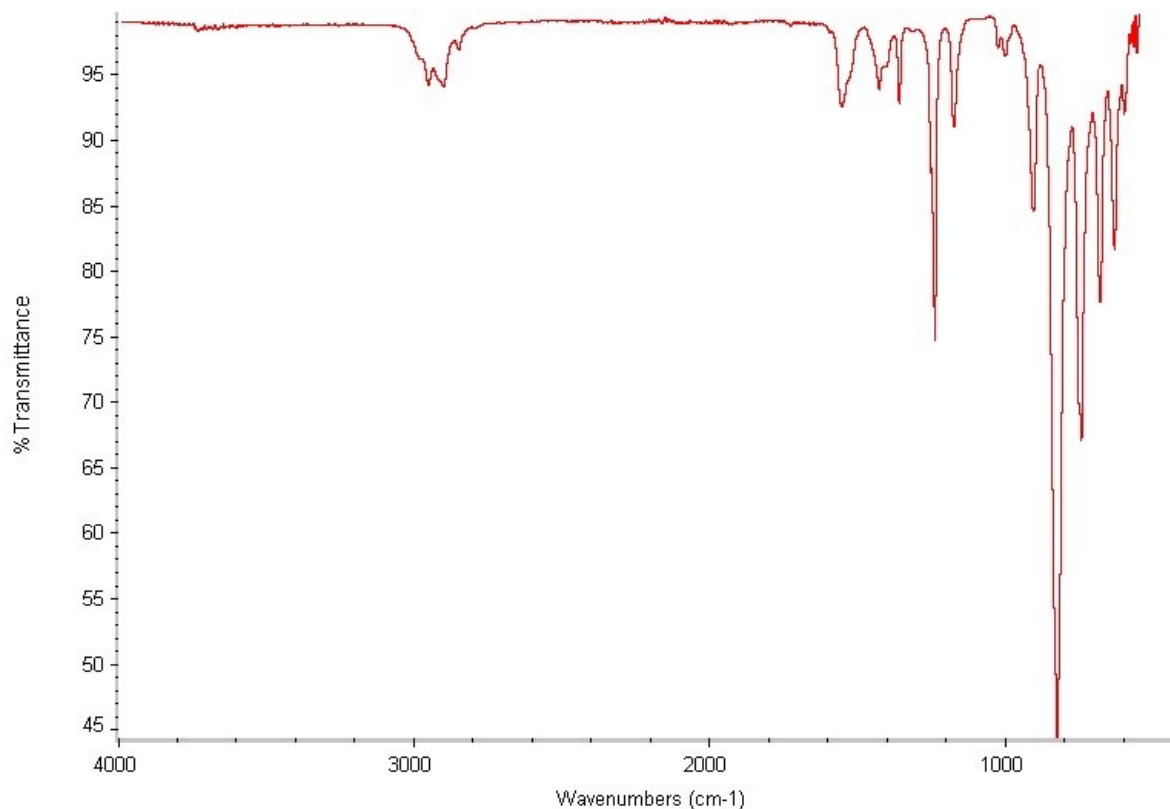


**Figure A.1** FT-IR spectra of a membrane containing crosslinked PTMSP with 1.5wt% BAA

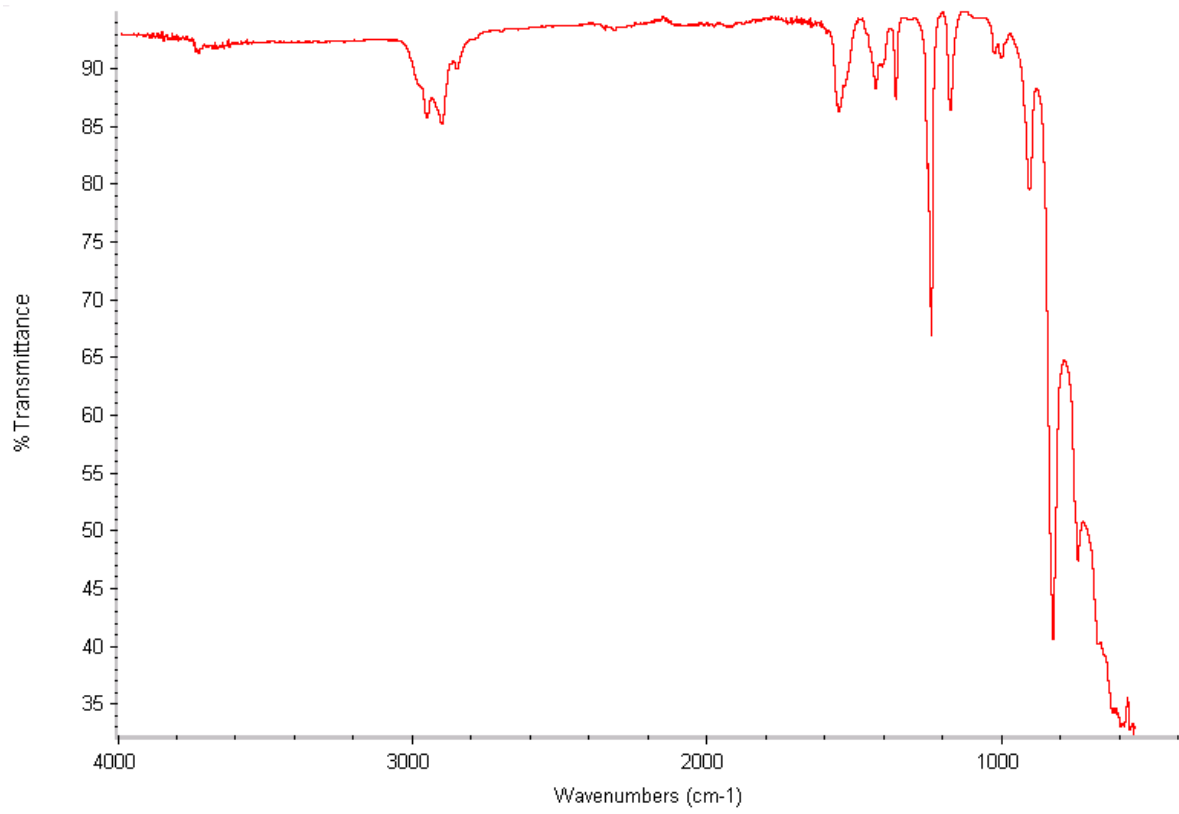


**Figure A.2** FT-IR spectra of a membrane containing crosslinked nanofilled PTMSP with 1.5wt% BAA and 10wt% TiO<sub>2</sub> nanoparticles

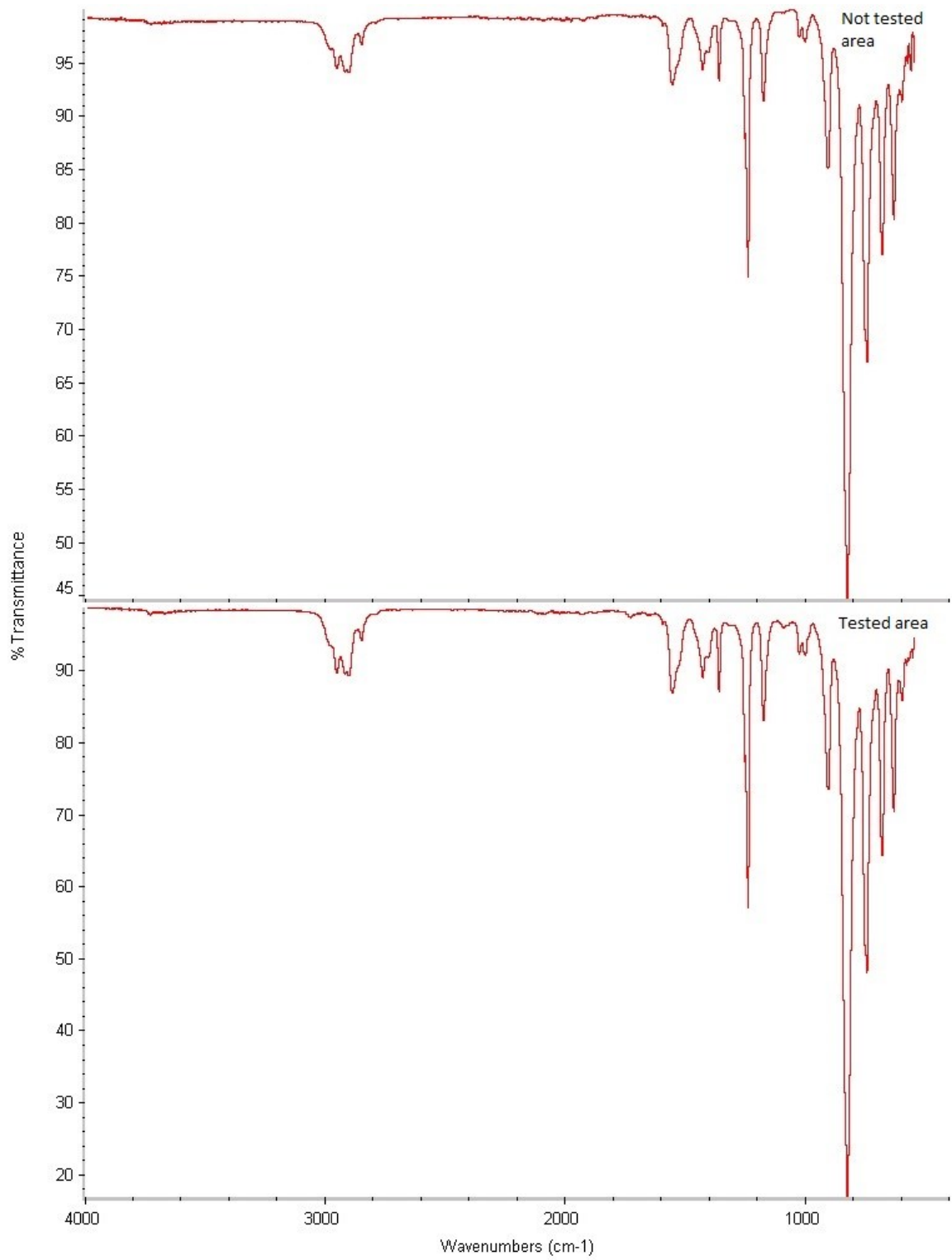


**Figure A.3** FT-IR spectra of a membrane containing crosslinked PTMSP with 2wt% BAA in a non-gas tested- and gas tested area

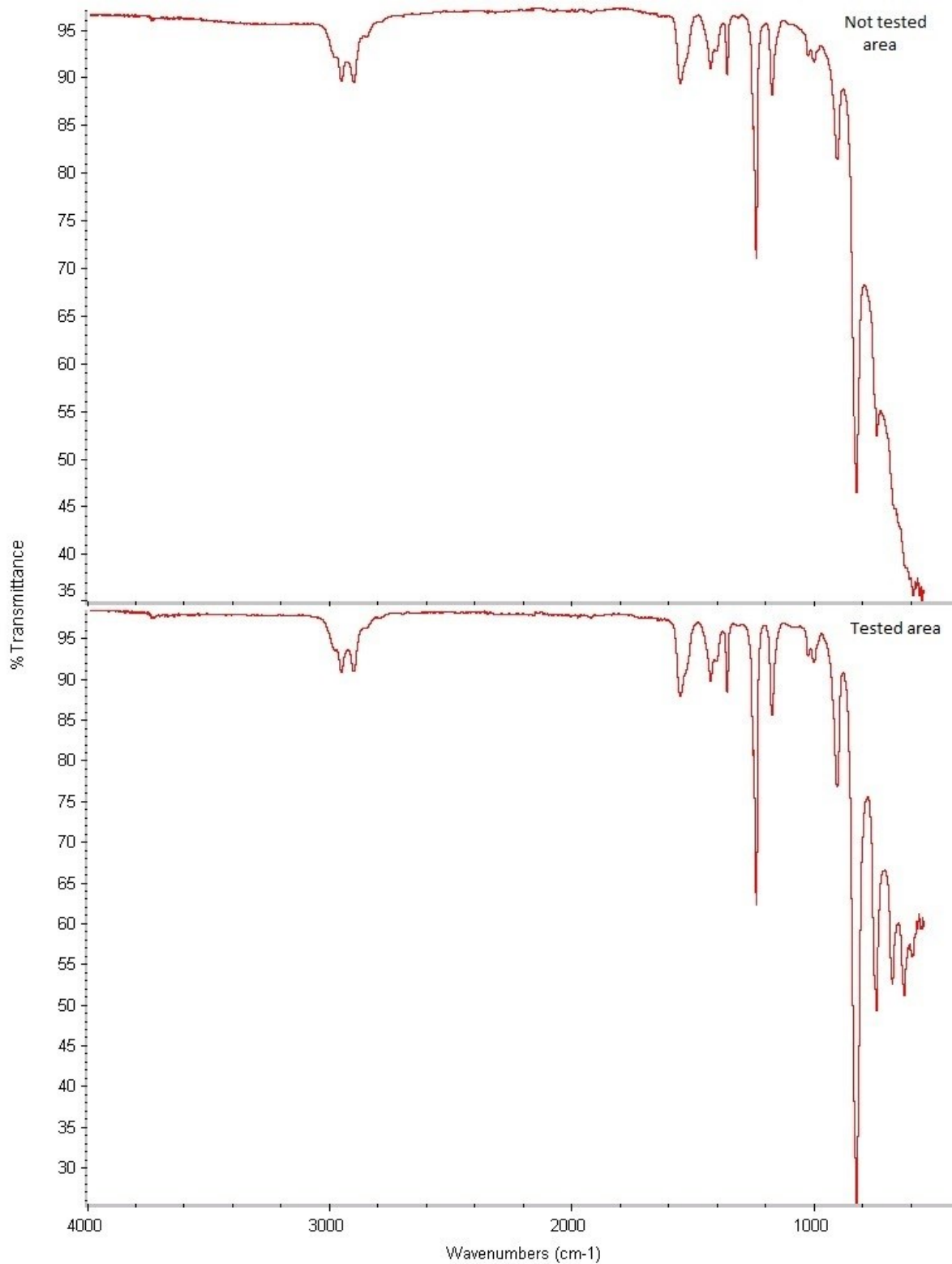


**Figure A.4** FT-IR spectra of a membrane containing nanofilled PTMSP with 20wt% TiO<sub>2</sub> nanoparticles in a non-gas tested- and gas tested area

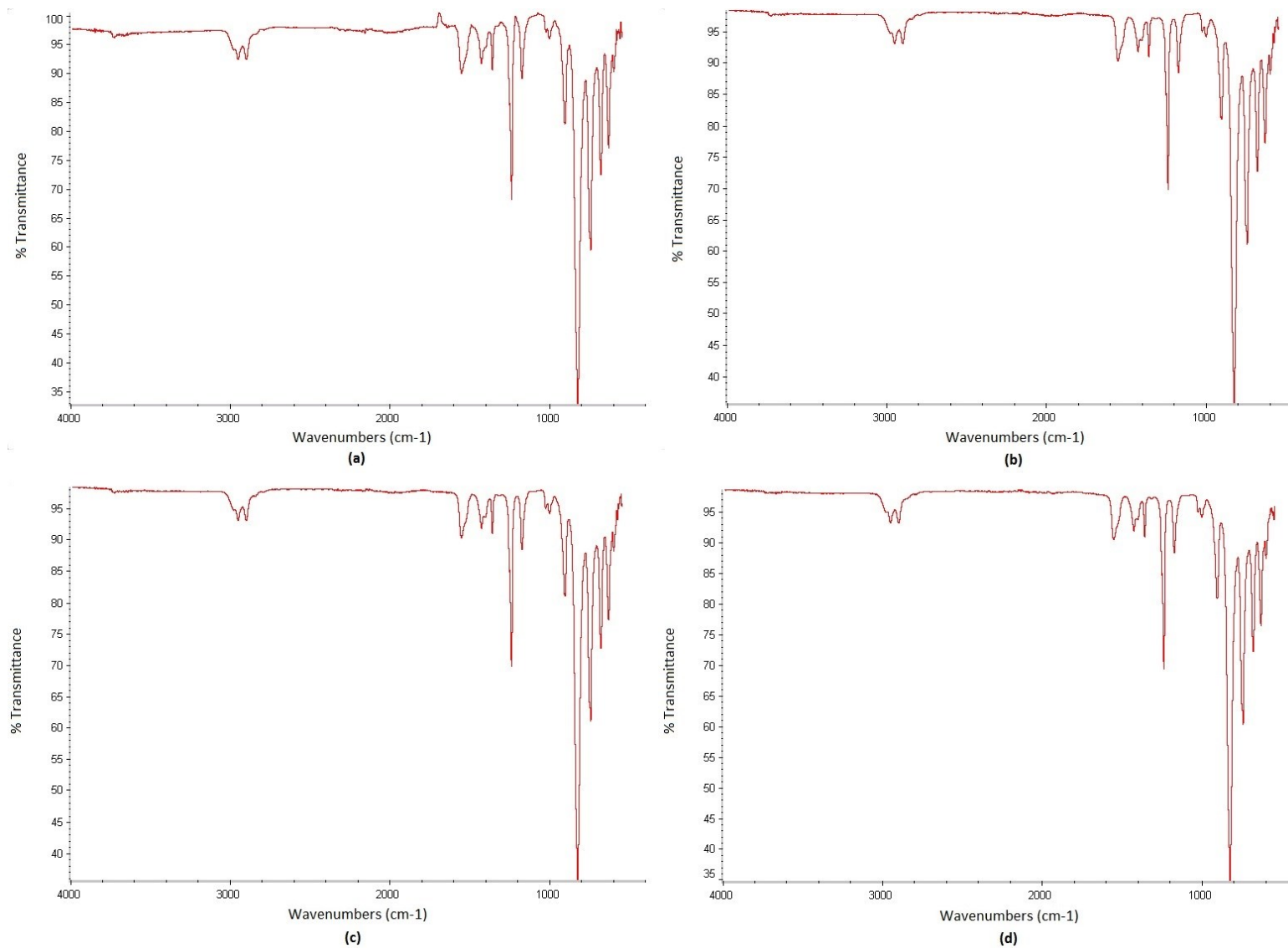


**Figure A.5** FT-IR spectra of PTMSP membranes treated with (a) no solution (b) distilled water (c) 2 M MDEA and (d) 4.2 M MDEA for 2 weeks

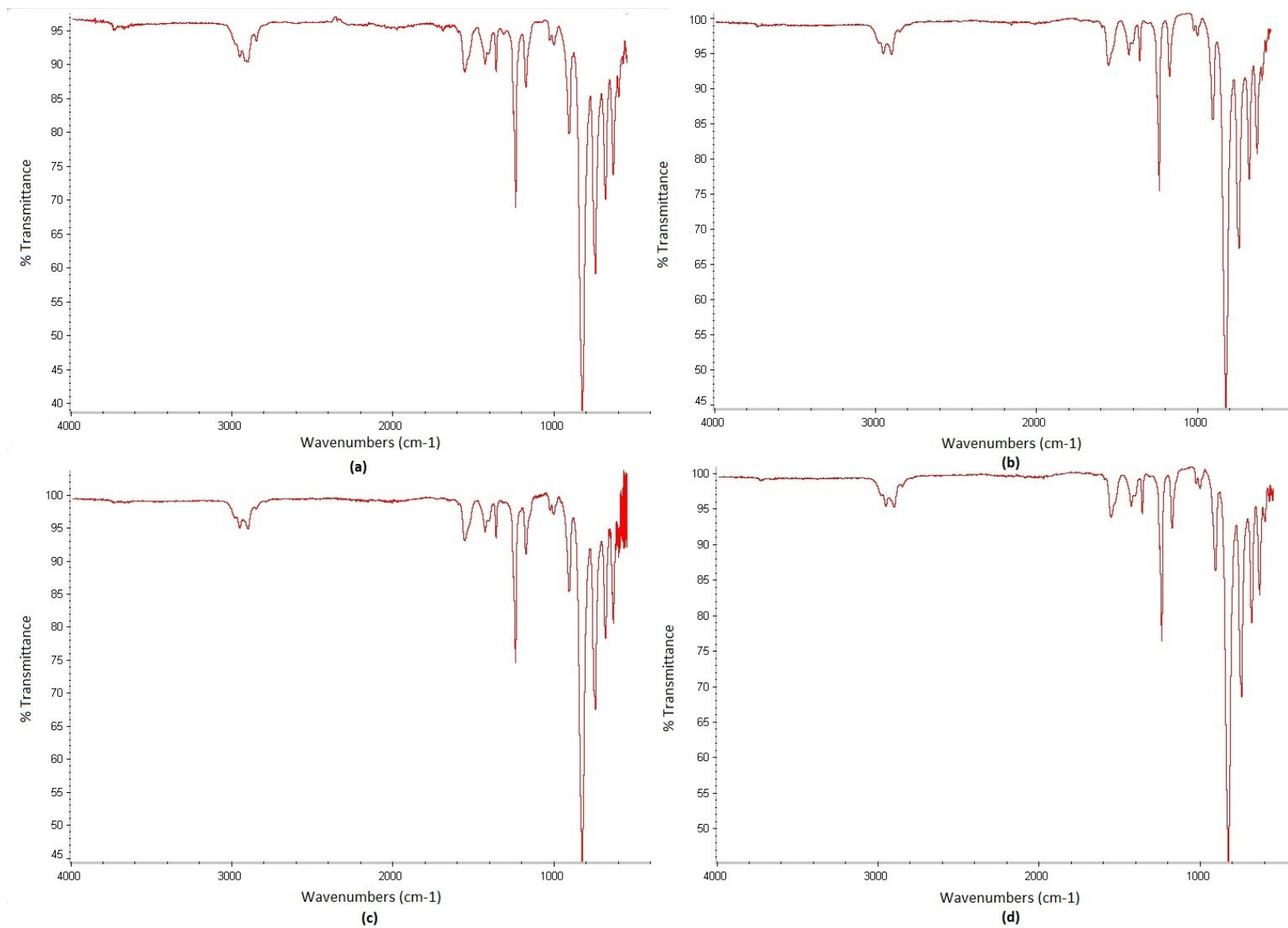


**Figure A.6** FT-IR spectra of crosslinked PTMSP with 3wt% BAA membranes treated with (a) no solution (b) distilled water (c) 2M MDEA and (d) 4.2M MDEA for 2 weeks



## B. GAS PERMEABILITY CALCULATIONS AND RESULTS

### B.1 Gas permeability calculations

The gas permeability calculations were done by the following equation:

$$P = \frac{l}{A T p_0} \frac{V T_0}{(p_1 - p_2)} \frac{dp}{dt} \quad (\text{B.1})$$

The parameters and values of an example with N<sub>2</sub> permeability in a membrane of pure PTMSP are given in Table B.1.

**Table B.1** Values of the parameters for gas permeability of N<sub>2</sub> at 2 bar for a pure PTMSP membrane

Symbol	Description	Value
l [μm]	Membrane thickness	28
V [cm <sup>3</sup> ]	Volume in the chamber	173
T <sub>0</sub> [K]	Standard temperature	273.15
dp/dt [mbar/s]	Steady state pressure change	0.1994
A [cm <sup>2</sup> ]	Membrane area	1.5394
T [K]	Gas temperature	295
p <sub>0</sub> [bar]	Standard pressure	1.0133
p <sub>1</sub> [bar]	Feed pressure	2.22
p <sub>2</sub> [mbar]	Permeate pressure	16.47

The thickness *l* was measured by using an instrument, Digitrix II Disc Micrometer. The steady state pressure change on the permeate side was detected by a MKS Baraton® 0-100 mbar pressure transducer which was logged in the software LabView. With linear regression of permeate pressure (*p*<sub>2</sub>) versus time (*t*) in Excel, the steady state pressure change was found. The permeability for this example was calculated in the following way:

$$P \left[ \frac{\text{m}^3(\text{STP})\text{m}}{\text{m}^2\text{hbar}} \right] = \frac{(l [\mu\text{m}] \cdot 10^{-6} \left[ \frac{\text{m}}{\mu\text{m}} \right]) (V [\text{cm}^3] \cdot 10^{-6} \left[ \frac{\text{m}^3}{\text{cm}^3} \right]) \cdot T_0 [\text{K}] \cdot \left( \frac{dp [\text{mbar}]}{dt [\text{s}]} \right) \cdot 10^{-3} \left[ \frac{\text{bar}}{\text{mbar}} \right] \cdot 3600 \left[ \frac{\text{s}}{\text{h}} \right]}{A [\text{cm}^2] \cdot 10^{-4} \left[ \frac{\text{m}^2}{\text{cm}^2} \right] \cdot T [\text{K}] \cdot p_0 [\text{bar}] \cdot (p_1 [\text{bar}] - p_2 [\text{mbar}] \cdot 10^{-3} \left[ \frac{\text{bar}}{\text{mbar}} \right])} \quad (\text{B.2})$$

Insertion of the values from Table B.1 into Eq. B.2 gives a permeability of 3 505 Barrer (= m<sup>3</sup>(STP)m.m<sup>-2</sup>h<sup>-1</sup>bar<sup>-1</sup>).

## **B.2 Gas permeability results**

All the gas permeabilities of the membranes tested in this work are presented in Table B.2, Table B.3, Table B.4 and Table B.5. In addition to permeabilities, information about aging is given. The membrane ID consists of several numbers. The six first numbers represent the date the membranes were casted from the polymer solutions. The following three numbers represents the polymer, BAA and TiO<sub>2</sub> concentration, respectively. This means that for pure PTMSP, the numbers are given as 2-0-0, and for PTMSP with 20 wt% TiO<sub>2</sub> nanoparticles the numbers are 2-0-20, and so on. The last number represents the membrane parallel.

**Table B.2** Gas permeabilities of membranes from DOE

Membrane ID	Membrane thickness [μm]	Aging [days]	Permeability [Barrer]								
			N <sub>2</sub>			CH <sub>4</sub>			CO <sub>2</sub>		
			2 bar	4 bar	6 bar	2 bar	4 bar	6 bar	2 bar	4 bar	6 bar
<i>Pure PTMSP membranes</i>											
28.01.13_2-0-0_1	64.0	17	3 972	3 956	3 943	9 082	9 173	9 144	27 036	26 777	26 149
06.02.13_2-0-0_1	28.8	11	2 026	2 055	2 088	3 444	3 587	3 722	14 812	15 120	15 145
06.02.13_2-0-0_2	28.0	13	3 505	3 533	3 579	5 327	7 602	7 729	20 446	20 891	20 869
06.02.13_2-0-0_3	28.2	15	3 532	3 579	3 625	7 626	7884	8 068	23 011	23 424	23 336
06.02.13_2-0-0_5	26.8	59	-	-	-	3 045	3 188	3 327	16 377	16 586	16 698
06.02.13_2-0-0_6	27.2	93	-	-	-	4 217	4 190	3 934	11 646	13 290	14 982
<i>Crosslinked PTMSP with 3 wt% BAA</i>											
12.02.13_2-3-0_1	35.4	14	242	240	241	566	564	556	3 271	3 208	3 121
12.02.13_2-3-0_2	36.4	15	251	244	246	572	571	559	3 206	3 124	3 001
12.02.13_2-3-0_7	29.2	44	-	-	-	714	711	702	3 919	3 830	3 660
12.02.13_2-3-0_8	31.0	82	-	-	-	311	314	302	1 772	1 741	1 586
<i>Crosslinked nanofilled PTMSP with 3wt% BAA and 20 wt% TiO<sub>2</sub></i>											
14.02.13_2-3-20_1	33.6	15	760	544	607	926	1 020	1 091	3 206	3 229	3 110
14.02.13_2-3-20_2	33.0	18	170	168	168	398	397	390	2 258	2 226	2 154
14.02.13_2-3-20_3	32.6	20	90	89	90	211	213	215	1 319	1 342	1 325
<i>Crosslinked nanofilled PTMSP with 1.5 wt% BAA and 10 wt% TiO<sub>2</sub></i>											
25.02.13_2-1.5-10_1	34.6	11	1 226	1 224	1 228	2 718	2 733	2 718	10 389	10 312	9 938
25.02.13_2-1.5-10_2	39.6	14	1 131	1 131	1 133	2 490	2 487	2 463	10 472	10 257	9 843
25.02.13_2-1.5-10_3	37.4	16	586	585	587	1 292	1 294	1 277	5 516	5 429	5 088
<i>Nanofilled PTMSP with 20wt% TiO<sub>2</sub></i>											
04.03.13_2-0-20_1	35.6	11	3 118	3 187	3 262	6 502	6 818	7 075	22 796	23 175	23 414
04.03.13_2-0-20_2	34.1	14	3 024	3 051	3 097	6 720	6 879	6 999	22 351	22 417	22 227
<i>Crosslinked PTMSP with 1.5 wt% BAA</i>											
21.03.13_2-1.5-0_1	32.6	14	-	-	-	2 213	2 229	2 213	8 950	8 840	8 361
<i>Crosslinked PTMSP with 2 wt% BAA</i>											
21.03.13_2-2-0_1	28.8	15	-	-	-	753	775	767	3 971	3 924	3 751
<i>Crosslinked nanofilled PTMSP with 2wt% BAA and 20 wt% TiO<sub>2</sub></i>											
21.02.13_2-2-20_2	42.4	17	-	-	-	947	965	968	4 825	4 827	4 651

**Table B.3** Permeability and selectivity of pure PTMSP membranes which have been treated with distilled water, 2M MDEA and 4.2M MDEA up to 10 weeks

Membrane ID	Solution	Time in solution [weeks]	Aging [days]	Permeability [Barrer]						Selectivity [-]		
				CH <sub>4</sub>			CO <sub>2</sub>			CO <sub>2</sub> / CH <sub>4</sub>		
				2 bar	4 bar	6 bar	2 bar	4 bar	6 bar	2 bar	4 bar	6 bar
06.02.13_2-0-0_7	Distilled water	0.143	41	5 914	6 162	6 318	20 668	21 059	20 839	3.49	3.42	3.30
05.03.13_2-0-0_3	Distilled water	1	29	6 513	6 795	6 986	23 959	24 244	24 306	3.68	3.57	3.48
05.03.13_2-0-0_6	Distilled water	2	33	4 858	5 097	5 286	19 515	20 140	20 333	4.02	3.95	3.85
04.03.13_2-0-0_13	Distilled water	3	35	4 830	5 111	5 278	20 070	20 515	20 518	4.16	4.01	3.89
04.03.13_2-0-0_10	Distilled water	4	42	3 703	3 874	3 977	15 965	16 252	16 280	4.31	4.20	4.09
04.03.13_2-0-0_7	Distilled water	6	57	3 048	3 212	3 377	14 729	15 213	15 609	4.83	4.74	4.62
04.03.13_2-0-0_4	Distilled water	8	70	2 303	2 442	2 417	9 280	9 706	9 744	4.03	3.98	4.03
04.03.13_2-0-0_1	Distilled water	10	83	3 317	3 476	3 666	15 063	15 714	16 143	4.54	4.52	4.40
06.02.13_2-0-0_8	2M MDEA	0.143	42	5 521	5 781	5 957	20 343	20 718	20 957	3.68	3.58	3.52
05.03.13_2-0-0_4	2M MDEA	1	30	5 025	5 173	5 297	19 528	19 660	19 538	3.89	3.80	3.69
05.03.13_2-0-0_7	2M MDEA	2	34	4 042	4 168	4 289	15 940	16 132	16 142	3.94	3.87	3.76
05.03.13_2-0-0_1	2M MDEA	3	35	5 202	5 600	5 732	20 563	21 111	21 205	3.95	3.77	3.70
04.03.13_2-0-0_11	2M MDEA	4	43	3 725	3 967	4 200	18 265	18 846	19 186	4.90	4.75	4.57
04.03.13_2-0-0_8	2M MDEA	6	58	4 389	4 600	4 785	17 559	17 898	18 176	4.00	3.89	3.80
04.03.13_2-0-0_6	2M MDEA	8	71	2 160	4 294	3 950	9 140	10 999	9 923	4.23	2.56	2.51
04.03.13_2-0-0_2	2M MDEA	10	84	2 912	3 073	3 243	15 302	16 264	16 787	5.26	5.29	5.18
06.02.13_2-0-0_9	4.2M MDEA	0.143	43	5 941	6 177	6 945	22 801	22 873	22 479	3.84	3.70	3.24
05.03.13_2-0-0_5	4.2M MDEA	1	31	5 272	5 510	5 723	21 459	21 828	21 932	4.07	3.96	3.83
05.03.13_2-0-0_8	4.2M MDEA	2	35	4 909	5 151	5 388	20 417	21 057	21 282	4.16	4.09	3.95
05.03.13_2-0-0_3	4.2M MDEA	3	36	4 662	4 929	5 052	20 383	20 918	21 071	4.37	4.24	4.17
04.03.13_2-0-0_12	4.2M MDEA	4	44	3 587	3 808	3 986	17 820	18 110	18 327	4.97	4.76	4.60
04.03.13_2-0-0_9	4.2M MDEA	6	59	4 221	4 434	4 644	17 191	17 611	17 734	4.07	3.97	3.82
04.03.13_2-0-0_6	4.2M MDEA	8	72	3 352	3 369	3 285	9 360	10 612	9 496	2.79	3.15	2.89
04.03.13_2-0-0_3	4.2M MDEA	10	85	4 229	4 448	4 616	15 727	16 634	17 102	3.72	3.74	3.71

**Table B.4** Permeability and selectivity of crosslinked PTMSP membranes with 3 wt% BAA which have been treated with distilled water, 2M MDEA and 4.2M MDEA up to 10 weeks

Membrane ID	Solution	Time in solution [weeks]	Aging [days]	Permeability [Barrer]						Selectivity [-]		
				CH <sub>4</sub>			CO <sub>2</sub>			CO <sub>2</sub> / CH <sub>4</sub>		
				2 bar	4 bar	6 bar	2 bar	4 bar	6 bar	2 bar	4 bar	6 bar
13.03.13_2-3-0_7	Distilled water	0.143	28	3 594	3 586	3 557	12 976	12 842	12 427	3.61	3.58	3.49
13.03.13_2-3-0_4	Distilled water	1	36	2 189	2 223	2 243	9 856	9 885	9 731	4.50	4.45	4.34
12.03.13_2-3-0_10	Distilled water	2	30	3 023	3 040	3 027	11 422	11 407	11 162	3.78	3.75	3.69
13.03.13_2-3-0_7	Distilled water	3	40	2 415	2 430	2 434	10 265	10 320	10 125	4.25	4.25	4.16
12.03.13_2-3-0_4	Distilled water	4	44	2 547	2 576	2 593	10 982	11 023	10 905	4.31	4.28	4.21
12.03.13_2-3-0_1	Distilled water	6	56	2 511	2 487	2 379	10 278	10 169	9 629	4.09	4.09	4.05
25.02.13_2-3-0_1	Distilled water	8	84	1 531	1 533	1 534	6 822	6 776	6 562	4.46	4.42	4.28
12.02.13_2-3-0_3	Distilled water	10	91	189	200	194	1 308	1 326	1 326	6.93	6.63	6.83
13.03.13_2-3-0_8	2M MDEA	0.143	29	2 241	2 253	2 256	10 062	10 030	9 876	4.49	4.45	4.38
13.03.13_2-3-0_5	2M MDEA	1	37	2 189	2 174	2 148	9 242	8 909	8 469	4.22	4.10	3.94
13.03.13_2-3-0_1	2M MDEA	2	30	2 894	2 952	2 948	11 269	11 281	11 070	3.89	3.82	3.75
12.03.13_2-3-0_8	2M MDEA	3	42	2 077	2 125	2 142	8 660	8 846	8 756	4.17	4.16	4.09
12.03.13_2-3-0_5	2M MDEA	4	45	1 834	1 853	1 868	7 980	7 914	7 861	4.35	4.27	4.21
12.03.13_2-3-0_2	2M MDEA	6	57	2 546	2 450	2 224	9 329	9 270	8 527	3.66	3.78	3.83
13.03.13_2-3-0_9	2M MDEA	8	68	1 520	1 657	1 630	3 162	3 361	3 369	2.08	2.03	2.07
12.02.13_2-3-0_4	2M MDEA	10	92	417	418	413	2 549	2 506	2 451	6.11	6.00	5.94
12.02.13_2-3-0_6	4.2M MDEA	0.143	59	215	218	221	1 550	1 555	1 560	7.20	7.13	7.07
13.03.13_2-3-0_6	4.2M MDEA	1	39	2 601	2 631	2 641	11 720	11 661	11 241	4.51	4.43	4.26
13.03.13_2-3-0_2	4.2M MDEA	2	32	1 838	1 879	1 867	6 878	6 855	6 754	3.74	3.65	3.62
12.03.13_2-3-0_9	4.2M MDEA	3	43	1 102	1 111	1 114	5 355	5 368	5 223	4.86	4.83	4.69
12.03.13_2-3-0_6	4.2M MDEA	4	48	1 002	1 014	1 017	5 108	5 107	5 006	5.10	5.04	4.92
12.03.13_2-3-0_3	4.2M MDEA	6	58	3 318	4 231	4 543	5 367	6 629	6 505	1.62	1.57	1.43
13.03.13_2-3-0_10	4.2M MDEA	8	69	1 376	1 378	1 366	6 242	6 218	5 952	4.53	4.51	4.36
12.02.13_2-3-0_5	4.2M MDEA	10	93	311	308	308	1 952	1 891	1 878	6.28	6.15	6.10

**Table B.5** Permeability and selectivity of crosslinked nanofilled PTMSP membranes with 3wt% BAA and 20wt% TiO<sub>2</sub> which have been treated with distilled water, 2M MDEA and 4.2M MDEA up to 4 weeks

Membrane ID	Solution	Time in solution [weeks]	Aging [days]	Permeability [Barrer]						Selectivity [-]		
				CH <sub>4</sub>			CO <sub>2</sub>			CO <sub>2</sub> / CH <sub>4</sub>		
				2 bar	4 bar	6 bar	2 bar	4 bar	6 bar	2 bar	4 bar	6 bar
17.04.13_2-2-20_1	Distilled water	2	29	59	62	62	313	407	428	5.31	6.58	6.92
17.04.13_2-2-20_4	Distilled water	4	39	55	60	61	345	395	420	6.33	6.59	6.94
17.04.13_2-2-20_2	2M MDEA	2	31	43	44	45	325	336	352	7.55	7.57	7.82
17.04.13_2-2-20_5	2M MDEA	4	40	49	53	52	305	345	363	6.27	6.45	6.92
17.04.13_2-2-20_3	4.2M MDEA	2	31	31	34	35	173	225	245	5.64	6.60	7.10
17.04.13_2-2-20_6	4.2M MDEA	4	41	31	35	35	199	227	244	6.39	6.54	7.04

## C. CONTACT ANGLE MEASUREMENTS

The results from the water contact angle measurements are given in Table C.1. Three parallels were performed per membrane. Each measurement was done after 10 minutes from the water droplet hit the membrane. The mean value is presented with a standard deviation.

**Table C.1** Water contact angles of the membranes prepared for DOE

Membrane Composition		Contact angle, $\Theta$ [°]			
wt% BAA	wt% TiO <sub>2</sub>	Parallel 1	Parallel 2	Parallel 3	Mean value
None	None	120	129	123	124 ± 3.78
1.5	None	94	99	95	96 ± 2.04
2.0	None	90	97	96	95 ± 2.99
3.0	None	103	103	22	102 ± 1.90
None	20.0	142	130	135	136 ± 4.89
1.5	10.0	93	93	96	93 ± 1.27
2.0	20.0	90	97	96	95 ± 2.99
3.0	20.0	88	75	73	79 ± 6.92

The results of the contact angles of the membrane that have been in contact with distilled water, 2M MDEA and 4.2M MDEA for several weeks are presented in Table C.2, Table C.3, Table C.4.

The membrane ID consists of several numbers. The six first numbers represent the date the membranes were casted from the polymer solutions. The following three numbers represents the polymer, BAA and TiO<sub>2</sub> concentration, respectively. This means that for pure PTMSP, the numbers are given as 2-0-0, for crosslinked PTMSP with 3wt% BAA: 2-3-0, and for crosslinked nanofilled PTMSP membranes with 2 wt% BAA and 20wt% TiO<sub>2</sub>: 2-2-20. The last number represents the membrane parallel.

**Table C.2** Contact angles of pure PTMSP membranes which have been treated with distilled water, 2M MDEA and 4.2M MDEA up to 10 weeks. The measurements are taken 10 minutes after the drop was in contact with the membrane.

Membrane ID	Solution	Time in solution [weeks]	Contact angles, $\Theta$ [°]				Standard deviation
			Parallel 1	Parallel 2	Parallel 3	Mean $\Theta$	
06.02.13_2-0-0_7	Distilled water	0.143	92.40	95.68	95.86	94.65	1.59
05.03.13_2-0-0_3	Distilled water	1	95.02	95.78	97.47	96.09	1.02
05.03.13_2-0-0_6	Distilled water	2	91.90	92.11	90.61	91.54	0.66
04.03.13_2-0-0_13	Distilled water	3	90.39	92.29	91.85	91.51	0.81
04.03.13_2-0-0_10	Distilled water	4	83.38	82.33	88.77	84.83	2.82
04.03.13_2-0-0_7	Distilled water	6	87.61	93.03	90.15	90.26	2.21
04.03.13_2-0-0_4	Distilled water	8	87.02	87.88	76.46	83.79	5.19
04.03.13_2-0-0_1	Distilled water	10	94.59	95.49	106.16	98.75	5.25
06.02.13_2-0-0_8	2M MDEA	0.143	90.43	90.05	87.97	89.48	90.43
05.03.13_2-0-0_4	2M MDEA	1	95.66	93.02	95.22	94.63	95.66
05.03.13_2-0-0_7	2M MDEA	2	95.99	103.72	100.82	100.18	95.99
05.03.13_2-0-0_1	2M MDEA	3	101.19	98.54	101.48	100.40	101.19
04.03.13_2-0-0_11	2M MDEA	4	97.59	103.78	102.59	101.32	97.59
04.03.13_2-0-0_8	2M MDEA	6	96.32	97.46	98.84	97.54	96.32
04.03.13_2-0-0_6	2M MDEA	8	98.25	96.88	95.08	96.74	98.25
04.03.13_2-0-0_2	2M MDEA	10	87.59	79.41	80.56	82.52	87.59
06.02.13_2-0-0_9	4.2M MDEA	0.143	-	-	-	-	-
05.03.13_2-0-0_5	4.2M MDEA	1	94.72	92.99	95.66	94.46	1.11
05.03.13_2-0-0_8	4.2M MDEA	2	108.52	108.91	111.79	109.74	1.46
05.03.13_2-0-0_3	4.2M MDEA	3	102.14	103.99	108.45	104.86	2.65
04.03.13_2-0-0_12	4.2M MDEA	4	105.44	105.98	100.83	104.08	2.31
04.03.13_2-0-0_9	4.2M MDEA	6	95.11	90.24	106.39	97.25	6.76
04.03.13_2-0-0_6	4.2M MDEA	8	102.08	102.93	100.58	101.86	0.97
04.03.13_2-0-0_3	4.2M MDEA	10	124.38	120.7	123.45	122.84	1.56



**Table C.3** Contact angles of crosslinked PTMSP with 3wt% BAA which have been treated with distilled water, 2M MDEA and 4.2M MDEA up to 10 weeks. The measurements are taken 10 minutes after the drop was in contact with the membrane.

Membrane ID	Solution	Time in solution [weeks]	Contact angles, $\Theta$ [°]				Standard deviation
			Parallel 1	Parallel 2	Parallel 3	Mean $\Theta$	
13.03.13_2-3-0_7	Distilled water	0.143	94.08	113.82	118.02	108.64	10.44
13.03.13_2-3-0_4	Distilled water	1	94.44	91.35	94.72	93.50	1.53
12.03.13_2-3-0_10	Distilled water	2	95.38	97.02	91.67	94.69	2.24
13.03.13_2-3-0_7	Distilled water	3	93.99	97.36	96.06	95.80	1.39
12.03.13_2-3-0_4	Distilled water	4	92.4	95.17	88.38	91.98	2.79
12.03.13_2-3-0_1	Distilled water	6	91.78	94.17	93.5	93.15	1.01
25.02.13_2-3-0_1	Distilled water	8	92.37	93.99	92.3	92.89	0.78
12.02.13_2-3-0_3	Distilled water	10	91.32	80.45	88.85	86.87	4.65
13.03.13_2-3-0_8	2M MDEA	0.143	96.91	99.39	96.02	97.44	1.43
13.03.13_2-3-0_5	2M MDEA	1	96.75	98.24	95.44	96.81	1.14
13.03.13_2-3-0_1	2M MDEA	2	98.37	95.26	95.33	96.32	1.45
12.03.13_2-3-0_8	2M MDEA	3	98.09	95.34	91.92	95.12	2.52
12.03.13_2-3-0_5	2M MDEA	4	94.61	98.69	100.88	98.06	2.60
12.03.13_2-3-0_2	2M MDEA	6	94.68	99.17	99.6	97.82	2.22
13.03.13_2-3-0_9	2M MDEA	8	90.04	93.31	94.74	92.70	1.97
12.02.13_2-3-0_4	2M MDEA	10	86.43	81.46	78.88	82.26	3.13
12.02.13_2-3-0_6	4.2M MDEA	0.143	110.91	111.26	117.83	113.33	3.18
13.03.13_2-3-0_6	4.2M MDEA	1	92.33	97.79	99.09	96.40	2.93
13.03.13_2-3-0_2	4.2M MDEA	2	129.76	131.28	130.52	130.52	0.62
12.03.13_2-3-0_9	4.2M MDEA	3	91.2	91.71	90.6	91.17	0.45
12.03.13_2-3-0_6	4.2M MDEA	4	107.9	101.15	105.72	104.92	2.81
12.03.13_2-3-0_3	4.2M MDEA	6	101.14	99.96	99.94	100.35	0.56
13.03.13_2-3-0_10	4.2M MDEA	8	96.61	99.83	101.61	99.35	2.07
12.02.13_2-3-0_5	4.2M MDEA	10	95.55	95	96.62	95.72	0.67



**Table C.4** Contact angles of crosslinked nanofilled PTMSP with 2wt% BAA and 20wt% TiO<sub>2</sub> which have been treated with distilled water, 2M MDEA and 4.2M MDEA up to 4 weeks. The measurements are taken 10 minutes after the drop was in contact with the membrane.

Membrane ID	Solution	Time in solution [weeks]	Contact angles, $\Theta$ [°]				Standard deviation
			Parallel 1	Parallel 2	Parallel 3	Mean $\Theta$	
17.04.13_2-2-20_1	Dest. water	2	119.94	123.05	119.17	120.72	1.68
17.04.13_2-2-20_4	Dest. water	4	106.96	102.4	106.43	105.26	2.04
17.04.13_2-2-20_2	2M MDEA	2	98.26	98.72	99.1	98.69	0.34
17.04.13_2-2-20_5	2M MDEA	4	84.76	89.36	80.75	84.96	3.52
17.04.13_2-2-20_3	4.2M MDEA	2	89.34	96.17	96.48	94.00	3.30
17.04.13_2-2-20_6	4.2M MDEA	4	95.21	88.22	90.73	91.39	2.89

## **D. RISK ASSESSMENT**

“Hazardous activity identification process” and “Risk assessment” for the following activities are attached:

- Gas permeation of N<sub>2</sub>, CH<sub>4</sub> and CO<sub>2</sub> through membranes in a single gas chamber
- Membrane preparation
- Use of chemicals during the testing of membrane properties

NTNU	Hazardous activity identification process	Prepared by	Number	Date	
		HSE section	HMSRV-26/01	01.12.2006	
HSE		Approved by	Page	Replaces	
		The Rector	XVIII out of 1	15.12.2003	


**Unit:** Dep. Chemical Engineering

**Date:** 15.01.2013

**Participants in the identification process (including their function):** Tina Tomasa (master student), Karen Nessler Seglem (co-supervisor)

**Short description of the main activity/main process:** Gas permeation of N<sub>2</sub>, CH<sub>4</sub> and CO<sub>2</sub> through membranes in a single gas chamber

Activity/process	Responsible person	Laws, regulations etc.	Existing documentation	Existing safety measures	Comment
Gas permeation of N <sub>2</sub>	Karen Nessler Seglem	Local operation manual	Use glasses	-	
Gas permeation of CH <sub>4</sub>	Karen Nessler Seglem	Local operation manual	Use glasses	-	
Gas permeation of CO <sub>2</sub>	Karen Nessler Seglem	Local operation manual	Use glasses	-	

NTNU	<b>Risk assessment</b>	Prepared by	Number	Date	
		HSE section	HMSRV-26/03	01.12.2006	
HSE/KS		Approved by	Page	Replaces	
		The Rector	XIX out of 1	15.12.2003	

**Unit:** Dep. Chemical Engineering

**Date:** 15.01.2013

**Line manager:** Øyvind Gregersen

**Participants in the risk assessment (including their function):** Tina Tomasa (master student), Karen Nessler Seglem (co-supervisor)

Activity from the identification process form	Potential undesirable incident/strain	Likelihood:	Consequence:				Risk value	Comments/status Suggested measures
		Likelihood (1-4)	Human (1-4)	Environment (1-4)	Economy / materiel (1-4)	Likelihood (1-4)		
Gas permeation of N <sub>2</sub>	Pressure build up which can cause rupture of membranes because of malfunction valves	2	A	A	A	A	2A	Check the pressure, vent the system, change membranes or valves if they have lost some of their function
	Leakage	2	A	A	A	A	2A	
	Explosion	1	C	C	C	C	1C	
Gas permeation of CH <sub>4</sub>	Pressure build up which can cause rupture of membranes because of malfunction valves	2	A	A	A	A	2A	Check the pressure, vent the system, change membranes or valves if they have lost some of their function.
	Leakage	2	A	A	A	A	2A	
	Fire, flammable gas	1	B	B	B	B	1B	Leakage of CH <sub>4</sub> in combination with a sparkle may cause fire and explosion
	Explosion	1	C	C	C	C	1C	
Gas permeation of CO <sub>2</sub>	Pressure build up which can cause rupture of membranes because of malfunction valves,	2	A	A	A	A	2A	Check the pressure, vent the system, change membranes or valves if they have lost some of their function
	Leakage	2	A	A	A	A	2A	
	Explosion	1	C	C	C	C	1C	

**Likelihood, e.g.:**

1. Minimal
2. Low
3. Medium
4. High
5. Very high

**Consequence, e.g.:**



- A. Very little
- B. Little
- C. Moderate
- D. Critical
- E. Very critical

**Risk value (each one to be estimated separately):**

**Human = Likelihood x Human Consequence**

**Environmental = Likelihood x Environmental consequence**

**Financial/material = Likelihood x Consequence for Economy/materiel**

NTNU	Hazardous activity identification process	Prepared by	Number	Date	
		HSE section	HMSRV-26/01	01.12.2006	
HSE		Approved by	Page	Replaces	
		The Rector	XX out of 1	15.12.2003	



**Unit:** Dep. Chemical Engineering

**Date:** 15.01.2013

**Participants in the identification process (including their function):** Tina Tomasa (master student), Karen Nessler Seglem (co-supervisor)

**Short description of the main activity/main process:** Membrane preparation

Activity/process	Responsible person	Laws, regulations etc.	Existing documentation	Existing safety measures	Comment
Weighting of toluene and nanoparticles	Karen Nessler Seglem	HSE-datasheet	Lab safety equipment	HSE-datasheet	
Closed rolling of solution	Karen Nessler Seglem	-	Lab safety equipment	-	
Ultrasound	Karen Nessler Seglem	Local operation manual	Lab safety equipment, use ice to avoid solvent evaporation	-	

NTNU	<b>Risk assessment</b>	Prepared by	Number	Date	
		HSE section	HMSRV-26/03	01.12.2006	
HSE/KS		Approved by	Page	Replaces	
		The Rector	XXI out of 1	15.12.2003	

**Unit:** Dep. Chemical Engineering

**Date:** 15.01.2013

**Line manager:** Øyvind Gregersen

**Participants in the risk assessment (including their function):** Tina Tomasa (master student), Karen Nessler Seglem (co-supervisor)

Activity from the identification process form	Potential undesirable incident/strain	Likelihood:	Consequence:				Risk value	Comments/status Suggested measures
		Likelihood (1-4)	Human (1-4)	Environment (1-4)	Economy / materiel (1-4)	Likelihood (1-4)		
Weighting of toluene and nanoparticles	Inhalation	4	A	A	A	A	4A	Use foam cupboard, gloves and glasses. Use a mask with P2 filter when weighting the nanoparticles
	Spill	4	A	A	A	A	4A	
	Skin and eye irritation	3	A	A	A	A	3A	
	Flammable (toluene)	1	B	B	B	B	1B	
Closed rolling of solution	The glass can fall of the roller and break	1	A	A	A	A	1A	Use foam cupboard, gloves and glasses
Ultrasound	Inhalation	3	A	A	A	A	3A	Use foam cupboard, gloves and glasses. Cover the sample with a coating or cool down the sample to avoid evaporation

**Likelihood, e.g.:**

1. Minimal
2. Low
3. Medium
4. High
5. Very high

**Consequence, e.g.:**



- A. Very little
- B. Little
- C. Moderate
- D. Critical
- E. Very critical

**Risk value (each one to be estimated separately):**

**Human = Likelihood x Human Consequence**

**Environmental = Likelihood x Environmental consequence**

**Financial/material = Likelihood x Consequence for Economy/materiel**

NTNU	Hazardous activity identification process	Prepared by	Number	Date	
		HSE section	HMSRV-26/01	01.12.2006	
HSE		Approved by	Page	Replaces	
		The Rector	XXII out of 1	15.12.2003	

**Unit:** Dep. Chemical Engineering

**Date:** 15.01.2013

**Participants in the identification process (including their function):** Tina Tomasa (master student), Karen Nessler Seglem (co-supervisor)

**Short description of the main activity/main process:** Use of chemicals during the testing of membrane properties

Activity/process	Responsible person	Laws, regulations etc.	Existing documentation	Existing safety measures	Comment
Use of N-Methyldiethanolamine (MDEA)	Karen Nessler Seglem	HSE-datasheet	Lab safety equipment	HSE-datasheet	



NTNU	<b>Risk assessment</b>	Prepared by	Number	Date	
		HSE section	HMSRV-26/03	01.12.2006	
HSE/KS		Approved by	Page	Replaces	
		The Rector	XXIII out of 1	15.12.2003	

**Unit:** Dep. Chemical Engineering

**Date:** 15.01.2013

**Line manager:** Øyvind Gregersen

**Participants in the risk assessment (including their function):** Tina Tomasa (master student), Karen Nessler Seglem (co-supervisor)

Activity from the identification process form	Potential undesirable incident/strain	Likelihood:	Consequence:				Risk value	Comments/status Suggested measures
		Likelihood (1-4)	Human (1-4)	Environment (1-4)	Economy / materiel (1-4)	Likelihood (1-4)		
Use of N-Methyldiethanolamine (MDEA)	Inhalation	4	A	A	A	A	4A	Use foam cupboard, gloves and glasses.
	Spill	4	A	A	A	A	4A	
	Skin and eye irritation	3	A	A	A	A	3A	

**Likelihood, e.g.:**

1. Minimal
2. Low
3. Medium
4. High
5. Very high

**Consequence, e.g.:**

- A. Very little
- B. Little
- C. Moderate
- D. Critical
- E. Very critical

**Risk value (each one to be estimated separately):**

**Human = Likelihood x Human Consequence**

**Environmental = Likelihood x Environmental consequence**

**Financial/material = Likelihood x Consequence for Economy/materiel**